Vaccine Lipid-Biopolymer Cross-Linked Nanoparticles Against Infectious Diseases and Cancer

by
Yuchen Fan

A dissertation submitted in partial fulfillment
of the requirements for the degree of
Doctor of Philosophy
(Pharmaceutical Sciences)
in The University of Michigan
2019

Doctoral Committee:

Associate Professor James J. Moon, Chair
Professor Maria G. Castro
Professor Steven P. Schwendeman
Professor Duxin Sun

Yuchen Fan

yuchfan@med.umich.edu

ORCID iD 0000-0001-7868-2919

ACKNOWLEDGMENTS

Pursuing a PhD degree has brought me unforgettable challenges in not only research work but also personal growth. Fortunately, I've got generous help and support from many friendly people, including my advisors, colleagues, families and friends, without whom I can't complete this long journey.

First and foremost, I would like to thank my advisor, Prof. James Moon. It is my pleasure to be his early generations of students and learn from him the essential skills, both scientifically and emotionally, to be a successful independent researcher. His insightful and critical thinking towards scientific questions, as well as passion for work have always been inspiring me during my graduate study and impacting my future career. I am also appreciated for the great freedom and opportunities he has offered me during these years, especially the valuable training in fellowship applications, paper and proposal writing, and conference presentations.

I should also send my great gratitude to my dissertation committee members, Prof. Steven P. Schwendeman, Prof. Duxin Sun, and Prof. Maria G. Castro. Their valuable critics and suggestions during my data meetings have helped me improve my research projects and move toward the defense.

I’d like to thank my lab members and alumni for their help during these years, including Dr. Jutaek Nam and Dr. Lukasz Ochyl who helped me accommodate to the lab and shared their experiment protocols with me. Special thanks to Dr. Rui Kuai and his wife Dr. Wenmin Yuan for their help in not only lab work but also life, and I’d treasure those experiences. Also, thank Charles Park and Xiaoqi Sun for their time for discussions and fun together. I’d like to thank our lab manager Yao Xu for daily maintenance of the lab and help in ELISPOT studies, and the staff in the Immunology Core, Flow Cytometry Core, and Microscopy and Image Analysis Laboratory for their help in my experiments. Thank Dr. Christopher Cooper and his lab at the USAMRIID for the collaboration on Ebola vaccine studies.

I’d like to thank my families and friends for their generous help and supports during these years. And finally, I am appreciated for partial of my funding sources including the Rackham Pre-doctoral Fellowship, Rackham Graduate Student Research Grant, and Elizabeth Broomfield Fellowship to support my PhD study.

TABLE OF CONTENTS

List of Figures

List of Tables

List of Abbreviations

NP	Nanoparticle
HA-SH	Thiolated hyaluronic acid
OVA	Ovalbumin
PEG	Polyethylene glycol
BMDCs	Bone marrow dendritic cells
MVP	Multilamellar vaccine particle
ICMV	Interbilayer-crosslinked multilamellar vesicle
GP	Glycoprotein
ICD	Immunogenic cell death
DAMPs	Damage-associated molecular patterns
TLR	Toll-like receptor
APCs	Antigen-presenting cells
MHC	Major histocompatibility complex
dLNs	Draining lymph nodes
MPLA	Monophosphoryl lipid A
CTLs	Cytotoxic T lymphocytes
HMGB1	High mobility group protein B1
DOTAP	1,2-dioleoyl-3-trimethylammonium-propane
DOBAQ	N-(4-carboxybenzyl)-N,N-dimethyl-2,3-bis(oleoyloxy)propan-1-aminium
DLS	Dynamic light scattering
NTA	Nanoparticle tracking analysis
FRET	Fluorescence resonance energy transfer
PBMCs	Peripheral blood mononuclear cells
ELISA	Enzyme linked immunosorbent assay
ELISPOT	Enzyme linked immunospot
ICS	Intracellular cytokine staining
PBS	Phosphate buffered saline
FBS	Fetal bovine serum
TLC	Thin layer chromatography
HPLC	High performance liquid chromatography
EE%	Encapsulation efficiency

ICBs	Immune checkpoint blockers
MAL	Maleimide
Mit	Mitoxantrone
MFI	Geometric mean fluorescence intensity
ANOVA	Analysis of variance
SEM	Standard error of mean

ABSTRACT

Prophylactic vaccines can induce long-term, antigen-specific cellular and humoral immunity, and provide effective countermeasures against emerging infectious diseases, such as the recent epidemics of Ebola and Zika. Compared to inactivated or live-attenuated pathogens, subunit proteins derived from whole-pathogens provide a safer antigen source but are often limited by unstable delivery in their soluble forms and low immunogenicity. Nanoparticle (NP) vaccines have shown promise to protect antigens from rapid enzymatic degradation, and achieve co-localized delivery of antigens and adjuvants to antigen-presenting cells, thus enhancing cellular and humoral immune responses. In this thesis, I hypothesize that delivery of subunit protein antigens and/or molecular adjuvants by nanoparticles can improve immune stimulation and vaccine efficacy. Specifically, I have developed a new cationic lipid-hyaluronic acid (HA) hybrid NP platform and demonstrated the improved vaccine efficacy using plague, Ebola, and cancer models.

In the first section, I present the characterization of these NPs as an intranasal vaccine using the model antigen ovalbumin (OVA) and F1-V, a candidate recombinant antigen against the plague. These NPs exhibited improved colloidal stability, and reduced

cytotoxicity associated with cationic liposomes by at least 20 fold in dendritic cell (DC) culture. Furthermore, NPs co-loaded with OVA and a molecular adjuvant, the Toll-like receptor (TLR)-4 agonist monophosphoryl lipid A (MPLA), promoted DC maturation *in vitro*, and elicited robust OVA-specific $CD8^+$ T cell and antibody responses *in vivo*. Importantly, intranasal vaccination with NPs co-loaded with F1-V and MPLA increased endpoint serum titers of F1-V-specific total IgG, IgG_1, and IgG_{2c} by 11-, 23-, and 15-fold, respectively, compared with the lack of sero-conversion in mice immunized with the equivalent doses of soluble F1-V vaccine.

In the second section, I modified the hybrid NP design by promoting inter-lipid layer crosslinking and particle surface decoration with HA, and constructed the multilamellar vaccine particle (MVP) platform. Compared with the previously developed interbilayer-crosslinked multilamellar vesicle (ICMV) platform without HA decoration, MVP accumulated more in CD44-expressing DCs, increased antigen processing in DCs, and elicited significantly stronger antigen-specific $CD8^+$ and $CD4^+$ T cell immune responses tested using the OVA antigen. A single dose of the Ebola glycoprotein (GP)/MPLA co-loaded MVP protected 80% of mice against a lethal viral challenge, suggesting it could be a potent delivery platform for subunit vaccines.

Inspired by these promising results, I further explored the MVP for delivery of molecular adjuvants and developed a novel whole-cell cancer vaccination strategy in the third section. Recent studies have shown that cancer cells treated with certain

chemotherapeutics, such as mitoxantrone, can undergo immunogenic cell death (ICD) and initiate anti-tumor immune responses. However, it remains unclear how to exploit ICD for cancer immunotherapy. In this section, I synthesized and demonstrated immunogenically dying tumor cells surface-modified with MVP encapsulating CpG, a TLR-9 agonist, efficiently promoted activation and antigen cross-presentation by DCs *in vitro*, and elicited robust antigen-specific $CD8^+$ T cells *in vivo*. Furthermore, whole tumor-cell vaccination combined with immune checkpoint blockade led to complete tumor regression in 78% of CT26 tumor-bearing mice and established long-term immunity against tumor recurrence. Our strategy may open new doors to “personalized” cancer immunotherapy tailored to individual patient’s tumor cells.

Overall, our results presented in this thesis suggest lipid-HA crosslinked MVP could be a promising platform for vaccine delivery of subunit protein antigens and molecular adjuvants, thus promoting clinical translation of vaccine candidates against infectious diseases and cancer.

Chapter 1 Introduction

1.1. Immune defense against pathogens

Vertebrates are protected by the immune system from pathogens such as viruses, bacteria, fungi, and parasites. The immune response can be classified into two categories: innate and adaptive immunity. Innate immune responses act as the first line of defense with physical barriers including the skin epithelium and mucosal surface, chemical barriers including the stomach acidity and secreted anti-microbial peptides, and cellular barriers including neutrophils, macrophages, dendritic cells, and natural killer cells.[1-2] Pathogen recognition by innate immunity relies on pathogen-associated molecular patterns (PAMPs) and pattern recognition receptors (PRRs) expressed on microorganisms and immune cells, respectively.[3] To date, four types of PRRs have been identified: Toll-like receptors (TLRs), C-type lectin receptors (CLRs), Nod-like receptors (NLRs) and retinoic acid-inducible gene-I-like receptors (RLRs), among which TLRs have been mostly characterized.[4] The innate immunity provides rapid defense before the elicitation of adaptive immunity, but without immune memory. In contrast, adaptive immunity requires the processing of pathogens by antigen-presenting cells, which will present immunogenic

antigens to T cells and B cells, eliciting cellular and humoral immune responses, respectively. For cancer, theoretically, the immune system can inhibit oncogenesis by actively identifying and eliminating cancerous cells, a process referred to as immunosurveillance.[5] However, this defense mechanism often failed due to down-regulation of tumor antigens expressed in cancerous cells and/or immune suppression within the tumor microenvironment.[6] Below I will introduce in detail about key factors governing innate and adaptive immunity; then present the rationale and advantages of nanoparticles for vaccine delivery.

1.1.1. Antigen presentation and activation of T and B cells

Antigen-presenting cells (APCs) play a pivotal role in both innate and adaptive immune responses. Professional APCs include B cells, macrophages, and DCs, among which DCs have been shown as the most efficient APC population.[7] DCs can process and load endogenous and exogenous antigens onto major histocompatibility complex (MHC) class I (MHC-I) in endoplasmic reticulum and MHC class II (MHC-II) in endosomes, respectively, and then present the complex of MHC/antigen peptide as the activation signal one to $CD8^+$ and $CD4^+$ T cells, respectively. To fully activate T cells, there should be signal two provided by the recognition between co-stimulatory markers CD80/86 on DCs and CD28 on T cells, as well as polarizing cytokines secreted from APCs as the third signal. Although MHC-I is constitutively expressed by the majority of mammalian cells,

non-professional APCs cannot provide the additional signal two and three to alert the immune system when infected with pathogens. Therefore, DCs evolve an alternative mechanism termed cross-presentation to process exogenous pathogens and activate $CD8^+$ T cells.

Although the exact mechanism of cross-presentation is still under investigation, there are potentially two different pathways, i.e. vacuolar and cytosolic pathways, as shown in the **Figure 1.1**.[8] The main difference between the two is the subcellular location for processing and loading of antigens to MHC-I: endosomes designated for the vacuolar pathway while cytosol for the cytosolic pathway. Endosomes with relatively high pH and low levels of proteases are thought to be beneficial to cross-presentation, and some subtypes of DCs such as $CD8^+$ DCs and $CD103^+$ DCs have been identified as efficient cross-presenting DC subtypes.[9]

There are two signals required for activation of B cells: (1) recognition of antigens by B cell receptors (BCRs); and (2) additional activation signals provided from activated $CD4^+$ T cells that are ligated with B cells (thymus-dependent mechanism) or less commonly, cross-linking of BCRs by antigens or signaling through TLRs (thymus-independent mechanism). Follicular helper T cells (Tfh) have been identified as the main helper $CD4^+$ T cell subtype that promotes B-cell activation and following humoral immune responses. Upon activated in lymph nodes (LNs), B cells rapidly proliferate to form germinal centers where the generation of antibody-secreting plasma

cells, memory B cells, and high-affinity antibodies occur. In general, pathogens are cleared by antigen-specific antibodies through neutralization or phagocytosis following opsonization or complement activation. Isotype switching of antibodies is mediated by different cytokines secreted from $CD4^+$ helper T cells, e.g. the Th2 cytokine IL-4 induces IgE and IgG_1, TGF-α induces IgA, while the Th1 cytokine IFN-β induces IgG_{2a}. Balanced Th1/Th2 IgG titers are advantageous for clearance of systemically disseminated pathogens, while IgA plays an important role in immune protection at mucosal membranes.[10]

1.1.2. TLR agonists as vaccine adjuvants

TLRs are important mediators of innate immunity by sensing exogenous PAMPs and endogenous damage-associated molecular patterns (DAMPs) released by dying cells or damaged tissues. To date, 13 types of TLRs have been identified with distinctive specificities in mice and humans, and ligands of TLR-1-9 are intensively investigated as adjuvants. A summary of characteristics of common TLRs and their ligands are listed in **Table 1.1**.

Upon ligand binding, TLRs will dimerize and initiate signaling pathways through MyD88 which is the adaptor molecule for most TLRs, or TRIF which is only associated with TLR-3 and intracellular TLR-4.[11] Although gene transcription and cytokine release profile vary following the activation of different TLRs, a common response is the

production of type I IFNs by activation of intracellular TLRs, especially by TLR-3.[12]

The TLR-4 agonist MPLA has been approved as adjuvants for the HPV vaccine Cervarix and the HBV vaccine Fendrix, while the TLR-7 agonist Imiquimod approved for the treatment of topical basal cell carcinoma.[13] Several agonists of TLR-4, 7, 8, and 9 are now investigated as vaccine adjuvants in clinical trials.[14] Furthermore, recent studies reveal synergistic effects among certain TLR agonists, especially those with different signaling pathways, such as poly I:C plus CpG, and MPLA plus CpG.[15-16]

1.2. Hyaluronic acid

Hyaluronic acid (HA) is a linear polysaccharide composed of repeating disaccharide units of D-glucuronic acid and N-acetyl-D-glucosamine.[17] The molecular weight of natural HA ranges between 1 kDa and 2 MDa, and each glucoronate unit carries an anionic charge associated with its carboxylate group at the physiological pH. These anionic charges are usually balanced with mobile cations such as Na^+ and K^+, and significantly increase the water solubility of HA since the uncharged hyaluronan is insoluble in water. HA is biocompatible and abundant in various tissues, such as skin, the vitreous of eyes, the umbilical cord, synovial fluid, heart valves, and skeletal tissues,[18] with 50% of HA found in the human body is associated with skin and acts as a major component of the extracellular matrix (ECM).[19] In nature, HA is synthesized by three types of membrane-bound synthases and is degraded by two pathways: (1) enzymatic degradation

by hyaluronidases; and (2) nonspecific oxidation-reduction degradation reaction induced by reactive oxygen species.[20]

1.2.1. HA in immune modulation

HA plays an important role in regulating immune responses, mainly through ligation with its major receptor CD44, which is expressed on several immune cell populations.[21] Binding of HA expressed on DCs with CD44 expressed on T cells promote the formation of DC-T cell clusters and provide additional stimulatory signals for T cell proliferation.[22] The HA-CD44 ligation also promotes adhesion, migration, and extravasation of T cells and neutrophils in inflamed tissues.[18] In addition, CD44 regulates the phagocytosis by macrophages, especially the clearance of apoptotic neutrophils and HA fragments.[23] Noticeably, the immunomodulatory properties of HA are dependent on its molecular weights. High molecular weight HA (> 1000 kDa) is unable to induce inflammatory responses, whereas low molecular weight (< 500 kDa), fragmented HA is immunostimulatory by promoting DC maturation.[18] Furthermore, only high molecular weight HA enhances the suppression activity of $CD4^+CD25^+$ regulatory T cells.[24]

1.2.2. Use of HA for vaccine delivery systems

HA, which is biocompatible and shows multiple immunological functions, has been widely investigated for vaccine delivery. HA has been incorporated in nano- or

micro-structures to improve mucosal vaccine delivery, and significantly increased titers of both antigen-specific IgG in serum and IgA in nasal wash.[25-26] HA has also been used to assist transdermal vaccine delivery in the form of microneedles or a non-invasive topical patch.[27-28] Nanoparticles can be coated with HA on their surfaces to achieve targeted delivery of antigens to dendritic cells via HA-CD44 ligation.[29-30] Alternatively, antigens and adjuvants can also be chemically conjugated onto the HA polymer backbone, thus enhancing their delivery efficiency to local draining lymph nodes due to the propensity of HA for trafficking through ECM and the increase of molecular weight by polymer grafting.[31-33]

1.3. Nanoparticle (NP) platforms for vaccine delivery

The particulate delivery approach has been widely investigated for the development of vaccines, e.g. virus-like particles as a natural mimic of inactivated pathogens, and synthetic PLGA nano/microparticles and cationic liposomes for the stable delivery of protein and DNA subunit antigens, respectively. Repurposing these nanomaterials to target the immune system may offer new opportunities to tune immunity with several key advantages: (1) nanocarriers with finely tuned size and a defined surface chemistry can achieve selective delivery to lymphoid tissues;[34-36] and (2) nanoparticles carrying both antigens and adjuvants can stably co-deliver vaccine components to APCs, thus potentially promote cross-presentation of antigens.[37-38]

1.3.1. Improvement of LN draining of antigens by NP vaccines

Nanocarriers can improve delivery efficiency of antigens to lymphoid tissues by their prolonged tissue residence as well as controlled release of antigens and adjuvants. Particle size is one of the primary factors determining the efficiency of lymphatic draining. Large particles (> 500 nm in diameter) can be physically trapped at the injection site by interaction with extracellular matrix proteins, whereas ultra-small nanoparticles (< 10 nm in diameter) or soluble antigen molecules can rapidly diffuse not only into but out of lymph nodes, thus minimizing the chance of APCs phagocytizing sufficient amount of vaccine particles.[39] On the other hand, particles of an intermediate size (10-100 nm in diameter) can both efficiently drain to regional draining lymph nodes and become retained there, thereby increasing the chance of antigen uptake and presentation by APCs.[35, 39] Indeed, one study has compared the immunogenicity of protein or peptide antigen-conjugated nanobeads with sizes ranging from 0.02 to 2 μm. Following intradermal injection of these nanobeads into mice, a 40 nm nanovaccine formulation drained most efficiently to lymph nodes and elicited the strongest antigen-specific T-cell immune responses than other formulations, including vaccines with conventional adjuvants such as Alum, MPLA, or Quil-A.[40] However, it remains to be seen whether the delivery advantage to LNs achieved by NP systems can be successfully translated into clinics since most studies were performed on murine models. Indeed, upon subdermal

injection into the breast region of breast cancer patients, large (> 300 nm) radio-labeled colloids were drained slowly through the lymph vessels and retained longer in sentinel lymph nodes, compared with their small (< 50 nm) counterparts that rapidly visualized lymphatic vessels, sentinel lymph nodes, and second- and third-tier lymph nodes.[41] In addition, lymphatic draining of particulate vaccines also depends on the material composition, morphology, and surface chemistry of particles.[36]

1.3.2. Improvement of mucosal immunity by NP vaccines

Mucosal vaccination would preferentially elicit T- and B-cell immune responses in local and distal mucosal surfaces, including respiratory, gastrointestinal, and reproductive tracts, thereby establishing immunity in the frontline of protection against pathogens.[42-43] Compared with soluble antigens that are subjected to fast clearance or degradation, particulate vaccines could improve colloidal stability, increase residence time in mucosal tissues, and promote induction of antigen-specific IgA titers and peripheral tissue-resident effector $CD4^+$ and $CD8^+$ T cells.

Pulmonary vaccine delivery is noninvasive and needle-free. Intranasal administration of NP vaccines allows targeting antigens to the nasal cavity, which is characterized by highly permeable nasal epithelium for the absorption of biomolecules and large amounts of immune cells within nasal-associated lymphoid tissues. One example utilized interbilayer-crosslinked multilamellar vesicles (ICMVs) for pulmonary

vaccine delivery.[44] The NP systems co-loaded with protein or peptide antigens and two TLR agonists (poly I:C and MPLA) were efficiently processed by DCs in lungs and mediastinal LNs, and elicited antigen-specific $CD8^+$ T-cell immunity not only in the lung but also disseminated systemically to distal mucosal sites. This NP vaccine led to ~100% protection of immunized mice in subcutaneous tumor challenge or intratracheal viral challenge models, whereas the soluble admix counterpart exerted low prophylactic efficacy. Alternatively, the adjuvant-free mucoadhesive nanogel system has been prepared by self-assembly of the polysaccharide pullulan modified with cholesteryl and amino groups.[45] Compared with a soluble vaccine, the nanogel significantly increased the residence time of antigen in nasal epithelium following intranasal vaccination and elicited robust antigen-specific mucosal IgA and systemic IgG responses, achieving complete protection of animals against an intraperitoneal or intranasal challenge with C. botulinum neurotoxin.

Oral vaccines may be most amenable to mass vaccination campaigns and also most efficacious for immunization against enteric pathogens.[46] Indeed, oral vaccine delivery has been exploited for currently licensed and candidate cholera vaccines. However, one of the major challenges in oral vaccination lies in rapid denaturation and degradation of antigens in contact with acidic pH and abundant proteases in the gastrointestinal tract. Thus, it would be valuable to investigate particulate carriers composed of biopolymers that can endure the harsh gastric environment or liposomes stabilized by bile salts or

archaeobacterial lipids that can maintain antigenicity and immunogenicity of antigens.[47] In addition, vaccine carriers targeted to M cells and/or intestinal dendritic cells could be examined to further improve the efficacy of oral vaccines.

1.3.3. Co-delivery of antigens and adjuvants by NPs

Nanoparticle delivery systems can co-deliver antigens together with adjuvants, thereby enhancing cross-presentation and/or skewing immune responses to desired $CD4^+$ T helper phenotypes. Th1 responses elicited by activation of TLR-3, 7, and 9 contribute to $CD8^+$ T cell responses.[48-49] The TLR-9 agonist CpG, which is an unmethylated oligonucleotide containing CpG motif, has been complexed with cationic polymers via the electrostatic interaction or conjugated with nanocarriers, which improved immune activation compared with administration of the soluble adjuvant.[50-51] The charge-mediated entrapment was also exploited to co-load an anionic TLR-3 agonist poly I:C and cationic antigen peptides onto gold nanoparticles via the "layer-by-layer" strategy, leading to the elicitation of robust antigen-specific $CD8^+$ T cells when tested with a model antigen *in vivo*.[52] Furthermore, nanoparticles designed for multifaceted drug loading can support a combinational use of adjuvants, thus permitting exploitation of synergy among certain TLR agonists, as introduced above. For example, CpG and poly I:C have been co-loaded into polyester nanoparticles,[53] while the TLR-4 agonist glucopyranosyl lipid A and the TLR-7 agonist imiquimod have been co-encapsulated into liposomes.[54] In both cases, the

Th1 response was significantly improved by the dual TLR agonists-loaded particles, compared with that elicited by a single adjuvant. Alternatively, TLR agonists can be combined with siRNAs inhibiting the immunosuppressive pathways. Co-delivery of CpG and siRNA targeting IL-10, the inducer of Th2 and Treg cells, skewed immune responses to the Th1 type.[55] The combination of an epitope peptide of Trp2 and CpG-based nanovaccine with siRNA against TGF-β, which is one of the major cytokines responsible for induction and maintenance of immunosuppressive tumor microenvironment, has significantly improved the therapeutic efficacy of the nanoparticle-based cancer vaccine in a late-stage murine melanoma model.[56]

1.3.4. Promotion of cross-presentation by NP vaccines

Extracellular antigens are usually processed and presented via MHC-II by APCs to $CD4^+$ T cells; whereas antigens engulfed by APCs need to be presented via MHC-I to elicit cytotoxic T lymphocytes (CTLs). Thus, traditional vaccine approaches relying on soluble protein or peptide antigens may skew immune responses to $CD4^+$ T cell responses, while failing to induce sufficient CTL responses. In contrast, antigens delivered by functional nanomaterials designed to promote endosomal escape (i.e., translocation of antigens from endosomes/phagosomes to cytosol) may promote cross-presentation and favorably elicit $CD8^+$ T-cell responses.[9] To this end, extensive research efforts have been focused on pH-sensitive delivery systems that can retain their cargo under the physiological pH

condition while triggering release of antigens and disruption of endocytic vacuoles at the acidic (~ pH 6) endosomal microenvironment.[57] For example, a liposomal antigen delivery system modified with a pH-sensitive dextran derivative has been shown to promote cytosolic delivery of antigens.[58] In addition, a micellar system composed of an amphiphilic polymer with a pH-sensitive building block forming the particle core has been devised to induce fusion of the nanomaterials to endosomal vesicles, thus transporting protein antigen surface-displayed on micelles from endosome to cytosol and promoting antigen cross-presentation and $CD8^+$ T cell responses.[59] An alternative approach includes an oxidation-sensitive polymersome that can respond to the oxidative environment of endosomes and deliver antigens and adjuvants to cytosol.[60] Additionally, liposomes modified with a cell-penetrating peptide octaarginine or gold nanoparticles displaying tumor antigens were also shown to promote cross-presentation.[61-62]

1.4. NP subunit vaccines against infectious diseases

For decades, research efforts on countermeasures against emerging infectious pathogens have been focused on attenuated or inactivated whole-bacterium or whole-virus vaccines. Despite their strong immunostimulatory efficacy, preclinical and clinical studies performed with these traditional vaccines have raised serious concerns, as they have induced unacceptable levels of reactogenicity and caused inadvertent pathogenic infections with ill-prepared live-cell vaccines in the past.[63-65] In contrast, molecularly

defined subunit antigens derived from whole pathogens offer safer alternatives. However, subunit antigens are usually far less immunogenic than live and attenuated vaccines and are also more susceptible to deactivation and degradation. Recent advances in particulate vaccine delivery systems have addressed these challenges faced by subunit antigen-based vaccines.

1.4.1. NP subunit vaccines against plague

Plague, caused by infection with *Yersinia pestis (Y. pestis)*, is an ancient zoonotic disease that is naturally carried in rodent reservoirs. The disease can be transmitted to humans by direct contact with infected rodents or bites from infected fleas from these rodents, causing the bubonic plague; or by pathogenic aerosols that cause pneumonic plague. *Y. pestis* prefers to attack certain types of lymphocytes, especially macrophages, and alveolar epithelial cells of the lung. In a typical natural transmission via bites by infected fleas, the bacteria enter the host's subcutaneous tissues, followed by ingestion by macrophages, which become an intracellular niche for the pathogen.[66] After the onset of an infection, *Y. pestis* suppresses the host immune responses by producing a variety of virulence factors, initiates the extracellular life cycle, and rapidly multiplies with a biphasic phase.[67] The bacteria multiply first in draining lymph nodes near the site of flea bites, followed by dissemination into the blood and colonization in the liver, spleen, and lungs. The initial host immune responses are evidenced by phagocyte infiltration,

production of inflammatory cytokines, and tissue necrosis.[68]

Historically, the plague has been one of the most devastating epidemic diseases, including the infamous Black Death pandemic in the 14th century that killed one-third of the European population. In particular, aerosolized *Y. pestis* can result in deadly pneumonic diseases with a mortality rate of 50-90% without treatment.[69] Although intensive antibiotic therapy can reduce the mortality rate of pneumonic plague down to ~15%, it must be given within 24-36 h after exposure.[69] In addition, there are reported cases of multidrug-resistant strains, raising concerns about antibiotic therapies.[70] Therefore, vaccine development against plague is an indispensable strategy for biodefense. Two types of plague vaccines have been used since the late 19th century: a killed whole-cell vaccine, which is only protective against bubonic plague, and a live whole-cell vaccine, which generates protective immunity against both bubonic and pneumonic plagues.[63] However, both vaccines have been discontinued due to local and systemic side effects, such as regional lymphadenopathy, anorexia, and mild fever, long-term booster doses required, and safety concerns with the live bacterial vectors. Current research efforts have been mainly focused on the development of safer subunit vaccines utilizing the capsular subunit protein F1 and low-calcium response V antigen (LcrV). F1 and V, screened from a panel of key virulent factors from *Y. pestis*, have been reported to be promising antigens against bubonic and pneumonic plagues in various animal models.[71] Polymeric microspheres have been tested as vaccine carriers to

potentiate the efficacy of subunit plague antigens.[72-74] PLA microspheres co-encapsulating F1 and V were shown to elicit superior humoral immune responses compared with soluble vaccines irrespective of administration routes.[72] A recent study on F1-loaded PLGA/PEG microspheres showed that a single vaccine dose was sufficient to protect mice from bacterial challenge.[74]

Nanoparticle delivery systems composed of poly (anhydride),[75-76] gold,[77] and lipoproteins[78] have been developed for plague vaccines. A single intranasal dose of recombinant F1-V-loaded poly(anhydride) nanoparticles led to prolonged lung disposition[76] and generated high levels of antigen-specific antibody responses,[75] with the overall kinetics dictated by the chemical composition, hydrophobicity, and degradation rate of poly(anhydride) particles.[79] In another approach, F1 antigen was conjugated on the surfaces of gold nanoparticles via carbodiimide (EDC/NHS) chemistry, and the conjugates were resuspended in Alhydrogel.[77] This vaccine system elicited higher titers of both anti-F1 IgG_1 and IgG_{2a} than those elicited by the vaccine without Alhydrogel as well as the soluble F1 mixed with the adjuvant. Lipid-based delivery systems have also shown promising results for the delivery of subunit plague antigens. Nanolipoprotein particles were constructed with lipids, cholate, and apolipoprotein that self-assembled into nanostructures mimicking high-density lipoproteins.[78] The LcrV antigen was terminally modified with polyhistidine for complexation with nickel-modified lipids while MPLA or cholesterol-modified CpG was co-encapsulated via lipid insertion. The

resulting vaccine particles significantly enhanced LcrV-specific IgG titers in mice compared with the physical mixture of LcrV antigen and soluble or particulate adjuvants.

1.4.2. NP subunit vaccines against Filoviruses

Filoviruses, including Marburg virus and Ebola virus, are the main causative pathogens for hemorrhagic fever in humans, which is a deadly disease transmitted by direct contact with body fluids of infected subjects. Ebola virus preferentially and initially replicate in macrophages and dendritic cells,[80] which transport the virus through the lymphatic system to blood, liver, and spleen, where the virus can infect endothelial and epithelial cells, hepatocytes, Kupffer cells, and cells of adrenal gland tissue. Typically, Ebola virus infection runs its course within 14 to 21 days. Initial infection is manifested by nonspecific flu-like symptoms. Patients with progressive disease exhibit severe bleeding and coagulation abnormalities. The terminal stages of Ebola virus infection usually include diffuse bleeding, and hypotensive shock causing the majority of fatality.[81]

Since the discovery of the Ebola virus in the 1970s, several outbreaks resulted in fatality rates ranging from 25 to 90%. Currently, no vaccine or specific antiviral drug is available for the disease. The recent Ebola outbreaks in Africa have intensified research efforts to develop Ebola vaccines, resulting in two vaccine candidates, rVSV-EBOV and ChAd3-ZEBOV, both of which have entered Phase III trials in the late 2015.[82] Historically, development of vaccines against Ebola began with inactivated whole viruses,

and a whole virion inactivated by formalin was shown to provide better protection than the γ-irradiation approach.[83] More recently, a replication-defective whole-virus vaccine showed complete protection in a pilot trial on non-human primates.[84] Given the variable potency of inactivated viruses and emergence of mutant strains, the primary vaccine approach has shifted from the direct use of whole virions to overexpression of genes encoding the Ebola glycoprotein (GP) and nucleoprotein (NP) in the host to elicit potent humoral and cellular immune responses. Specifically, immunity can be elicited by replication-deficient recombinant adenoviruses or plasmid vectors that transduce Ebola antigens or by attenuated recombinant viruses bearing Ebola GPs on their surfaces.[85] However, booster immunizations are often required, and safety concerns remain for viral vectors. For instance, although recombinant vesicular stomatitis virus (rVSV) expressing Ebola GPs achieved complete protection under a 'ring vaccination' scheme in a recent clinical trial,[86] previous preclinical studies in non-human primates have reported cases of vector-induced viremia.[87-88] As an alternative to the viral vector-based approaches described above, virus-like particles (VLPs) are the most promising vector-free vaccine platforms in the preclinical pipeline for Ebola vaccines. Filovirus GPs along with a viral matrix protein VP40 have been produced from mammalian cell lines and self-assembled into VLPs.[89] Immunization with Ebola VLPs completely protected mice and non-human primates from a viral challenge.[90-91] Follow-up studies revealed that the protection was dependent on type I IFNs,[92] and VLPs combined with the TLR-3 agonist poly I:C,[93]

which is capable of driving the production of type I IFNs, significantly augmented cellular and humoral immune responses. In addition, a trimeric hybrid VLP was constructed to express GPs of the Marburg virus, Ebola Zaire virus, and Sudan virus.[94] Immunization with these VLPs induced protection rates higher than 70% against a Marburg challenge but varying rates from 20 to 70% against an Ebola challenge depending on subunits of the Ebola GP used for the VLPs. In a separate line of studies, a liposomal formulation encapsulating irradiated Ebola virions and lipid A as the adjuvant has been shown to elicit CTL responses and achieve a protection rate of ~100% in a murine model; however, this liposomal vaccine failed to protect non-human primates from a lethal challenge.[95-96]

1.5. Cancer immunotherapy

Immunotherapy has been explored for more than a century as a potential therapeutic approach to combat against cancer. Dating back to 1891 when neither chemotherapy nor radiotherapy was developed, a surgeon named William B. Coley successfully treated his cancer patients with bacterial products, which are now recognized to have induced non-specific anti-tumor inflammation.[97] However, immunotherapeutic strategies for cancer treatment have been doubted for a long time due to disappointing failures in various clinical trials. It was not until recent years that dendritic cell-based vaccines and immune checkpoint blockers (ICBs) have each ushered new lines of cancer therapy and

raised the hope for unleashing patients' own immune system to eradicate tumors.[98-99] Cancer immunity consists of several key steps, including release of antigens from tumor beds, presentation of tumor antigens by antigen-presenting cells (APCs), priming and activation of T cells by activated APCs, migration and infiltration of effector T cells back to the tumor, and finally the recognition and killing of tumor cells by effector T cells.[100] In theory, each of these steps can be targeted with various therapeutic approaches, as shown in **Figure 1.2.** The current advancement in cancer immunotherapy is mainly driven by striking results obtained with inhibitors of negative immune checkpoint molecules. However, this approach is mostly aimed at augmenting the potency of pre-existing tumor-specific T cells and benefits only a portion of patients as seen in clinical trials.[101-102] In contrast, cancer vaccines targeting early steps of antigen processing can potentially improve both therapeutic and prophylactic efficacy against not only the primary tumor but also inoperable metastasis or relapse, and benefit more patients, especially those that lack sufficient levels of pre-existing anti-tumor T cells and/or immune checkpoint molecules.

1.5.1. Whole-cell cancer vaccines

Compared with a single peptide or protein antigen, whole-cell cancer vaccines may elicit multivalent immune responses by broadening epitope recognition and help to achieve personalized immunotherapy. Whole-cell antigens can be obtained from tumor cell

lysates with necrotic features or inactivated whole tumor cells with apoptotic features. Similar to subunit vaccine nanocarriers, tumor cell lysates and TLR agonists have been co-encapsulated into particulate delivery systems, including liposomes or PLGA micro/nanoparticles.[103-104] Whole-cell cancer vaccine has also been delivered by a biodegradable,"infection-mimicking" PLGA matrix containing tumor cell lysates as the source of tumor antigens, granulocyte macrophage colony-stimulating factor (GM-CSF) for recruitment of DCs *in situ*, and CpG for activation of recruited DCs.[105] This PLGA matrix-based whole-cell cancer vaccine successfully elicited antigen-specific $CD8^+$ T cells and improved both prophylactic and therapeutic anti-tumor efficacy, compared with a conventional whole-cell vaccine GVAX, composed of irradiated, GM-CSF-secreting tumor cells. In an alternative approach, the plasma membrane of tumor cells has been extracted and coated onto polymeric nanoparticle cores along with the TLR-4 agonist MPLA or the TLR-9 agonist CpG to form a tumor cell-mimicking cancer vaccine.[106-107]

1.5.2. Immune checkpoint blockers (ICBs)

Cancer therapy by reversion of immunosuppression has achieved striking success in recent years. The CTLA-4 antibody Ipilimumab has improved the survival of patients with advanced, untreatable melanoma by 3.7 months, and is the first approved cancer therapeutic in this category.[108] However, Ipilimumab also causes a high rate of adverse effects since CTLA-4 is mainly up-regulated during T-cell activation in lymph nodes and

is a natural controller of immune activation. The anti-PD-1 antibodies Nivolumab and Pembrolizumab were approved for the treatment of malignant melanoma in 2014. In contrast to CTLA-4, PD-1 mainly inhibits tumor-infiltrating T cells within the tumor microenvironment. Blockade of PD-1 mitigated side effects and improved response rates,[109] especially among patients bearing tumors positive for PD-L1.[102, 110] In addition, dual inhibition of CTLA-4 and PD-1 proves to be more efficacious than a single therapy, mainly due to their distinctive mechanisms of action.[111]

On the other hand, there are also stimulatory checkpoints such as OX40 (CD134) and 4-1BB (CD137) that can be activated to improve anti-tumor immunity. Both two molecules belong to the TNFR family and directly mediate T-cell activation. Ligation of OX40 on T cells with OX40 ligand on APCs results in activation of both $CD4^+$ and $CD8^+$ T cells, with a general inhibitory effect on tumor growth.[112] In a phase I trial on patients with advanced cancers, an agonistic antibody against OX40 showed acceptable toxicity profile and regressed metastatic lesions in 12 out of 30 patients, although no patients achieved partial response defined by the Response Evaluation Criteria in Solid Tumors (RECIST) criteria.[113] Notably, previous results are controversial about the expansion of Tregs by activation of OX40.[114-115] Since all $CD4^+$ T cell subtypes can be activated by this pathway, it is likely that the differentiation of Tregs depends on different polarizing cytokine milieus. In contrast to OX40, 4-1BB signaling preferentially activates $CD8^+$ rather than $CD4^+$ T cells.[116] It is indeed up-regulated as a surrogate for CD28 which is

already outperformed by CTLA-4 in terms of binding with co-stimulatory molecules during the late or secondary immune response.[117] A phase I trial of anti-4-1BB agonist antibody has been done on patients with different cancers, showing good tolerance across various dose ranges.[118]

1.5.3. Lipid-based NP systems for cancer immunotherapy

Recent progress in cancer immunotherapy has excited the interest in nanoparticle systems to efficiently deliver tumor antigens and adjuvants to augment immune responses. Liposomes are biocompatible and have been used to incorporate TLR agonists by either lipid insertion of lipophylic molecules or charge-mediated complexation between cationic lipids and negatively charged agonists such as CpG and poly I:C.[119] However, simple unilamellar liposomes may be subjected to instability *in vivo*. One solution is to crosslink lipid layers by chemical bonds to increase both loading capability and stability. The previously developed ICMVs have efficiently and stably delivered protein antigens and the TLR-4 agonist MPLA, thus eliciting robust adaptive immune responses.[120-121] Particulate systems have also been applied to ICB-based therapies to relieve off-target toxicity caused by the current systemic administration route for these therapeutic antibodies. For example, intratumoral administration of anti-CTLA-4 antibody encapsulated in micron-size mesoporous silica enhanced anti-tumor efficacy, compared with soluble antibody injected intraperitoneally in a murine melanoma model, possibly

due to the controlled release of the antibody from an *in situ* depot.[122] An PD-L1 antibody can also be conjugated on the surfaces of platelets to hijack the inflammation-targeted delivery of platelet-bound ICBs for cancer adjuvant therapy.[123] Alternatively, targeted delivery of siRNA against PD-L1 has also been investigated with cationic lipoid and polymeric nanoparticles.[124-125] PD-L1 expressed on cancer cells were efficiently silenced by siRNA complexed with folic acid-modified polyethylenemine, resulting in enhanced *in vitro* T-cell activation.[125]

1.6. Immunogenic cell death (ICD)

Cell death is classically cataloged into two instances: necrosis which is accidental and pro-inflammatory, and apoptosis which is finely regulated and immunologically silent. The immunogenicity of dying cells mostly derives from the release of DAMPs, which are normally hidden in the interior of cells but can stimulate immune responses like PAMPs when exposed or released from dying cells.[126] Physiological apoptosis is immunologically tolerated due to phagocytosis, during which DAMPs are not released until their degradation in phagocytes. However, inflammatory responses can still occur if the apoptotic cells are not efficiently cleared and undergo secondary necrosis. In terms of cancer, recent studies revealed the immunogenicity of dying tumor cells under certain chemotherapies or radiotherapy. Although systemic administration of chemotherapeutics is generally immunosuppressive, *in situ* treatment with few types of chemodrugs

especially anthracyclines prove to induce ICD.[127-128] In addition, the abscopal effect observed during radiotherapy, i.e. regression of distant, non-irradiated tumors, is also caused by systemic immune responses elicited by the killing of primary tumor cells.[129]

1.6.1. Biomarkers of ICD

There are at least three identified markers of cancer cells undergoing ICD: the exposure of calreticulin (CRT), the release of ATP and high mobility group protein B1 (HMGB1).[130] CRT is normally located inside endoplasmic reticulum as a necessary chaperone protein for the binding of peptides to MHC-I complex, thus facilitating MHC-I presentation. However, it can be translocated on the cell surface during ICD and becomes an “eat-me” signal when recognized by CD91 on DCs.[131] Extracellular ATP not only acts as a “find-me” signal by recruiting DCs to dying cells, but also is a potentiator of CTL response. The binding of ATP to purinergic receptor P2RX7 on DCs activates NLRP3 inflammasome, thereby promoting maturation and secretion of IL-1β, which is necessary for the priming of IFN-γ-producing $CD8^+$ T cells.[132] HMGB1 is an intracellular DNA-binding protein that stabilizes nucleosomes and regulates transcription. The released HMGB1 can be recognized by TLR-4 in DCs, thereby promoting antigen presentation through inhibiting lysosomal degradation of engulfed antigens and promoting the secretion of IL-1β by DCs.[130]

1.6.2. ICD inducers

Anthracyclines such as doxorubicin, daunorubicin, and the anthracycline analog mitoxantrone were first identified as ICD inducers.[133] Several other chemodrugs such as oxaliplatin and cyclophosphamide, and γ-irradiation were also shown to induce ICD. Notably, except the anthracycline family, these chemodrugs are diverse in terms of their pharmacological mechanisms and chemical structure, making it difficult to predict ICD-inducing agents by simple structure-function relationship. For instance, although cisplatin belongs to the same category of chemotherapeutics as oxaliplatin, it is not an ICD inducer since it fails to elicit the apoptotic exposure of CRT.[134] One classification system has been proposed based on whether an ICD inducer directly acts on endoplasmic reticulum (ER),[135] which is the main site for the release of DAMPs during ICD. Most ICD inducers have focused effects on cytoplasm or nucleus, along with collateral effects on ER, and are classified as type I inducers. In contrast, type II inducers including Hypericin-based photodynamic therapy and Coxsackievirus B3 exert stress on ER as the focused effect. In addition to the release of DAMPs following ER stress, these agents differ in other pharmacological properties, such as killing potency of cancer cells and tumor inhibition, and potential inhibition of infiltrating anti-tumor immune cells.[135] Therefore the most efficient ICD inducer remains to be determined.

1.6.3. Exploiting ICD for cancer immunotherapy

The immune responses elicited by ICD and their potential for cancer immunotherapy is shown in **Figure 1.3**. Since the discovery of ICD, many clinical trials have been initiated to test the immune-mediated anti-tumor effects of ICD-inducing agents. Indeed, trials of GVAX may all involve the mechanisms of ICD since tumor cells are inactivated by γ-irradiation, which may increase the immunogenicity of those whole-cell vaccines. Chemodrug ICD inducers have been widely tested in combination with other cancer immunotherapies, such as vaccines, adoptive cell transfer, and checkpoint inhibitors.[136] ICD also suggests an alternative approach to formulating whole-cell cancer vaccines, in particular with the potential to achieve personalized cancer immunotherapy. In pre-clinical settings, mice vaccinated with anthracycline-treated tumor cells were highly protected from a following challenge of the homologous tumor, suggesting the successful elicitation of anti-tumor immunity.[127, 137] Furthermore, NP delivery systems have been investigated for the delivery of ICD inducers. Compared with the free drug, oxaliplatin delivered by PLGA-PEG micelles was shown to elicit higher ICD markers *in vitro* and stronger antigen-specific anti-tumor immunity *in vivo* in a pancreatic tumor model.[138] However, the therapeutic efficacy of these cancer vaccines was always limited, demonstrated by the slow progression of tumors instead of complete tumor regression.[127, 138-139] Therefore, this vaccine approach needs to be further potentiated either by adjuvants which can stimulate antigen presentation and CTL responses or by combining approaches that can reverse the immunosuppressive tumor microenvironment, e.g. the inhibition of

suppressive immune checkpoints. For example, PLGA microparticles have been employed to encapsulate doxorubicin and CpG and intratumorally injected to induce ICD.[140] Alternatively, doxorubicin-based *in situ* vaccination combined with anti-CTLA-4 and anti-OX40 antibodies has been shown to improve infiltration of T cells into distant tumors, leading to tumor eradication and increased survival.[141] Recently, a lipid-supported mesoporous silica nanoparticle system was used to co-deliver oxaliplatin and a small molecule inhibitor of IDO, and achieved dramatic tumor inhibition in an orthotropic pancreatic ductal adenocarcinoma model.[142]

1.7.Conclusion

Overall, various nanoparticle platforms have shown promise for vaccine delivery by increasing accumulation of loaded antigens in draining lymph nodes, enhancing activation of DCs by co-delivering antigens and adjuvants, and promoting cross-presentation of antigens by DCs thus eliciting both antigen-specific T cell and B cell immune responses. Nanoparticle systems composed of lipids and hyaluronic acid are biocompatible. A facile hybrid nanostructure design may offer a novel solution for efficient delivery of subunit protein antigens and molecular adjuvants, therefore promoting the clinical translation of vaccine candidates against emerging infectious diseases and cancer.

1.8. Figures and tables

Table 1.1. Characteristics of major TLRs and their ligands.

TLRs	Cellular localization	Types of ligand	Examples of ligand
TLR-1/2[a]	Plasma membrane	Triacyl lipopeptides, peptidoglycans	Pam3CSK4
TLR-2/6[a]	Plasma membrane	Diacyl lipopeptides, extracellular membrane proteins	HSPs, HMGB1, Zymosan
TLR-3	Endosome	dsRNA	Poly I:C, poly A:U
TLR-4	Plasma membrane/endosome[b]	LPS	MPLA, HMGB1, HSPs
TLR-5	Plasma membrane	Bacterial flagellum	Flagellin
TLR-7	Endosome	ssRNA and base analogs	Imiquimod, R848
TLR-8	Endosome	ssRNA and base analogs	R848
TLR-9	Endosome	ssDNA	CpG-ODN

a: Upon activation, TLR-1/2 and TLR-2/6 form heterodimers, respectively, whereas other TLRs form homodimers;

b: Upon activation, TLR-4 will be internalized from cell membrane into endosomes.

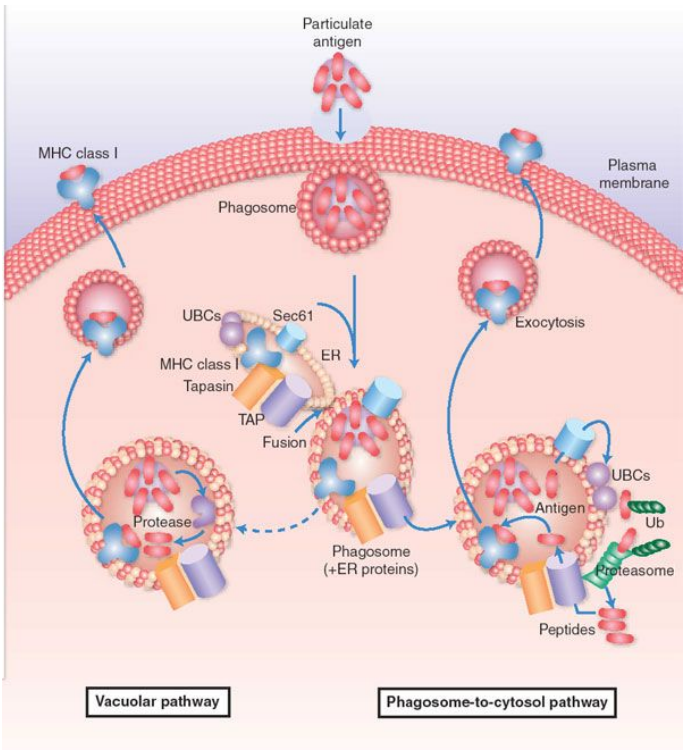

Figure 1.1. Pathways of antigen cross-presentation. Adapted from *Nat Immunol* 2003, *4* (10), 941-3.

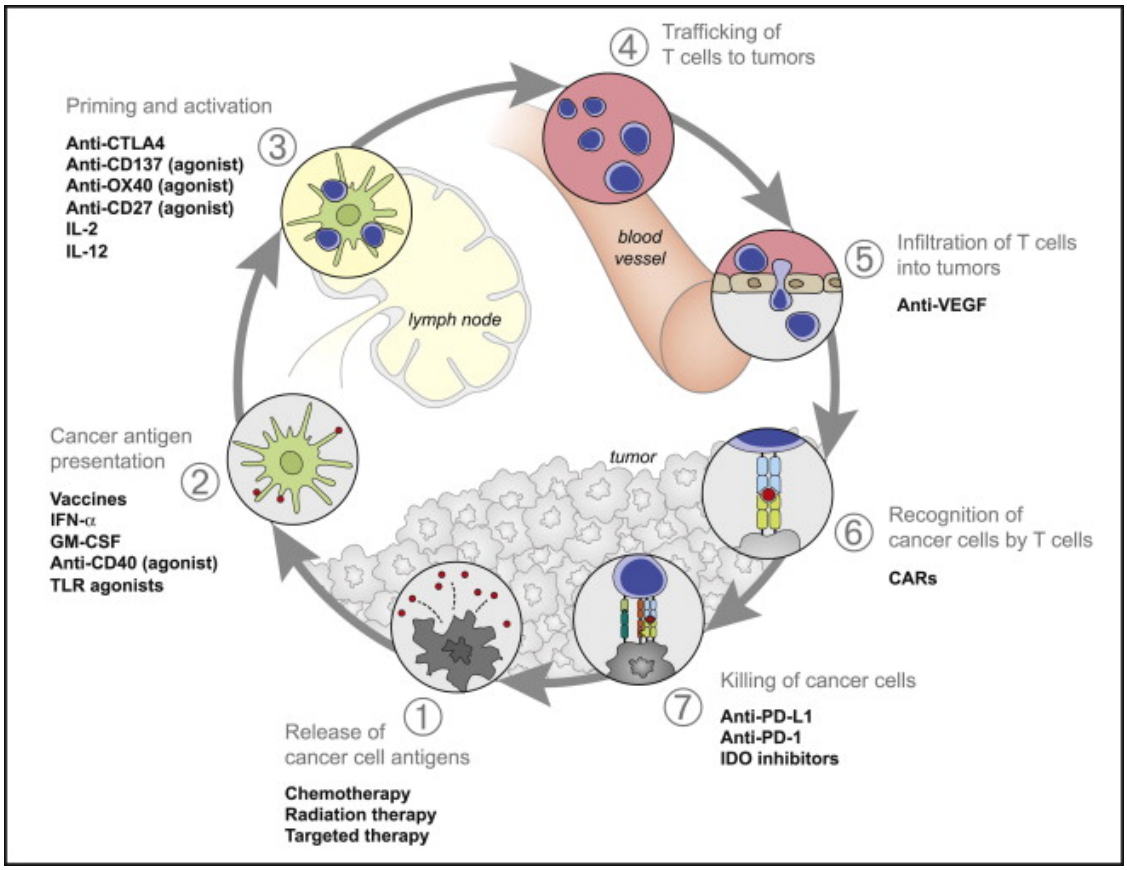

Figure 1.2. Therapeutic strategies targeting important steps in the cancer immunity circle. Adapted from *Immunity* 2013, *39* (1), 1-10.

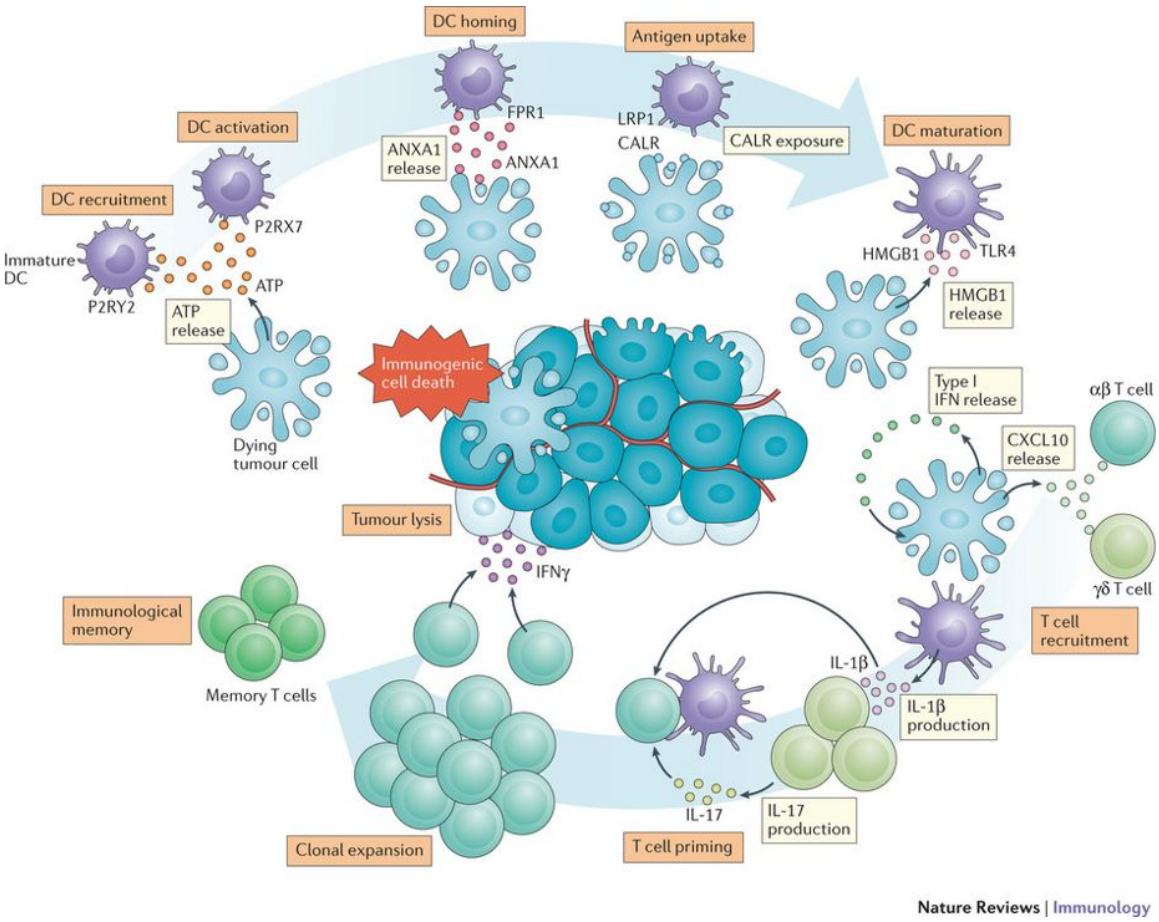

Figure 1.3. Immune responses elicited by following the initiation of immunogenic cell death. Adapted from *Nat Rev Immunol* 2017, *17* (2), 97-111.

1.9. References

1. Medzhitov, R.; Janeway, C., Jr. Innate immunity. *N Engl J Med* **2000,** *343* (5), 338-44.

2. Spits, H.; Di Santo, J. P. The expanding family of innate lymphoid cells: regulators and effectors of immunity and tissue remodeling. *Nat Immunol* **2011,** *12* (1), 21-7.

3. Akira, S., *et al.* Pathogen recognition and innate immunity. *Cell* **2006,** *124* (4), 783-801.

4. Takeuchi, O.; Akira, S. Pattern recognition receptors and inflammation. *Cell* **2010,** *140* (6), 805-20.

5. Dunn, G. P., *et al.* Cancer immunoediting: from immunosurveillance to tumor escape. *Nat Immunol* **2002,** *3* (11), 991-8.

6. Schreiber, R. D., *et al.* Cancer immunoediting: integrating immunity's roles in cancer suppression and promotion. *Science* **2011,** *331* (6024), 1565-70.

7. Jung, S., *et al.* In vivo depletion of CD11c+ dendritic cells abrogates priming of CD8+ T cells by exogenous cell-associated antigens. *Immunity* **2002,** *17* (2), 211-20.

8. Rock, K. L. The ins and outs of cross-presentation. *Nat Immunol* **2003,** *4* (10), 941-3.

9. Joffre, O. P., *et al.* Cross-presentation by dendritic cells. *Nat Rev Immunol* **2012,** *12* (8), 557-69.

10. Macpherson, A. J., *et al.* The immune geography of IgA induction and function. *Mucosal Immunol* **2008,** *1* (1), 11-22.

11. Kaczanowska, S., *et al.* TLR agonists: our best frenemy in cancer immunotherapy. *J Leukoc Biol* **2013,** *93* (6), 847-63.

12. Kawai, T.; Akira, S. The role of pattern-recognition receptors in innate immunity: update on Toll-like receptors. *Nat Immunol* **2010,** *11* (5), 373-84.

13. Vacchelli, E., *et al.* Trial watch: FDA-approved Toll-like receptor agonists for cancer therapy. *Oncoimmunology* **2012,** *1* (6), 894-907.

14. Steinhagen, F., *et al.* TLR-based immune adjuvants. *Vaccine* **2011,** *29* (17), 3341-55.

15. Napolitani, G., *et al.* Selected Toll-like receptor agonist combinations synergistically trigger a T helper type 1-polarizing program in dendritic cells. *Nat Immunol* **2005,** *6* (8), 769-76.

16. Duthie, M. S., *et al.* Use of defined TLR ligands as adjuvants within human vaccines. *Immunol Rev* **2011,** *239* (1), 178-96.

17. Sahdev, P., *et al.* Biomaterials for nanoparticle vaccine delivery systems. *Pharm Res* **2014,** *31* (10), 2563-82.

18. Jiang, D., *et al.* Hyaluronan as an immune regulator in human diseases. *Physiol Rev* **2011,** *91* (1), 221-64.

19. Fraser, J. R., *et al.* Hyaluronan: its nature, distribution, functions and turnover. *J Intern Med* **1997,** *242* (1), 27-33.

20. Knopf-Marques, H., *et al.* Hyaluronic Acid and Its Derivatives in Coating and Delivery Systems: Applications in Tissue Engineering, Regenerative Medicine and Immunomodulation. *Adv Healthc Mater* **2016,** *5* (22), 2841-2855.

21. Sherman, L., *et al.* Hyaluronate receptors: key players in growth, differentiation, migration and tumor progression. *Curr Opin Cell Biol* **1994,** *6* (5), 726-33.

22. Bollyky, P. L., *et al.* Th1 cytokines promote T-cell binding to antigen-presenting cells via enhanced hyaluronan production and accumulation at the immune synapse. *Cell Mol Immunol* **2010,** *7* (3), 211-20.

23. Teder, P., *et al.* Resolution of lung inflammation by CD44. *Science* **2002,** *296* (5565), 155-8.

24. Bollyky, P. L., *et al.* Cutting edge: high molecular weight hyaluronan promotes the suppressive effects of CD4+CD25+ regulatory T cells. *J Immunol* **2007,** *179* (2), 744-7.

25. Verheul, R. J., *et al.* Covalently stabilized trimethyl chitosan-hyaluronic acid nanoparticles for nasal and intradermal vaccination. *J Control Release* **2011,** *156* (1), 46-52.

26. Singh, M., *et al.* A novel bioadhesive intranasal delivery system for inactivated influenza vaccines. *J Control Release* **2001,** *70* (3), 267-76.

27. Matsuo, K., *et al.* A low-invasive and effective transcutaneous immunization system using a novel dissolving microneedle array for soluble and particulate antigens. *J Control Release* **2012,** *161* (1), 10-7.

28. Kim, K. S., *et al.* Noninvasive Transdermal Vaccination Using Hyaluronan Nanocarriers and Laser Adjuvant. *Adv Funct Mater* **2016,** *26* (15), 2512-2522.

29. Gennari, A., *et al.* Mannosylation Allows for Synergic (CD44/C-Type Lectin) Uptake of Hyaluronic Acid Nanoparticles in Dendritic Cells, but Only upon Correct Ligand Presentation. *Adv Healthc Mater* **2016,** *5* (8), 966-76.

30. Liang, X., *et al.* Nanoparticles with CD44 Targeting and ROS Triggering Properties as Effective in Vivo Antigen Delivery System. *Mol Pharm* **2018,** *15* (2), 508-518.

31. Sestak, J., *et al.* Single-step grafting of aminooxy-peptides to hyaluronan: a simple approach to multifunctional therapeutics for experimental autoimmune encephalomyelitis. *J Control Release* **2013,** *168* (3), 334-40.

32. Chittasupho, C., *et al.* Hyaluronic acid graft polymers displaying peptide antigen modulate dendritic cell response in vitro. *Mol Pharm* **2014,** *11* (1), 367-73.

33. Yoo, E., *et al.* Hyaluronic Acid Conjugates of TLR7/8 Agonists for Targeted Delivery to Secondary Lymphoid Tissue. *Bioconjug Chem* **2018,** *29* (8), 2741-2754.

34. Nune, S. K., *et al.* Advances in lymphatic imaging and drug delivery. *Adv Drug Deliv Rev* **2011,** *63* (10-11), 876-85.

35. Swartz, M. A., *et al.* Engineering approaches to immunotherapy. *Sci Transl Med* **2012,** *4* (148), 148rv9.

36. Irvine, D. J., *et al.* Synthetic Nanoparticles for Vaccines and Immunotherapy. *Chem Rev* **2015,** *115* (19), 11109-46.

37. Silva, J. M., *et al.* Immune system targeting by biodegradable nanoparticles for cancer vaccines. *J Control Release* **2013,** *168* (2), 179-99.

38. Fan, Y.; Moon, J. J. Nanoparticle Drug Delivery Systems Designed to Improve Cancer Vaccines and Immunotherapy. *Vaccines (Basel)* **2015,** *3* (3), 662-85.

39. Irvine, D. J., *et al.* Engineering synthetic vaccines using cues from natural immunity. *Nat Mater* **2013,** *12* (11), 978-90.

40. Fifis, T., *et al.* Size-dependent immunogenicity: therapeutic and protective properties of nano-vaccines against tumors. *J Immunol* **2004,** *173* (5), 3148-54.

41. Mariani, G., *et al.* Radioguided sentinel lymph node biopsy in breast cancer surgery. *J Nucl Med* **2001,** *42* (8), 1198-215.

42. Holmgren, J.; Czerkinsky, C. Mucosal immunity and vaccines. *Nat Med* **2005,** *11* (4 Suppl), S45-53.

43. Neutra, M. R.; Kozlowski, P. A. Mucosal vaccines: the promise and the challenge. *Nat Rev Immunol* **2006,** *6* (2), 148-58.

44. Li, A. V., *et al.* Generation of effector memory T cell-based mucosal and systemic immunity with pulmonary nanoparticle vaccination. *Sci Transl Med* **2013,** *5* (204), 204ra130.

45. Nochi, T., *et al.* Nanogel antigenic protein-delivery system for adjuvant-free intranasal vaccines. *Nat Mater* **2010,** *9* (7), 572-8.

46. Davitt, C. J.; Lavelle, E. C. Delivery strategies to enhance oral vaccination against enteric infections. *Adv Drug Deliv Rev* **2015,** *91*, 52-69.

47. Marasini, N., *et al.* Oral delivery of nanoparticle-based vaccines. *Expert Rev Vaccines* **2014,** *13* (11), 1361-76.

48. Oh, J. Z., *et al.* TLR7 enables cross-presentation by multiple dendritic cell subsets through a type I IFN-dependent pathway. *Blood* **2011,** *118* (11), 3028-38.

49. Mandraju, R., *et al.* Differential ability of surface and endosomal TLRs to induce CD8 T cell responses in vivo. *J Immunol* **2014,** *192* (9), 4303-15.

50. de Titta, A., *et al.* Nanoparticle conjugation of CpG enhances adjuvancy for cellular

immunity and memory recall at low dose. *Proc Natl Acad Sci U S A* **2013,** *110* (49), 19902-7.

51. Wilson, J. T., *et al.* pH-Responsive nanoparticle vaccines for dual-delivery of antigens and immunostimulatory oligonucleotides. *ACS Nano* **2013,** *7* (5), 3912-25.

52. Zhang, P., *et al.* Polyelectrolyte Multilayers Assembled Entirely from Immune Signals on Gold Nanoparticle Templates Promote Antigen-Specific T Cell Response. *ACS Nano* **2015,** *9* (6), 6465-77.

53. Silva, J. M., *et al.* In vivo delivery of peptides and Toll-like receptor ligands by mannose-functionalized polymeric nanoparticles induces prophylactic and therapeutic anti-tumor immune responses in a melanoma model. *J Control Release* **2015,** *198*, 91-103.

54. Fox, C. B., *et al.* A nanoliposome delivery system to synergistically trigger TLR4 AND TLR7. *J Nanobiotechnology* **2014,** *12*, 17.

55. Pradhan, P., *et al.* The effect of combined IL10 siRNA and CpG ODN as pathogen-mimicking microparticles on Th1/Th2 cytokine balance in dendritic cells and protective immunity against B cell lymphoma. *Biomaterials* **2014,** *35* (21), 5491-504.

56. Xu, Z., *et al.* Nanoparticle-delivered transforming growth factor-beta siRNA enhances vaccination against advanced melanoma by modifying tumor microenvironment. *ACS Nano* **2014,** *8* (4), 3636-45.

57. Sorkin, A.; Von Zastrow, M. Signal transduction and endocytosis: close encounters of many kinds. *Nat Rev Mol Cell Biol* **2002,** *3* (8), 600-14.

58. Yuba, E., *et al.* Dextran derivative-based pH-sensitive liposomes for cancer immunotherapy. *Biomaterials* **2014,** *35* (9), 3091-101.

59. Keller, S., *et al.* Neutral polymer micelle carriers with pH-responsive, endosome-releasing activity modulate antigen trafficking to enhance CD8(+) T cell responses. *J Control Release* **2014,** *191*, 24-33.

60. Scott, E. A., *et al.* Dendritic cell activation and T cell priming with adjuvant- and antigen-loaded oxidation-sensitive polymersomes. *Biomaterials* **2012,** *33* (26), 6211-9.

61. Nakamura, T., *et al.* Octaarginine-modified liposomes enhance cross-presentation by promoting the C-terminal trimming of antigen peptide. *Mol Pharm* **2014,** *11* (8), 2787-95.

62. Ahn, S., *et al.* Gold nanoparticles displaying tumor-associated self-antigens as a potential vaccine for cancer immunotherapy. *Adv Healthc Mater* **2014,** *3* (8), 1194-9.

63. Feodorova, V. A.; Motin, V. L. Plague vaccines: current developments and future perspectives. *Emerg Microbes Infect* **2012,** *1* (11), e36.

64. Webb, R. P.; Smith, L. A. What next for botulism vaccine development? *Expert Rev Vaccines* **2013,** *12* (5), 481-92.

65. Isherwood, K. E., *et al.* Vaccination strategies for Francisella tularensis. *Adv Drug Deliv Rev* **2005,** *57* (9), 1403-14.

66. Lukaszewski, R. A., *et al.* Pathogenesis of Yersinia pestis infection in BALB/c mice: effects on host macrophages and neutrophils. *Infect Immun* **2005,** *73* (11), 7142-50.

67. Sebbane, F., *et al.* Kinetics of disease progression and host response in a rat model of bubonic plague. *Am J Pathol* **2005,** *166* (5), 1427-39.

68. Du, Z.; Wang, X. Pathology and Pathogenesis of Yersinia pestis. *Adv Exp Med Biol* **2016,** *918*, 193-222.

69. Rosenzweig, J. A., *et al.* Progress on plague vaccine development. *Appl Microbiol Biotechnol* **2011,** *91* (2), 265-86.

70. Inglesby, T. V., *et al.* Plague as a biological weapon: medical and public health management. Working Group on Civilian Biodefense. *JAMA* **2000,** *283* (17), 2281-90.

71. Williamson, E. D.; Oyston, P. C. Protecting against plague: towards a next-generation vaccine. *Clin Exp Immunol* **2013,** *172* (1), 1-8.

72. Eyles, J. E., *et al.* Analysis of local and systemic immunological responses after intra-tracheal, intra-nasal and intra-muscular administration of microsphere co-encapsulated Yersinia pestis sub-unit vaccines. *Vaccine* **1998,** *16* (20), 2000-9.

73. Uppada, J. B., *et al.* Humoral immune responses and protective efficacy of sequential B- and T-cell epitopes of V antigen of Yersinia pestis by intranasal immunization in

microparticles. *Med Microbiol Immunol* **2009,** *198* (4), 247-56.

74. Huang, S. S., *et al.* Development of Yersinia pestis F1 antigen-loaded microspheres vaccine against plague. *Int J Nanomedicine* **2014,** *9*, 813-22.

75. Ulery, B. D., *et al.* Design of a protective single-dose intranasal nanoparticle-based vaccine platform for respiratory infectious diseases. *PLoS One* **2011,** *6* (3), e17642.

76. Ross, K. A., *et al.* Lung deposition and cellular uptake behavior of pathogen-mimicking nanovaccines in the first 48 hours. *Adv Healthc Mater* **2014,** *3* (7), 1071-7.

77. Gregory, A. E., *et al.* Conjugation of Y. pestis F1-antigen to gold nanoparticles improves immunogenicity. *Vaccine* **2012,** *30* (48), 6777-82.

78. Fischer, N. O., *et al.* Colocalized delivery of adjuvant and antigen using nanolipoprotein particles enhances the immune response to recombinant antigens. *J Am Chem Soc* **2013,** *135* (6), 2044-7.

79. Haughney, S. L., *et al.* Effect of nanovaccine chemistry on humoral immune response kinetics and maturation. *Nanoscale* **2014,** *6* (22), 13770-8.

80. Geisbert, T. W., *et al.* Pathogenesis of Ebola hemorrhagic fever in cynomolgus macaques: evidence that dendritic cells are early and sustained targets of infection. *Am J Pathol* **2003,** *163* (6), 2347-70.

81. Sullivan, N., *et al.* Ebola virus pathogenesis: implications for vaccines and therapies. *J Virol* **2003,** *77* (18), 9733-7.

82. de La Vega, M. A., *et al.* Ebolavirus Evolution: Past and Present. *PLoS Pathog* **2015,** *11* (11), e1005221.

83. Geisbert, T. W., *et al.* Prospects for immunisation against Marburg and Ebola viruses. *Rev Med Virol* **2010,** *20* (6), 344-57.

84. Marzi, A., *et al.* Vaccines. An Ebola whole-virus vaccine is protective in nonhuman primates. *Science* **2015,** *348* (6233), 439-42.

85. Choi, J. H.; Croyle, M. A. Emerging targets and novel approaches to Ebola virus

prophylaxis and treatment. *BioDrugs* **2013,** *27* (6), 565-83.

86. Henao-Restrepo, A. M., *et al.* Efficacy and effectiveness of an rVSV-vectored vaccine expressing Ebola surface glycoprotein: interim results from the Guinea ring vaccination cluster-randomised trial. *Lancet* **2015,** *386* (9996), 857-66.

87. Jones, S. M., *et al.* Live attenuated recombinant vaccine protects nonhuman primates against Ebola and Marburg viruses. *Nat Med* **2005,** *11* (7), 786-90.

88. Mire, C. E., *et al.* Single-dose attenuated Vesiculovax vaccines protect primates against Ebola Makona virus. *Nature* **2015,** *520* (7549), 688-691.

89. Warfield, K. L.; Aman, M. J. Advances in virus-like particle vaccines for filoviruses. *J Infect Dis* **2011,** *204 Suppl 3*, S1053-9.

90. Warfield, K. L., *et al.* Ebola virus-like particles protect from lethal Ebola virus infection. *Proc Natl Acad Sci U S A* **2003,** *100* (26), 15889-94.

91. Warfield, K. L., *et al.* Ebola virus-like particle-based vaccine protects nonhuman primates against lethal Ebola virus challenge. *J Infect Dis* **2007,** *196 Suppl 2*, S430-7.

92. Ayithan, N., *et al.* Virus-like particles activate type I interferon pathways to facilitate post-exposure protection against Ebola virus infection. *PLoS One* **2015,** *10* (2), e0118345.

93. Martins, K. A., *et al.* Toll-like receptor agonist augments virus-like particle-mediated protection from Ebola virus with transient immune activation. *PLoS One* **2014,** *9* (2), e89735.

94. Martins, K., *et al.* Cross-protection conferred by filovirus virus-like particles containing trimeric hybrid glycoprotein. *Viral Immunol* **2015,** *28* (1), 62-70.

95. Rao, M., *et al.* Cytotoxic T lymphocytes to Ebola Zaire virus are induced in mice by immunization with liposomes containing lipid A. *Vaccine* **1999,** *17* (23-24), 2991-8.

96. Rao, M., *et al.* Induction of immune responses in mice and monkeys to Ebola virus after immunization with liposome-encapsulated irradiated Ebola virus: protection in mice requires CD4(+) T cells. *J Virol* **2002,** *76* (18), 9176-85.

97. Starnes, C. O. Coley's toxins in perspective. *Nature* **1992,** *357* (6373), 11-2.

98. Mellman, I., *et al.* Cancer immunotherapy comes of age. *Nature* **2011,** *480* (7378), 480-9.

99. Couzin-Frankel, J. Breakthrough of the year 2013. Cancer immunotherapy. *Science* **2013,** *342* (6165), 1432-3.

100. Chen, D. S.; Mellman, I. Oncology meets immunology: the cancer-immunity cycle. *Immunity* **2013,** *39* (1), 1-10.

101. Downey, S. G., *et al.* Prognostic factors related to clinical response in patients with metastatic melanoma treated by CTL-associated antigen-4 blockade. *Clin Cancer Res* **2007,** *13* (22 Pt 1), 6681-8.

102. Topalian, S. L., *et al.* Safety, activity, and immune correlates of anti-PD-1 antibody in cancer. *N Engl J Med* **2012,** *366* (26), 2443-54.

103. Wang, C., *et al.* Toll-like receptor 3 agonist complexed with cationic liposome augments vaccine-elicited antitumor immunity by enhancing TLR3-IRF3 signaling and type I interferons in dendritic cells. *Vaccine* **2012,** *30* (32), 4790-9.

104. Gross, B. P., *et al.* A therapeutic microparticle-based tumor lysate vaccine reduces spontaneous metastases in murine breast cancer. *AAPS J* **2014,** *16* (6), 1194-203.

105. Ali, O. A., *et al.* Infection-mimicking materials to program dendritic cells in situ. *Nat Mater* **2009,** *8* (2), 151-8.

106. Fang, R. H., *et al.* Cancer cell membrane-coated nanoparticles for anticancer vaccination and drug delivery. *Nano Lett* **2014,** *14* (4), 2181-8.

107. Kroll, A. V., *et al.* Nanoparticulate Delivery of Cancer Cell Membrane Elicits Multiantigenic Antitumor Immunity. *Adv Mater* **2017,** *29* (47).

108. Hodi, F. S., *et al.* Improved survival with ipilimumab in patients with metastatic melanoma. *N Engl J Med* **2010,** *363* (8), 711-23.

109. Robert, C., *et al.* Pembrolizumab versus Ipilimumab in Advanced Melanoma. *N Engl J Med* **2015,** *372* (26), 2521-32.

110. Garon, E. B., *et al.* Pembrolizumab for the treatment of non-small-cell lung cancer. *N Engl J Med* **2015,** *372* (21), 2018-28.

111. Wolchok, J. D., *et al.* Nivolumab plus ipilimumab in advanced melanoma. *N Engl J Med* **2013,** *369* (2), 122-33.

112. Croft, M. Control of immunity by the TNFR-related molecule OX40 (CD134). *Annu Rev Immunol* **2010,** *28*, 57-78.

113. Curti, B. D., *et al.* OX40 is a potent immune-stimulating target in late-stage cancer patients. *Cancer Res* **2013,** *73* (24), 7189-7198.

114. Moran, A. E., *et al.* The TNFRs OX40, 4-1BB, and CD40 as targets for cancer immunotherapy. *Curr Opin Immunol* **2013,** *25* (2), 230-7.

115. Xiao, X., *et al.* New insights on OX40 in the control of T cell immunity and immune tolerance in vivo. *J Immunol* **2012,** *188* (2), 892-901.

116. Lee, S. W., *et al.* Functional dichotomy between OX40 and 4-1BB in modulating effector CD8 T cell responses. *J Immunol* **2006,** *177* (7), 4464-72.

117. Cheuk, A. T., *et al.* Role of 4-1BB:4-1BB ligand in cancer immunotherapy. *Cancer Gene Ther* **2004,** *11* (3), 215-26.

118. Vinay, D. S.; Kwon, B. S. Immunotherapy of cancer with 4-1BB. *Mol Cancer Ther* **2012,** *11* (5), 1062-70.

119. Zaks, K., *et al.* Efficient immunization and cross-priming by vaccine adjuvants containing TLR3 or TLR9 agonists complexed to cationic liposomes. *J Immunol* **2006,** *176* (12), 7335-45.

120. Moon, J. J., *et al.* Interbilayer-crosslinked multilamellar vesicles as synthetic vaccines for potent humoral and cellular immune responses. *Nat Mater* **2011,** *10* (3), 243-51.

121. Moon, J. J., *et al.* Enhancing humoral responses to a malaria antigen with nanoparticle vaccines that expand Tfh cells and promote germinal center induction. *Proc Natl Acad Sci U S A* **2012,** *109* (4), 1080-5.

122. Lei, C., *et al.* Local release of highly loaded antibodies from functionalized nanoporous support for cancer immunotherapy. *J Am Chem Soc* **2010,** *132* (20), 6906-7.

123. Wang, C., *et al.* In situ activation of platelets with checkpoint inhibitors for post-surgical cancer immunotherapy. *Nat Biomed Eng* **2017,** *1* (2).

124. Roeven, M. W., *et al.* Efficient nontoxic delivery of PD-L1 and PD-L2 siRNA into dendritic cell vaccines using the cationic lipid SAINT-18. *J Immunother* **2015,** *38* (4), 145-54.

125. Teo, P. Y., *et al.* Ovarian cancer immunotherapy using PD-L1 siRNA targeted delivery from folic acid-functionalized polyethylenimine: strategies to enhance T cell killing. *Adv Healthc Mater* **2015,** *4* (8), 1180-9.

126. Kono, H.; Rock, K. L. How dying cells alert the immune system to danger. *Nat Rev Immunol* **2008,** *8* (4), 279-89.

127. Casares, N., *et al.* Caspase-dependent immunogenicity of doxorubicin-induced tumor cell death. *J Exp Med* **2005,** *202* (12), 1691-701.

128. Fucikova, J., *et al.* Human tumor cells killed by anthracyclines induce a tumor-specific immune response. *Cancer Res* **2011,** *71* (14), 4821-33.

129. Vacchelli, E., *et al.* Trial Watch: Anticancer radioimmunotherapy. *Oncoimmunology* **2013,** *2* (9), e25595.

130. Kepp, O., *et al.* Molecular determinants of immunogenic cell death elicited by anticancer chemotherapy. *Cancer Metastasis Rev* **2011,** *30* (1), 61-9.

131. Kroemer, G., *et al.* Immunogenic cell death in cancer therapy. *Annu Rev Immunol* **2013,** *31*, 51-72.

132. Ghiringhelli, F., *et al.* Activation of the NLRP3 inflammasome in dendritic cells induces IL-1beta-dependent adaptive immunity against tumors. *Nat Med* **2009,** *15* (10), 1170-8.

133. Dudek, A. M., *et al.* Inducers of immunogenic cancer cell death. *Cytokine Growth Factor Rev* **2013,** *24* (4), 319-33.

134. Galluzzi, L., *et al.* The secret ally: immunostimulation by anticancer drugs. *Nat Rev Drug Discov* **2012,** *11* (3), 215-33.

135. Krysko, D. V., *et al.* Immunogenic cell death and DAMPs in cancer therapy. *Nat Rev Cancer* **2012,** *12* (12), 860-75.

136. Vacchelli, E., *et al.* Trial watch: Chemotherapy with immunogenic cell death inducers. *Oncoimmunology* **2012,** *1* (2), 179-188.

137. Apetoh, L., *et al.* Toll-like receptor 4-dependent contribution of the immune system to anticancer chemotherapy and radiotherapy. *Nat Med* **2007,** *13* (9), 1050-9.

138. Zhao, X., *et al.* Inducing enhanced immunogenic cell death with nanocarrier-based drug delivery systems for pancreatic cancer therapy. *Biomaterials* **2016,** *102*, 187-97.

139. Tongu, M., *et al.* Immunogenic chemotherapy with cyclophosphamide and doxorubicin against established murine carcinoma. *Cancer Immunol Immunother* **2010,** *59* (5), 769-77.

140. Makkouk, A., *et al.* Biodegradable microparticles loaded with doxorubicin and CpG ODN for in situ immunization against cancer. *AAPS J* **2015,** *17* (1), 184-93.

141. Makkouk, A., *et al.* Three steps to breaking immune tolerance to lymphoma: a microparticle approach. *Cancer Immunol Res* **2015,** *3* (4), 389-98.

142. Lu, J., *et al.* Nano-enabled pancreas cancer immunotherapy using immunogenic cell death and reversing immunosuppression. *Nat Commun* **2017,** *8* (1), 1811.

Chapter 2: Lipid-polymer hybrid nanoparticles for intranasal delivery of subunit vaccines

2.1. Abstract

To improve mucosal delivery of subunit antigens, we here report the development of a new cationic liposome-hyaluronic acid (HA) hybrid nanoparticle (NP) system and present our characterization of these NPs as an intranasal vaccine platform using a model antigen and F1-V, a candidate recombinant protein antigen for *Yersinia pestis*, the causative agent of plague. Incubation of cationic liposomes composed of DOTAP and DOPE with anionic HA biopolymer led to efficient ionic complexation and formation of homogenous liposome-polymer hybrid NPs, as evidenced by fluorescence resonance energy transfer, dynamic light scattering, and nanoparticle tracking analyses. Incorporation of cationic liposomes with thiolated HA allowed for facile surface decoration of NPs with thiol-PEG, resulting in the formation of DOTAP/HA core-PEG shell nanostructures. These NPs, termed DOTAP-HA NPs, exhibited improved colloidal stability and prolonged antigen release. In addition, cytotoxicity associated with DOTAP liposomes (LC_{50} ~0.2 mg/ml) was significantly reduced by at least 20 fold with DOTAP-HA NPs (LC_{50} > 4 mg/ml), as

measured with bone marrow dendritic cells (BMDCs). Furthermore, NPs co-loaded with ovalbumin (OVA) and a molecular adjuvant, monophosphoryl lipid A (MPLA), promoted BMDC maturation and up-regulation of co-stimulatory markers, including CD40, CD86, and MHC-II, and C57BL/6 mice vaccinated with NPs via intranasal route generated robust OVA-specific $CD8^+$ T cell and antibody responses. Importantly, intranasal vaccination with NPs co-loaded with F1-V and MPLA induced potent humoral immune responses with 11-, 23-, and 15-fold increases in F1-V-specific total IgG, IgG_1, and IgG_{2c} titers in immune sera by day 77, respectively, and induced balanced Th1/Th2 humoral immune responses, compared with the lack of sero-conversion in mice immunized with the equivalent doses of soluble F1-V vaccine. Overall, these results suggest that liposome-polymer hybrid NPs may serve as a promising vaccine delivery platform for intranasal vaccination against *Y. pestis* and other infectious pathogens.

2.2. Introduction

Synthetic nanoparticles (NPs) are promising delivery systems for subunit vaccines composed of peptides, recombinant proteins, or DNA.[1-3] Advantages of particulate vaccines include efficient encapsulation of antigens, shielding of antigens from rapid enzymatic degradation, and ability to co-deliver antigens with molecular adjuvants to antigen-presenting cells (APCs), thus promoting cellular and humoral immune responses.[3] Among particulate vaccine delivery systems, liposomes of various lipid

compositions have been widely investigated as potential vaccine carriers. In particular, cationic liposomes composed of 1,2-dioleoyl-3-trimethylammonium-propane (DOTAP) have been extensively studied as they can readily form nano-complexes with anionic peptides, proteins, and plasmid DNA encoding for antigens and generate T and B cell immune responses *in vivo*.[4-8] Despite significant advances made in this field, there are still several major challenges remaining for liposomal vaccines, including cytotoxicity of cationic liposomes that can negatively impact immune responses at high concentrations as well as their *in vivo* instability for delivery of biomacromolecules.[6-10] We previously addressed some of these issues by developing a new lipid-based NP system formed by divalent cation-induced liposomal fusion into multilamellar vesicles and subsequent cross-linking of opposing lipid layers via maleimide-thiol reaction.[11] The resulting NPs released cargo protein in a stable manner and elicited robust humoral and cellular immune responses.[11-13] As an alternative approach to producing stable vaccine delivery systems, here we aimed to synthesize lipid-biopolymer hybrid NPs by exploiting ionic charge interactions between liposomes and hyaluronic acid (HA), which is a biodegradable polymer that has been shown to form complexes with liposomes [14] and investigated as a vaccine delivery agent.[15-17] Specifically, we utilized ionic complexation between cationic DOTAP-based liposomes and anionic HA-based biopolymers to form DOTAP-HA hybrid NPs, which were then surface-decorated with poly(ethylene glycol) (PEG), resulting in the formation of DOTAP-HA/core PEG-shell NPs. We report here

that these NPs may serve as a promising vaccine delivery platform for intranasal vaccination.

Yersinia pestis, a causative agent of pneumonic plague, is a Category A bioterrorism bacterial agent that can be easily transmitted through pulmonary inhalation, potentially causing a death rate near 100% within a week of infection.[18] However, there are currently no available vaccine products against pneumonic plague. Therefore, it is of high priority to develop a protective plague vaccine. For vaccination against *Y. pestis*, intranasal route of immunization is attractive due to the ease of vaccine administration and rapid deployment in the time of imminent biological threat. In addition, the nasal cavity is characterized by highly permeable nasal epithelium for the absorption of biomolecules and high frequency of immune cells within nasal-associated lymphoid tissues.[19] Thus, nasal vaccination against *Y. pestis* may drive the induction of local mucosal immune responses in the airway to prevent initial pneumonic infection while simultaneously eliciting systemic immune responses to inhibit transmission of bacterial infection. In particular, F1-V, a recombinant fusion protein of fraction 1 pilus and LcrV antigen from *Y. pestis*, has been demonstrated to be a promising candidate for plague vaccine in a number of previous studies.[18, 20] In addition, F1-V in combination with various types of adjuvants [21] or nanocarriers [22-23] have been shown to promote prophylactic humoral immune responses against *Y. pestis*.

In this study, we report the development of a new liposome-polymer hybrid NP

system and our initial characterization of these NPs as an intranasal vaccine platform using a model antigen as well as F1-V. We show that DOTAP liposomes can be readily incorporated with thiolated HA (HA-SH) by promoting ionic complexation between DOTAP and HA-SH. The resulting DOTAP-HA NPs were further stabilized by reacting the HA-SH layer on the outer shell with thiolated PEG (PEG-SH), generating stable DOTAP/HA core-PEG shell NPs (**Figure 2.1**). Importantly, cytotoxicity of DOTAP liposomes in BMDCs (LC50 ~0.2 mg/ml) was significantly reduced by at least 20 fold (LD50 > 4 mg/ml) for DOTAP-HA NPs. Toll-like receptor (TLR) 4 agonist, MPLA,[24] was chosen as a molecular adjuvant for both the model antigen OVA and F1-V. DOTAP-HA hybrid NPs co-loaded with antigens and MPLA promoted maturation of BMDCs *in vitro* and effectively stimulated antigen-specific cellular and humoral immune responses *in vivo* after intranasal vaccination, suggesting their potency as a promising nasal vaccine platform against infectious pathogens.

2.3. Materials and methods

2.3.1. Reagents

Lipids including 1,2-dioleoyl-3-trimethylammonium propane (DOTAP), 1,2-dioleoyl-sn-glycero-3-phosphoethanolamine (DOPE), nitrobenzoxadiazole (NBD)-labeled DOPE (DOPE-NBD), rhodamine (Rhod)-labeled DOPE (DOPE-Rhod), and MPLA were all purchased from Avanti Polar Lipids (Alabaster, AL). Sodium

hyaluronate (HA, average Mw = 29 kD) and 2 kDa PEG-SH were from Lifecore Biomedical (Chaska, MN) and Laysan Bio (Arab, AL), respectively. L-cysteine, N-(3-Dimethylaminopropyl)-N'-ethylcarbodiimide hydrochloride (EDC), N-hydroxysuccinimide (NHS), 5,5'-Dithiobis(2-nitrobenzoic acid) (DTNB) and chloramine T were obtained from Sigma-Aldrich (St. Louis, MO). Ovalbumin (OVA) and F1-V were obtained from Worthington (Lakewood, NJ) and NIH BEI Resources (Manassas, VA), respectively. RPMI 1640 media, fetal bovine serum (FBS), penicillin-streptomycin, β-mercaptoethanol, ACK lysis buffer and Texas Red N-hydroxysuccinimide ester were from Life Technologies (Grand Island, NY). Granulocyte macrophage colony stimulating factor (GM-CSF) was the product of PeproTech (Rocky Hill, NJ). Rat anti-mouse CD16/32, CD86-PE, CD40-APC, and MHC Class II-FITC were from eBioscience (San Diego, CA). Rat anti-mouse CD8-APC, hamster anti-mouse CD11c-PECy7 were from BD Bioscience (San Jose, CA). iTAg tetramer/PE-H-2 Kb OVA (SIINFEKL) was purchased from MBL International (Woburn, MA). Zymax Rabbit anti-mouse IgG and HRP Rat anti-mouse IgG_1 were purchased from Invitrogen (Grand Island, NY), and Goat anti-mouse IgG_{2c} was from Southern Biotech (Birmingham, AL). 3.3',5.5'-tetramethylbenzidine (TMB) substrate solution was purchased from Thermo Scientific (Waltham, MA).

2.3.2. Thiolation of hyaluronic acid

Thiolated HA was synthesized by conjugation of HA with L-cysteine via EDC/NHS reaction. In specific, 200 mg HA was dissolved by 20 ml deionized water containing 200 mM EDC and NHS. The pH was then adjusted to 5 with 1 M HCl. The reaction mixture was stirred for 0.5 h, followed by addition of 400 mg L-cysteine and stirred at room temperature for another 4 h. The thiolated HA (HA-SH) was purified by dialysis (MWCO 10 kDa) against dilute HCl (pH 5), 0.9% NaCl in dilute HCl, and then dilute HCl again. Finally, the dialyzed sample was lyophilized and stored at -80 ^{o}C. The free thiol content of HA-SH was measured by Ellman's assay as previously reported.[16-17]

2.3.3. Preparation of liposomes and liposome-polymer hybrid NPs

DOTAP and DOPE (each 0.5 mg) were dissolved in chloroform, followed by solvent evaporation to form lipid film. The dried lipid film was hydrated with 0.2 ml deionized water at room temperature for 1 h with intermittent vortex, followed by the addition of varying amounts of HA or HA-SH and incubation for 1 h. Next, 0.1 ml PEG-SH solution (5 mg/ml in 10 mM HEPES buffer, pH 7.4) was added and the pH was adjusted to 8 with 1 M sodium hydroxide. Then 50 µl of chloramine T solution (50 mM in HEPES buffer, pH 7.4) was added to induce thiol-mediated conjugation of PEG-SH onto HA-SH. After 1 h incubation at room temperature, the resulting particles were collected by centrifugation at 20,000 × g for 10 min, washed with PBS, resuspended in 0.2 ml PBS, briefly sonicated,

and stored at 4 ^{o}C till use. In some cases, the initial lipid film was prepared along with 2.9 µg of MPLA and hydrated with a solution containing 200 µg of OVA to synthesize OVA/MPLA-loaded DOTAP-HA NPs. Since MPLA with hydrophobic acyl chains has been previously shown to be efficiently incorporated into liposomes and lipid-based nanoparticles via self-assembly into lipid membranes,[11, 25] we assumed 100% loading efficiency for MPLA in DOTAP-HA NPs. The encapsulation efficiency of OVA in NPs was determined to be 11 ± 1.8%, as assessed by densitometry measurement of particle samples after running the samples through SDS-PAGE, followed by Coomassie staining.

Particle samples were diluted with deionized water or PBS, followed by size and zeta potential measurements by dynamic light scattering (DLS, Zetasizer Nano ZSP, Malvern, UK). In addition, detailed NP size distribution and NP concentration were obtained by nanoparticle tracking analysis (NTA, NanoSight NS300, Malvern, UK) as reported previously.[26] PEG content in the final particle was determined by complexation of PEG with barium iodide as reported previously.[27-28] Briefly, 200 µl of 5% (w/v) barium chloride dissolved in 1 M hydrochloride acid and 100 µl of iodide solution containing 0.05 M iodine and 2% (w/v) potassium iodide were added to 800 µl of ×200 diluted particle suspension, followed by incubation at room temperature for 15 min. Absorbance at 535 nm was measured for PEG quantification. The dry weight of particles after lyophilization was measured to report the PEG content in µmol/g of particles. For the *in vitro* release study, OVA was labeled with the Texas Red N-hydroxysuccinimide ester and

encapsulated into DOTAP-HA NPs. NPs were resuspended in phenol red-free RPMI 1640 supplemented with 10% FBS, loaded in dialysis cassettes (MWCO 300 kDa), and incubated at 37 ^{o}C under constant shaking. Release media were collected at pre-determined time points during three weeks, followed by fluorescence measurement at excitation and emission wavelengths of 585/615 nm using a microplate fluorometer (Synergy Neo, BioTek, USA). The extent of polymer-induced liposomal fusion was assessed by the fluorescence resonance energy transfer (FRET) method.[29-30] Briefly, liposomes incorporating 5 mM DOPE-NBD (donor) or DOPE-Rhod (acceptor) were prepared separately, then mixed at 1:1 volume ratio, followed by the addition of varying amounts of HA. After incubation at room temperature for 1 h, the samples were diluted 200 times and fluorescence intensity was measured by a microplate fluorometer with excitation at 480 nm and emission filters set at 540 nm and 600 nm. FRET index was calculated as fluorescence intensity at 600 nm divided by that at 540 nm.[31]

2.3.4. Preparation of BMDCs

BMDCs were prepared as described previously.[32] Briefly, femur and tibia of a mouse were harvested from C57BL/6 mice, and cells were collected by flushing bone marrow with a syringe and passing the cell suspension through a cell strainer (mesh size = 40 μm). After centrifugation, cells were seeded into non-tissue culture treated petri-dish at a density of 2×10^6 cells/dish and cultured in DC culture media (RPMI 1640 supplemented

with 10% FBS, 1% penicillin-streptomycin, 50 μM β-mercaptoethanol, and 20 ng/ml GM-CSF) at 37 ^{o}C with 5% CO_2. Culture media were refreshed on days 3, 6 and 8, and BMDCs were used on days 10-12.

2.3.5. Activation and viability of BMDCs

BMDCs were seeded at a density of 8×10^5 cells/ml into 24-well plates and cultured overnight. Cells were incubated with culture media, liposomes, or liposome-polymer hybrid NPs encapsulating 5 μg/ml of OVA, with or without 0.58 μg/ml of MPLA at 37 ^{o}C for 2 h, followed by washing with PBS and overnight culture. BMDCs were harvested, incubated with anti-CD16/32 at room temperature for 10 min, and then stained with fluorescent probe-labeled antibodies against CD11c, CD40, CD86, and MHC II at room temperature for 30 min. Finally, cells were washed and resuspended in 2 μg/ml DAPI solution and analyzed by flow cytometry (Cyan 5, Beckman Coulter, USA). BMDC viability following different treatments was measured by CCK-8 kit.[33] Briefly, BMDCs were seeded into 96-well plates (40,000 cells/well) and cultured overnight. Cells were then incubated with liposomes or liposome-polymer hybrid NPs encapsulating OVA, with or without MPLA, with various lipid concentrations. Following 2 h incubation at 37 ^{o}C, cells were washed by PBS and cultured overnight. Finally, cells were incubated with the CCK-8 reagent for 2 h at 37 ^{o}C and OD450 was measured with a microplate reader.

2.3.6. In vivo immunization studies

All *in vivo* experiments were performed under approval from the Institutional Animal Care and Use Committee (IACUC) at the University of Michigan. Female, 6-week old C57BL/6 mice (The Jackson Laboratory, USA) were randomly divided into 3 groups (n = 3-7) and administered with PBS, OVA plus MPLA solution, or hybrid NPs co-encapsulating OVA and MPLA via the intranasal route of immunization. Intranasal vaccination was performed by anesthetizing mice with isoflurane and administering both nostrils with a total vaccine dose of 50 μg of OVA and 0.58 μg of MPLA in 20-40 μl per mouse. A booster dose was given on day 28 after the prime vaccination. Serum samples were collected on days 21 and 49 for ELISA analysis. We also assessed the frequency of OVA-specific $CD8^+$ T cells among peripheral blood mononuclear cells (PBMCs) on day 7 post vaccination as we recently reported.[34] Briefly, blood samples were collected by retro-orbital bleeding, lysed with ACK lysis buffer, followed by centrifugation to collect pellets, which were then blocked by a CD16/32 blocking antibody and incubated with a PE-labeled SIINFEKL tetramer for 30 min on ice. Samples were then incubated with anti-CD8-APC for 20 min on ice. Cells were washed and resuspended in 2 μg/ml DAPI solution for analysis by flow cytometry.

In vivo biodistribution of antigen was investigated by injecting C57BL/6 mice (n = 3 per group) with PBS or 50 μg of Texas Red-labeled OVA either in free soluble or NP forms via intranasal or tail vein administration, and visualizing fluorescence signal from

major organs (e.g. heart, lungs, spleen, liver, and kidneys) with a Xenogen IVIS Spectrum Imaging System at 4 h post administration. For studies with F1-V, mice (n = 4) were intranasally immunized with F1-V plus MPLA solution, or hybrid NPs co-encapsulating F1-V and MPLA. The doses for prime vaccination on day zero and 1st booster vaccination on day 28 were 1 µg F1-V and 0.58 µg MPLA per mouse, while the 2nd booster dose given on day 56 was increased to 5 µg F1-V and 2.9 µg of MPLA per mouse. Serum samples were collected on days 0, 7, 21, 35, 49, 63 and 77 post the prime dose.

2.3.7. Enzyme-linked immunosorbent assay (ELISA)

ELISA was used to determine serum anti-OVA or anti-F1-V antibody titers post immunization. Microtiter plate was coated with OVA (1 µg/well) or F1-V (200 ng/well) dissolved in carbonate-bicarbonate buffer (pH 9.6) at 4 ^{o}C overnight. Wells were washed and blocked by 1 % BSA for 2 h, followed by incubation with serially diluted sera at room temperature for 1 h, incubation with HRP-conjugated anti-IgG, IgG_1, or IgG_{2c} antibodies for another hour, and colorization with the TMB substrate solution for 5 min. The reaction was stopped by 2 M H_2SO_4, and absorbance at 450 nm was measured by a microplate reader.

2.3.8. Statistical analysis

Data were analyzed by one- or two-way analysis of variance (ANOVA), followed by Bonferroni's test for comparison of multiple groups with Prism 5.0 (GraphPad Software). *P* values less than 0.05 were considered statistically significant. All values are reported as mean ± SEM with at least triplicate data points.

2.4. Results and discussion

2.4.1. Lipid-polymer hybrid NPs formed by ionic complexation of DOTAP liposomes and HA

Liposome-polymer hybrid NPs were synthesized by utilizing ionic complexation of positively charged liposomes and negatively charged HA. As shown in **Figure 2.2a**, the initial liposomes hydrated from lipid films composed of DOTAP and DOPE (henceforth referred to as DOTAP liposomes) had the particle size of 91.4 ± 0.4 nm. As an increasing amount of HA was added to the unilamellar liposomes, their size gradually increased, reaching 164.0 ± 1.4 nm with 150 μg HA added per 1 mg of liposome suspension. Addition of more than 300 μg of HA caused non-homogeneous aggregation shown by an abrupt increase in particle sizes (**Figure 2.2a**) and PDI values (**Figure 2.2b**). Similarly, the zeta potential of the lipid-polymer hybrid particles maintained values ranging from 47 - 55 mV with 0 - 150 μg HA added per one mg of liposome suspension (**Figure 2.2c**).

Addition of ≥ 300 μg of HA sharply decreased the surface charge of lipid-polymer hybrid particles, with their zeta potential readings reaching negative values with HA ≥ 1000 μg.

Liposomal fusion, which is a rapid process that generally occurs within 10 ms upon admixture of small unilamellar liposomes and fusogenic agent,[35] has been induced by the ionic interaction between lipids and charged small molecules such as Ca^{2+}, Mg^{2+},[35-36] fusogenic peptides,[37] or polymers such as dextran sulfate,[38] poly(malic acid),[30] or polylysine.[39] In this study, ionic complexation between DOTAP liposomes and HA biopolymer was further assessed by FRET assay, in which the efficiency of resonance energy transfer was measured between fluorescent NBD- (donor) and rhodamine- (acceptor) lipids initially on separate DOTAP liposomes and intermixed after addition of a varying amount of HA. As shown in **Figure 2.3**, the addition of 25 μg HA into liposomal suspension efficiently induced fusion of liposomes. The extent of fusion was decreased when more than 150 μg of HA was added to the batch of liposomes, suggesting that excess HA with anionic charge may reduce the extent of liposomal fusion by coating the external surfaces of cationic DOTAP liposomes. Based on the ability to induce ionic complexation between DOTAP liposomes and HA and form lipid-polymer hybrid NPs with homogeneous size, we chose to synthesize the hybrid NPs with 100 μg of HA for the subsequent studies.

2.4.2. PEGylated DOTAP-HA NPs exhibit colloidal stability and allow steady antigen release

In order to coat the external surfaces of liposome-HA hybrid particles with a hydrophilic PEG shell, we introduced free sulfhydryl groups to HA by EDC-mediated reaction between carboxylic groups in HA and amine group in L-cysteine (**Figure 2.1**). Ellman's assay indicated that thiolated HA contained 313.8 ± 1.8 μmol/g of free sulfhydryl groups. DOTAP liposomes incorporated with 100 μg of thiolated HA were PEGylated by incubation with 2 kDa MW thiol-PEG in the presence of an oxidizing agent, chloramine T, and the resulting NPs (henceforth referred to as DOTAP-HA NPs) were analyzed for their size and surface charge with Zetasizer Nano, as presented in **Table 2.1**. We measured the PEG content in DOTAP-HA NPs by assessing complexation of PEG with barium iodide as reported previously,[27-28] and the results indicated that ~24% of thiol-PEG initially added to the particle suspension was conjugated on the surfaces of DOTAP-HA NPs with PEG concentration of 47 ± 4 μmol per gram of particles (**Table 2.1**). We also carried out similar assays with DOTAP-HA NPs loaded with OVA, and the results showed that incorporation of OVA led to modest increases in particle size and PDI, whereas PEGylation efficiency and PEG content remained similar.

In addition, we performed more detailed size distribution analyses on DOTAP-HA NPs by nanoparticle tracking analysis (NTA), which has been reported to be a more accurate analytical tool than DLS analysis for assessing particle size distribution.[26] The

number distribution of particle size as measured with NTA indicated homogenous population of particles with the average diameter of ~ 210 nm for both blank DOTAP-HA NPs and OVA-DOTAP-HA NPs (**Figure 2.4**), thus corroborating the results of the DLS analyses of the particles.

Notably, DOTAP liposomes loaded with OVA immediately formed aggregates after resuspension in PBS, whereas OVA-DOTAP-HA NPs stably maintained their size distribution even after three days of incubation at 37 ^{o}C (**Figure 2.5**). Next, we examined antigen release from DOTAP-HA NPs loaded with Texas Red-labeled OVA (we omitted the DOTAP liposome group due to aggregation). When incubated in 10% FBS containing media at 37 ^{o}C, OVA-DOTAP-HA NPs steadily released ~ 40% of encapsulated OVA over three weeks, demonstrating the stability of the NPs (**Figure 2.6**).

2.4.3. Activation of BMDCs with adjuvant-loaded DOTAP-HA NPs

DCs are considered to be the most efficient antigen-presenting cells that play a key role in both innate and adaptive immune responses. Maturation of dendritic cells (DCs) involves up-regulation of a series of cell surface markers.[40] During DC maturation, elevated MHC-II present antigens to $CD4^{+}$ T cells (signal 1), while CD80/86 provide necessary co-stimulatory signal 2 for T cell activation. Increased CD40 is also necessary for DCs to receive further activation signals from $CD4^{+}$ T helper cells. We investigated DC

activation by incubating BMDCs with different particle formulations (**Figure 2.7**). After overnight culture, BMDCs exhibited a minor increase in the expression levels of CD86 and MHC-II after treatment with OVA-DOTAP liposomes. Treatment with OVA-DOTAP-HA NPs also led to a slight increase in the expression levels of MHC-II, indicating low immunogenicity of particles without any danger signals. To promote DC maturation, we incorporated MPLA, an FDA-approved TLR-4 agonist, into DOTAP-HA NPs by adding MPLA into the initial lipid film prior to hydration. Compared with OVA-DOTAP-HA NPs, DOTAP-HA NPs co-loaded with OVA and MPLA significantly up-regulated CD40 (**Figure 2.7a**), CD86 (**Figure 2.7b**), and MHC-II (**Figure 2.7c**) on DCs, indicating the immunostimulatory property of MPLA-loaded DOTAP-HA NPs.

2.4.4. Enhanced biocompatibility of DOTAP-HA NPs, compared with DOTAP liposomes

One of the major concerns of using cationic liposome as a delivery vehicle is its widely reported cytotoxicity.[9-10] To compare the cytotoxicity of DOTAP liposomes and DOTAP-HA NPs, we pulsed BMDCs with various concentrations of OVA-DOTAP liposomes or OVA-DOTAP-HA NPs with or without MPLA. Measurement of cell viability after overnight culture indicated that OVA-DOTAP liposome formulations with or without MPLA induced significant BMDC cytotoxicity with 50% of cell death observed at LC_{50} value of ~0.2 mg/ml (**Figure 2.8**). In contrast, BMDCs were able to

tolerate at least 20-fold higher concentration of lipids in OVA-DOTAP-HA NPs (LC_{50} > 4 mg/ml). In addition, BMDCs exhibited similar levels of viability when incubated with DOTAP-HA NPs with or without PEGylation (**Figure 2.9**). These results showed that ionic complexation of DOTAP liposomes with HA biopolymer significantly enhanced their biocompatibility. Overall, liposome-HA hybrid NPs potently activated DCs with significantly reduced cytotoxicity, compared with DOTAP liposomes.

2.4.5. Vaccination with DOTAP-HA NPs elicits adaptive immune responses

Next, we investigated the elicitation of humoral and cellular immune responses after intranasal delivery of OVA and MPLA in either soluble form or DOTAP-HA NPs. C57BL/6 mice were immunized with 50 μg of OVA and 0.58 μg of MPLA either in solution or DOTAP-HA NPs via intranasal administration on days 0 and 28. Immune sera were collected on days 21 and 49, three weeks post prime and boost, respectively, and analyzed for OVA-specific IgG responses with ELISA. Immunization with OVA/MPLA-DOTAP-HA NPs elicited significantly enhanced OVA-specific IgG responses, compared with immunization with soluble vaccines (**Figure 2.10a**). Among IgG subtypes, a robust level of OVA-specific IgG_1 response was observed in mice immunized with OVA/MPLA-DOTAP-HA NPs (**Figure 2.10b**); however, IgG_{2c} responses were not detected in any of the groups (**Figure 2.10c**), indicating strong

skewing toward Th2 over Th1 humoral immune responses with the OVA antigen.

We also examined the elicitation of OVA-specific cellular immune responses by assessing the frequency of OVA-specific $CD8^+$ T cells among PBMCs on day 7 after vaccination (**Figure 2.11**). Compared with the PBS group, vaccination with DOTAP-HA NPs significantly increased the frequency of OVA-specific CD8+ T cells among PBMCs as measured with fluorophore-conjugated tetramer with $OVA_{257-264}$ (SIINFEKL) in the context of $H\text{-}2K^b$. Although the difference was not statistically significant, there was a trend for increased OVA-specific CD8+ T cell responses in the DOTAP-HA NP group, compared with the soluble vaccine group. Overall, intranasal vaccination with DOTAP-HA NPs enhanced both B- and T-cell immune responses, compared with the equivalent dose of soluble vaccines. Similar advantages have been reported in nasal immunization with nanoparticles composed of other biodegradable polymers, such as trimethyl chitosan which increased sera anti-OVA IgG titers,[16, 41] and poly(γ-glutamic acid) which enhanced OVA-specific CD8 T cell response.[42]

In addition, we examined whether intranasal vaccination leads to systemic delivery of vaccine components. C57BL/6 mice were administered with Texas Red-labeled OVA in either free form or DOTAP-HA NPs, and after 4 h we examined heart, lungs, spleen, liver, and kidneys for the presence of OVA by measuring the fluorescence signal. We did not detect any accumulation of OVA in any of the major organs after intranasal vaccination with free OVA or OVA-DOTA-HA NPs (**Figure 2.12**). In contrast, as we

expected, intravenous injection of the same dose of OVA-DOTAP-HA NPs resulted in robust accumulation in the liver. These results suggest that there is minimal penetration of vaccine components into systemic compartments after intranasal administration, at least for the time window that we examined in our studies.

2.4.6. Intranasal vaccination with DOTAP-HA NPs elicits robust humoral immune responses against F1-V

As pneumonic plague can be easily transmitted by respiratory tract with deadly consequences, nasal vaccination has been the subject of various prior studies. A previous study comparing various routes of vaccination has reported that intranasal vaccination with F1-V resulted in humoral immune responses comparable to subcutaneous or intramuscular immunizations.[43-44] Moreover, adjuvants were shown to be indispensable for protection against *Y. pestis* infection by intranasal immunization of F1-V.[45] Recently, F1-V and MPLA have been intranasally delivered by polyanhydride nanoparticles, resulting in significantly improved lung residence of F1-V and plague protection.[22-23] These results highlight the benefits of particulate delivery systems for F1-V vaccine. In our current studies, DOTAP-HA NPs were also used to deliver F1-V via an intranasal route of vaccination. C57BL/6 mice were immunized with F1-V and MPLA either in soluble form or DOTAP-HA NPs, and the immune sera were analyzed for F1-V specific

antibody titers. The prime and first boost doses given on days 0 and 28 contained 1 μg F1-V and 0.58 μg MPLA per mouse. Although there was a detectable increase in anti-F1-V IgG titers after the first boost immunization, due to the low overall IgG responses, we decided to increase the second booster dose to 5 μg F1-V and 2.9 μg MPLA per mouse to ensure sero-conversion and to more clearly distinguish the potency of soluble *vs.* particulate vaccine formulations. After the second booster doses, the hybrid NP delivery system elicited substantially higher F1-V-specific total IgG titers, compared with soluble F1-V vaccines (an 11-fold increase on day 77, $p < 0.0001$, **Figure 2.13a**). Analyses of F1-V-specific IgG_1 (**Figure 2.13b**) and IgG_{2c} (**Figure 2.13c**) responses also revealed similar trend with 23-fold ($p < 0.05$) and 15-fold increases ($p < 0.001$) in serum titers on day 77, compared with immune sera from mice immunized with soluble F1-V vaccines. Notably, IgG_1 responses induced by DOTAP-HA NPs reached their peak on day 63 (one week post the second boost) and started to decrease by day 77. On the other hand, IgG_{2c} responses continued to increase after the second boost and reached substantially enhanced serum titer by day 77, contributing to the overall anti-F1-V total IgG titer. Thus, unlike the case with the OVA antigen (**Figure 2.10**), F1-V delivered by DOTAP-HA NPs exhibited Th1/Th2-balanced humoral immune responses, suggesting that the identity of subunit antigen formulated into these vaccine NPs may have a direct impact on the Th1/Th2 humoral immune responses. These results highlight the potency of DOTAP-HA NPs to generate potent immune responses against F1-V with significant dose sparing,

compared with conventional vaccine formulations.

2.5. Conclusion

In this work, we have utilized the ionic interaction between cationic DOTAP liposomes and anionic HA to form lipid-polymer hybrid NPs and examined their efficacy as delivery vehicles for protein antigens and immunostimulatory agents *in vitro* and *in vivo*. In specific, cationic DOTAP liposomes were incorporated with HA and PEGylated for enhanced biocompatibility, improved colloidal stability, and steady antigen release. Our results indicated that DOTAP-HA NPs carrying MPLA, a TLR-4 agonist, significantly improved BMDC activation while reducing cytotoxicity of DOTAP-based liposomes by at least 20-fold as indicated by their LC_{50} values. In addition, when administered via intranasal route, these vaccine NPs elicited significantly enhanced humoral immune responses against subunit protein antigens, compared with soluble vaccine formulations. Importantly, F1-V, a candidate antigen for *Y. pestis* was successfully formulated into DOTAP-HA NPs, and intranasal vaccination with these NPs induced substantially enhanced antigen-specific IgG titers with balanced Th1/Th2 IgG responses, compared with the soluble vaccine counterpart, suggesting their potential as a pulmonary vaccine platform. Our future studies will be directed to provide mechanistic insights into the process of NP-mediated antigen delivery to antigen-presenting cells within

nasal-associated lymphoid tissues and to delineate the impact of IgG_1/IgG_{2c}-balanced humoral immune responses on protection against *Y. pestis* infection.

2.6. Figures and tables

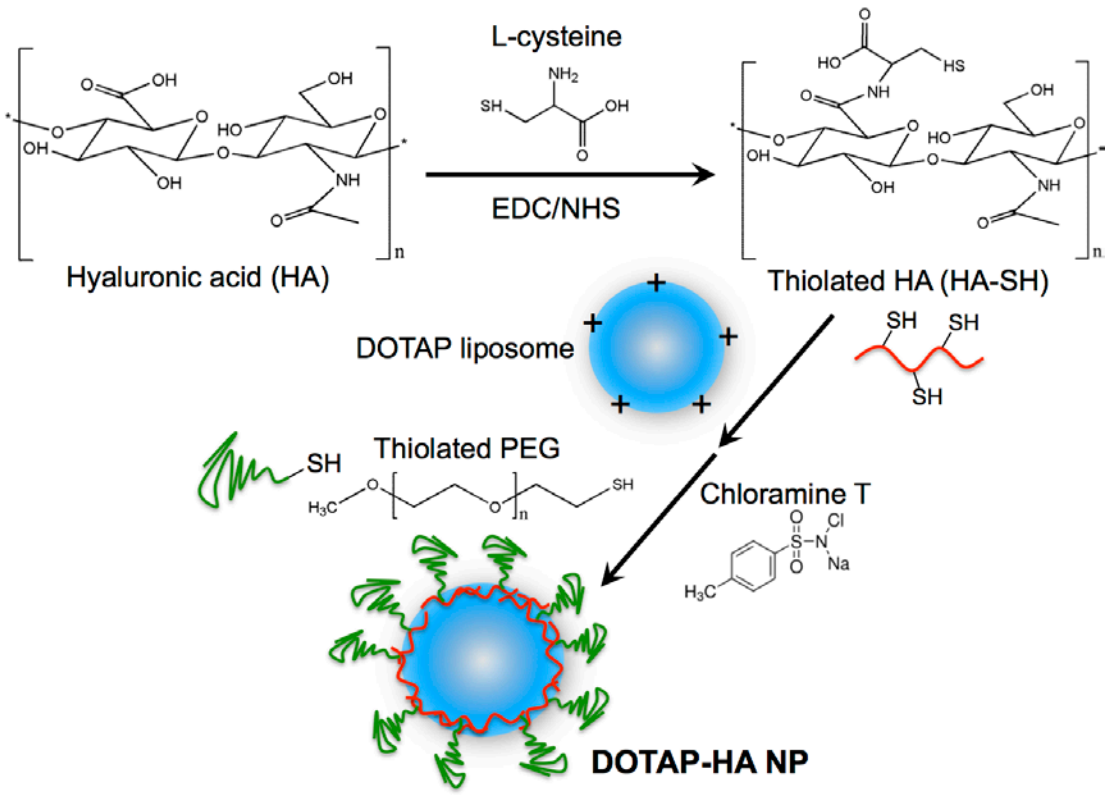

Figure 2.1. Schematic illustration of thiolation of hyaluronic acid and formation of lipid/polymer hybrid nanoparticles.

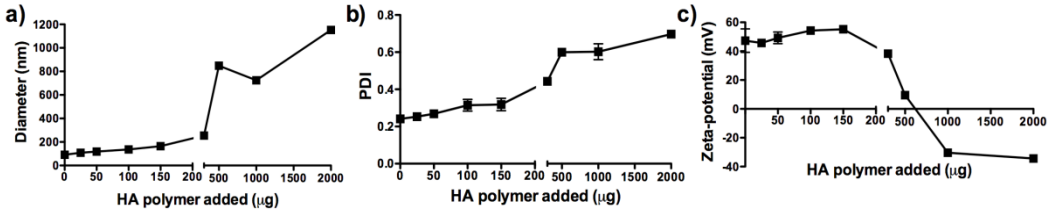

Figure 2.2. Characterization of liposomes interacting with varying amounts of HA polymer. HA in varying amounts was added per one mg of DOTAP:DOPE liposomes, and particle size **(a)**, PDI **(b),** and zeta potential **(c)** were measured. Results are reported as mean ± SEM (*n* = 3).

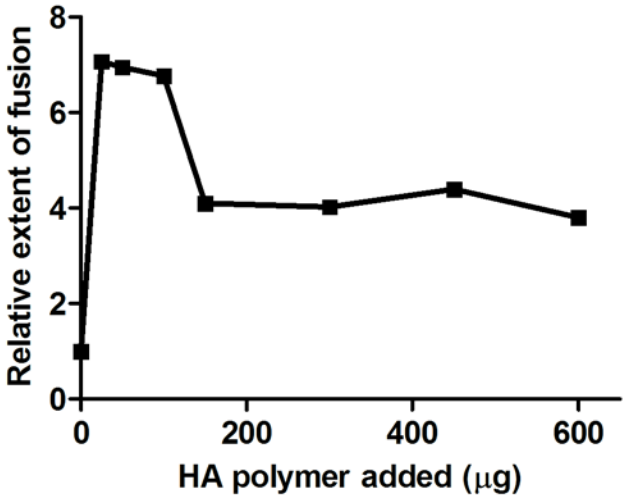

Figure 2.3. Ionic complexation of DOTAP liposomes and HA. DOTAP liposomes were separately prepared with NBD- or Rhod-labeled lipid, followed by addition of various amounts of HA. The efficiency of FRET was measured with respect to the control liposomes without HA. Results are mean ± SEM (n = 3).

Table 2.1. Characterization of DOTAP-HA NPs. Results are reported as mean ± SEM (*n* = 3).

	Size (nm)	PDI	Zeta potential (mV)	PEGylation efficiency (%)	PEG content (µmol/g particle)
Blank DOTAP-HA NPs	190 ± 1.3	0.184 ± 0.002	-16.8 ± 0.07	24 ± 5	47 ± 4
OVA-loaded DOTAP-HA NPs	250 ± 12	0.247 ± 0.005	-15.1 ± 0.9	22 ± 0.9	51 ± 13

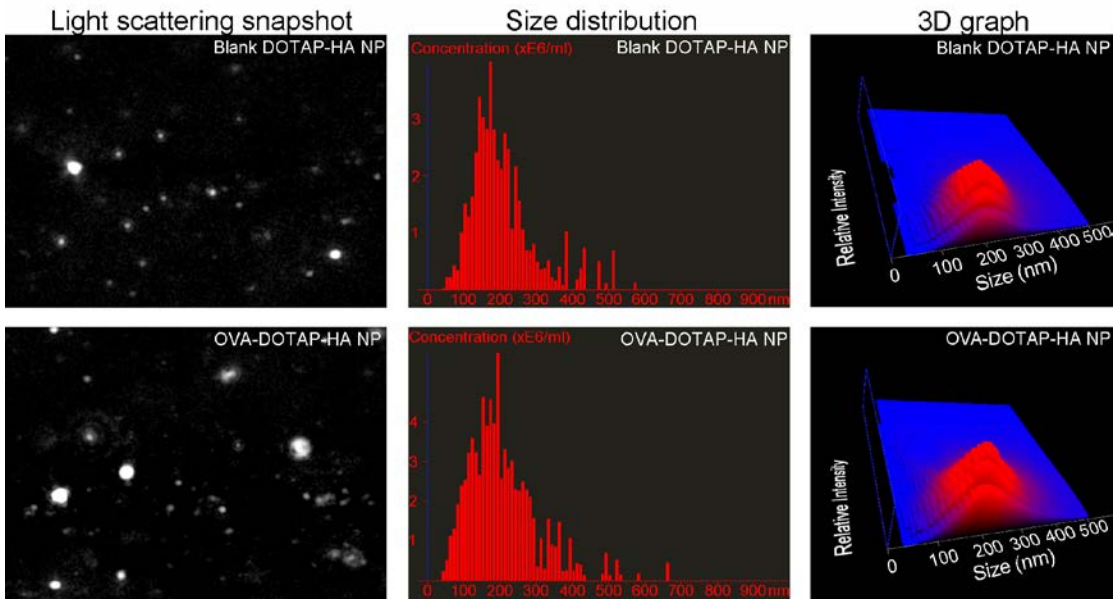

Figure 2.4. Nanoparticle tracking analysis of DOTAP-HA NP. Representative NTA video frame (left panel), size distribution (middle panel), and 3D graph (right panel showing size *vs.* light scattering intensity *vs.* particle concentration) are shown for blank and OVA-containing DOTAP-HA NPs.

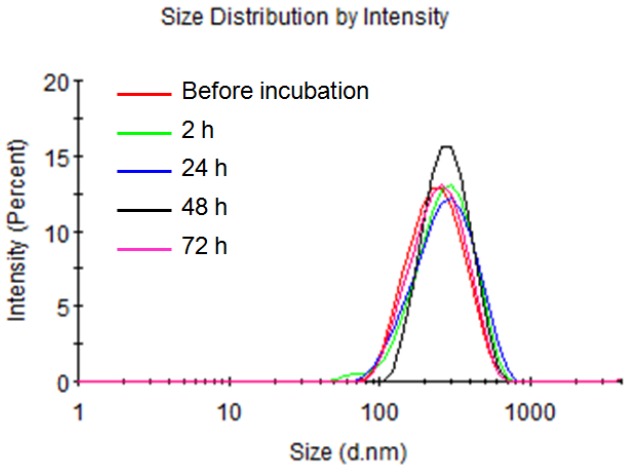

Figure 2.5. Stability of OVA-DOTAP-HA NPs. Particles were resuspended in PBS and incubated at 37 ^{o}C for different time periods, followed by the measurement of size distribution using DLS.

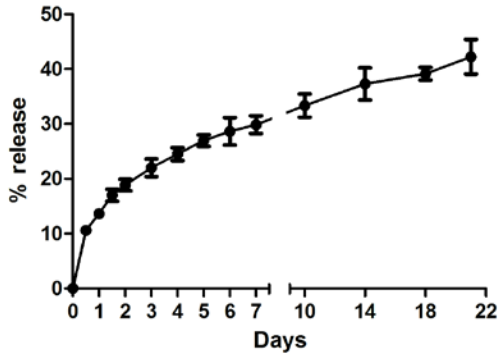

Figure 2.6. Steady release of protein antigen from DOTAP-HA NPs. DOTAP-HA NPs encapsulating Texas Red-labeled OVA were loaded in dialysis cassettes (MWCO 300 kDa) and incubated in RPMI 1640 supplemented with 10% FBS at 37 ^{o}C under constant shaking. Protein release was quantified by measuring fluorescence intensity of release media over three weeks with excitation/emission wavelengths of 585/615 nm. Results are mean ± SEM (n = 3).

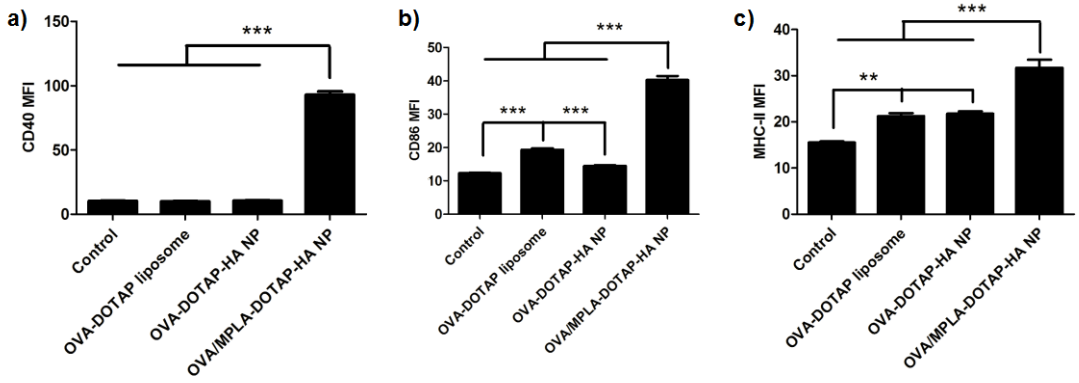

Figure 2.7. MPLA-loaded DOTAP-HA NPs induce maturation of BMDCs. BMDCs were pulsed with DOTAP liposomes or DOTAP-HA NPs containing 5 μg/ml of OVA with or without 0.58 μg/ml of MPLA for 2 h at 37 ^{o}C. After overnight culture, expression levels of CD40 **(a)**, CD86 **(b)** and MHC-II **(c)** were measured by flow cytometry. BMDCs treated with culture media served as the negative control. ** $p < 0.01$ and *** $p < 0.001$, as analyzed by one-way ANOVA followed by Bonferroni's test for comparison of multiple groups. Results are mean fluorescence intensity (MFI) ± SEM (n = 6).

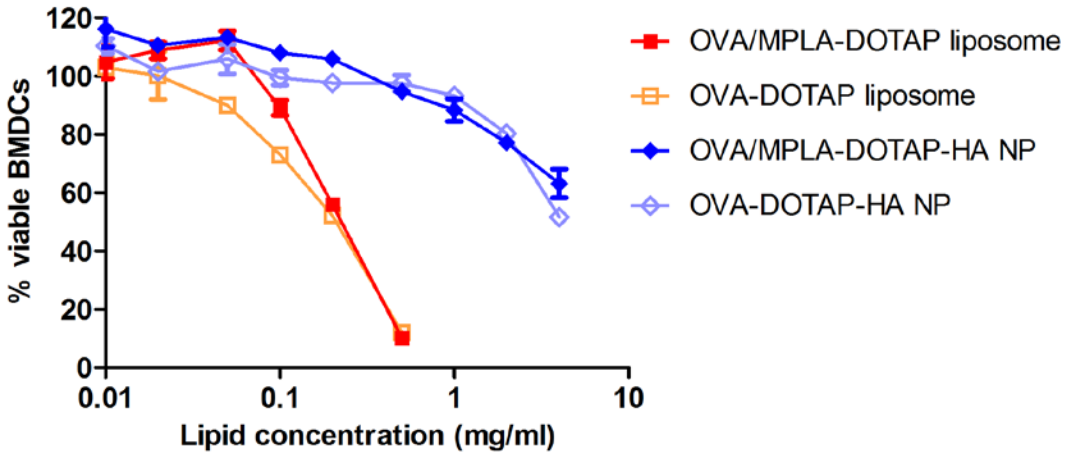

Figure 2.8. Cytotoxicity of DOTAP liposomes and DOTAP-HA NPs. BMDCs were pulsed with OVA-DOTAP liposomes or OVA-DOTAP-HA NPs with or without MPLA for 2 h at 37 ^{o}C. After overnight culture, BMDC viability was measured with a CCK-8 kit and reported as the percentage of viable BMDCs relative to the media treatment control group. Results are reported as mean ± SEM (n = 3).

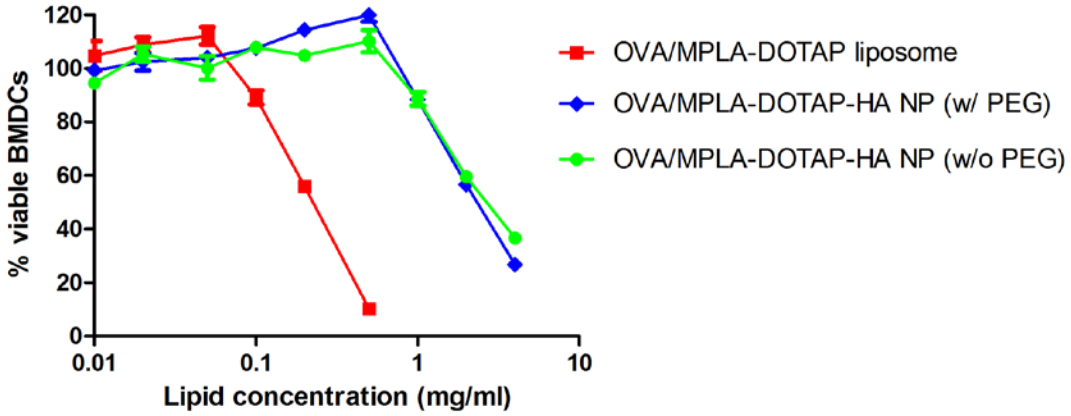

Figure 2.9. DOTAP-HA NPs with or without PEGylation exhibit enhanced biocompatibility, compared with DOTAP liposomes in BMDCs. BMDCs were pulsed with DOTAP liposomes or DOTAP-HA NPs with or without PEGylation in indicated lipid concentrations for 2 h at 37 ^{o}C. After overnight culture, BMDC viability was measured with a CCK-8 kit and reported as the percentage of viable BMDCs relative to the media treatment control group. Results are reported as mean ± SEM (n = 3).

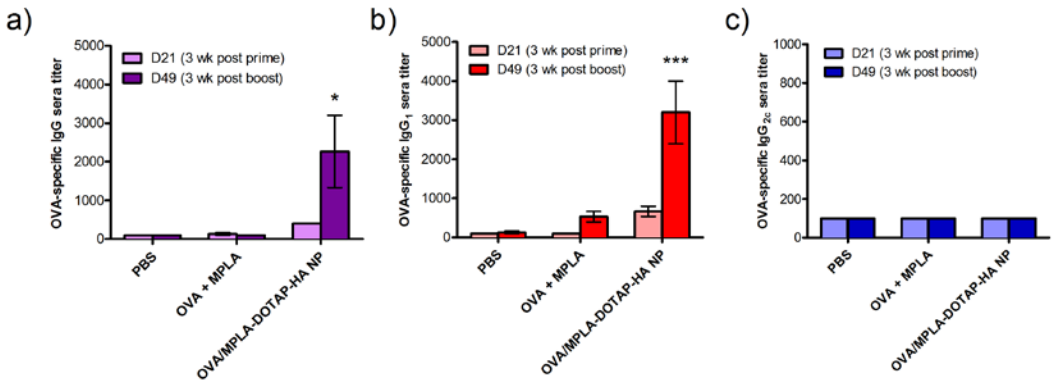

Figure 2.10. Vaccination with DOTAP-HA NPs elicits antigen-specific humoral immune responses. C57BL/6 mice were vaccinated with PBS, soluble OVA plus MPLA, or OVA and MPLA co-loaded in DOTAP-HA NPs on days 0 and 28 via intranasal route (OVA dose: 50 μg/mouse; MPLA dose: 0.58 μg/mouse). Serum samples were collected on days 21 and 49 for analysis of OVA-specific total IgG **(a)**, IgG_1 **(b)** and IgG_{2c} **(c)** titers by ELISA. * $p < 0.05$ and *** $p < 0.001$ in comparison to PBS and solution groups on day 49, as analyzed by two-way ANOVA, followed by Bonferroni's test for comparison of multiple groups. Results are reported as mean ± SEM ($n = 3$).

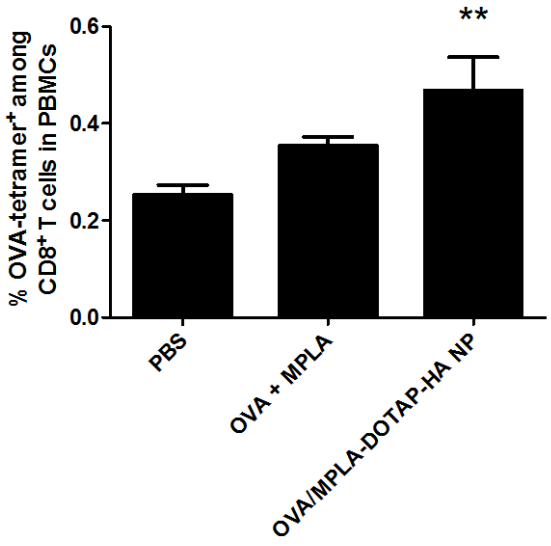

Figure 2.11. Vaccination with DOTAP-HA NPs elicits antigen-specific cellular immune responses. C57BL/6 mice were immunized via intranasal route with PBS, or OVA and MPLA either in soluble form or in DOTAP-HA NPs (OVA dose: 50 μg/mouse; MPLA dose: 0.58 μg/mouse). PBMCs were collected on day 7 and analyzed for OVA-specific $CD8^+$ T cells by tetramer staining and flow cytometry. ** $p < 0.01$ in comparison to PBS control, as analyzed by one-way ANOVA, followed by Bonferroni's test for comparison of multiple groups. Results are reported as mean ± SEM ($n = 7$).

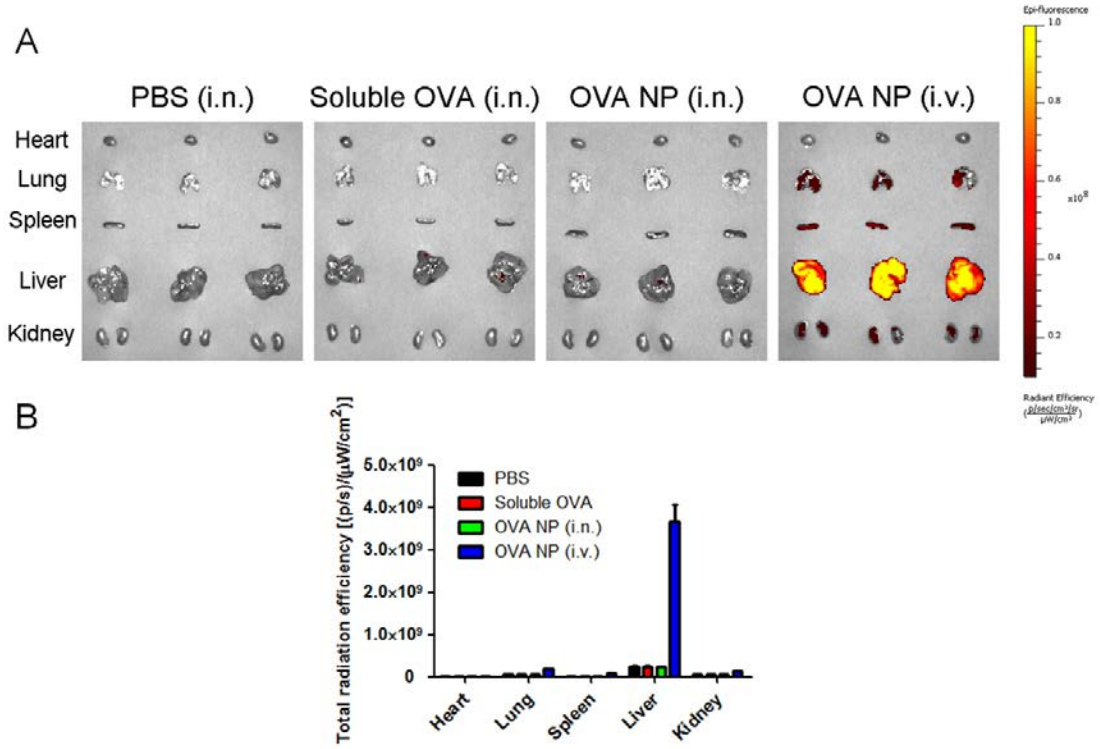

Figure 2.12. Biodistribution of vaccines administered via intranasal or intravenous routes. C57BL/6 mice (*n* = 3 per group) were intranasally administered with PBS, soluble Texas Red-labeled OVA, or DOTAP-HA NPs encapsulating Texas Red-labeled OVA. Mice administered with DOTAP-HA NPs via intravenous tail vein injection were included as a positive control group. Dose of labeled OVA was kept at 50 μg/mouse. **(A)** Mice were euthanized at 4 h post administration, and the major organs were excised and imaged for fluorescence signal. **(B)** Quantification of fluorescence signal from the major organs. Results are reported as mean ± SEM (*n* = 3).

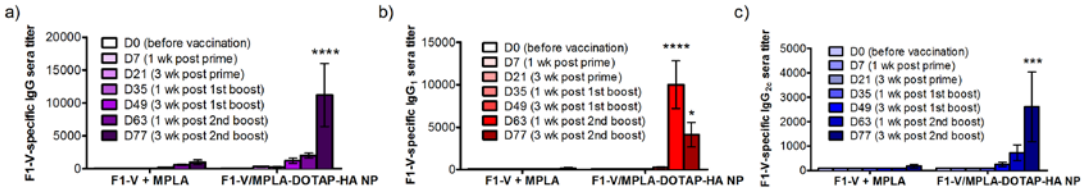

Figure 2.13. Vaccination with DOTAP-HA NPs induces F1-V-specific humoral immune responses. C57BL/6 mice were intranasally immunized with free F1-V and MPLA, or F1-V and MPLA co-loaded DOTAP-HA NPs on days 0 and 28 (F1-V dose: 1 μg/mouse; MPLA dose: 0.58 μg/mouse). The second booster dose given on day 56 was increased to 5 μg F1-V and 2.9 μg MPLA to ensure successful sero-conversion. Sera were collected on days 0, 7, 21, 35, 49, 63 and 77 and analyzed for F1-V-specific total IgG **(a)**, IgG_1 **(b)** and IgG_{2c} **(c)** titers by ELISA. * $p < 0.05$, *** $p < 0.001$ and **** $p < 0.0001$ in comparison to the soluble F1-V plus MPLA group of the same time point, as analyzed by two-way ANOVA, followed by Bonferroni's test for comparison of multiple groups. Results are reported as mean ± SEM (n = 4).

2.7. References

1. Irvine, D. J., *et al.* Engineering synthetic vaccines using cues from natural immunity. *Nat Mater* **2013,** *12* (11), 978-90.

2. Moon, J. J., *et al.* Engineering nano- and microparticles to tune immunity. *Adv Mater* **2012,** *24* (28), 3724-46.

3. Sahdev, P., *et al.* Biomaterials for nanoparticle vaccine delivery systems. *Pharm Res* **2014,** *31* (10), 2563-82.

4. Gregoriadis, G., *et al.* Liposome-mediated DNA vaccination. *FEBS Lett* **1997,** *402* (2-3), 107-10.

5. Perrie, Y., *et al.* Liposome-mediated DNA vaccination: the effect of vesicle composition. *Vaccine* **2001,** *19* (23-24), 3301-10.

6. Yan, W., *et al.* Reactive oxygen species play a central role in the activity of cationic liposome based cancer vaccine. *J Control Release* **2008,** *130* (1), 22-8.

7. Chen, W., *et al.* A simple but effective cancer vaccine consisting of an antigen and a cationic lipid. *Cancer Immunol Immunother* **2008,** *57* (4), 517-30.

8. Christensen, D., *et al.* Cationic liposomes as vaccine adjuvants. *Expert Rev Vaccines* **2011,** *10* (4), 513-21.

9. Lappalainen, K., *et al.* Comparison of cell proliferation and toxicity assays using two cationic liposomes. *Pharm Res* **1994,** *11* (8), 1127-31.

10. Lv, H., *et al.* Toxicity of cationic lipids and cationic polymers in gene delivery. *J Control Release* **2006,** *114* (1), 100-9.

11. Moon, J. J., *et al.* Interbilayer-crosslinked multilamellar vesicles as synthetic vaccines for potent humoral and cellular immune responses. *Nat Mater* **2011,** *10* (3), 243-51.

12. DeMuth, P. C., *et al.* Releasable layer-by-layer assembly of stabilized lipid nanocapsules on microneedles for enhanced transcutaneous vaccine delivery. *ACS Nano*

2012, *6* (9), 8041-51.

13. Li, A. V., *et al.* Generation of effector memory T cell-based mucosal and systemic immunity with pulmonary nanoparticle vaccination. *Sci Transl Med* **2013,** *5* (204), 204ra130.

14. Gasperini, A. A., *et al.* Association between cationic liposomes and low molecular weight hyaluronic acid. *Langmuir* **2015,** *31* (11), 3308-17.

15. Singh, M., *et al.* A novel bioadhesive intranasal delivery system for inactivated influenza vaccines. *J Control Release* **2001,** *70* (3), 267-76.

16. Verheul, R. J., *et al.* Covalently stabilized trimethyl chitosan-hyaluronic acid nanoparticles for nasal and intradermal vaccination. *J Control Release* **2011,** *156* (1), 46-52.

17. Verheul, R. J., *et al.* Tailorable thiolated trimethyl chitosans for covalently stabilized nanoparticles. *Biomacromolecules* **2010,** *11* (8), 1965-71.

18. Quenee, L. E., *et al.* Prevention of pneumonic plague in mice, rats, guinea pigs and non-human primates with clinical grade rV10, rV10-2 or F1-V vaccines. *Vaccine* **2011,** *29* (38), 6572-83.

19. Csaba, N., *et al.* Nanoparticles for nasal vaccination. *Adv Drug Deliv Rev* **2009,** *61* (2), 140-57.

20. Heath, D. G., *et al.* Protection against experimental bubonic and pneumonic plague by a recombinant capsular F1-V antigen fusion protein vaccine. *Vaccine* **1998,** *16* (11-12), 1131-7.

21. Uddowla, S., *et al.* Effect of adjuvants and route of immunizations on the immune response to recombinant plague antigens. *Vaccine* **2007,** *25* (47), 7984-93.

22. Ross, K. A., *et al.* Lung deposition and cellular uptake behavior of pathogen-mimicking nanovaccines in the first 48 hours. *Adv Healthc Mater* **2014,** *3* (7), 1071-7.

23. Ulery, B. D., *et al.* Design of a protective single-dose intranasal nanoparticle-based vaccine platform for respiratory infectious diseases. *PLoS One* **2011,** *6* (3), e17642.

24. Guy, B. The perfect mix: recent progress in adjuvant research. *Nat Rev Microbiol* **2007,** *5* (7), 505-17.

25. Alving, C. R., *et al.* Liposomes containing lipid A: an effective, safe, generic adjuvant system for synthetic vaccines. *Expert Rev Vaccines* **2012,** *11* (6), 733-44.

26. Filipe, V., *et al.* Critical evaluation of Nanoparticle Tracking Analysis (NTA) by NanoSight for the measurement of nanoparticles and protein aggregates. *Pharm Res* **2010,** *27* (5), 796-810.

27. Sims, G. E.; Snape, T. J. A method for the estimation of polyethylene glycol in plasma protein fractions. *Anal Biochem* **1980,** *107* (1), 60-3.

28. Gong, X. W., *et al.* Discarded free PEG-based assay for obtaining the modification extent of pegylated proteins. *Talanta* **2007,** *71* (1), 381-4.

29. Hoekstra, D. Role of lipid phase separations and membrane hydration in phospholipid vesicle fusion. *Biochemistry* **1982,** *21* (12), 2833-40.

30. Osanai, S.; Nakamura, K. Effects of complexation between liposome and poly(malic acid) on aggregation and leakage behaviour. *Biomaterials* **2000,** *21* (9), 867-76.

31. Berney, C.; Danuser, G. FRET or no FRET: a quantitative comparison. *Biophys J* **2003,** *84* (6), 3992-4010.

32. Lutz, M. B., *et al.* An advanced culture method for generating large quantities of highly pure dendritic cells from mouse bone marrow. *J Immunol Methods* **1999,** *223* (1), 77-92.

33. Ishiyama, M., *et al.* A highly water-soluble disulfonated tetrazolium salt as a chromogenic indicator for NADH as well as cell viability. *Talanta* **1997,** *44* (7), 1299-305.

34. Ochyl, L. J.; Moon, J. J. Whole-animal imaging and flow cytometric techniques for analysis of antigen-specific CD8+ T cell responses after nanoparticle vaccination. *J Vis Exp* **2015,** (98), e52771.

35. Miller, D. C.; Dahl, G. P. Early events in calcium-induced liposome fusion. *Biochim*

Biophys Acta **1982,** *689* (1), 165-9.

36. Papahadjopoulos, D., *et al.* Molecular mechanisms of calcium-induced membrane fusion. *J Bioenerg Biomembr* **1990,** *22* (2), 157-79.

37. Xia, Y., *et al.* Aggregation, fusion, and leakage of liposomes induced by peptides. *Langmuir* **2014,** *30* (25), 7334-42.

38. Arnold, K., *et al.* Interaction of dextran sulfate with phospholipid surfaces and liposome aggregation and fusion. *Chem Phys Lipids* **1990,** *55* (3), 301-7.

39. Yaroslavov, A. A., *et al.* Liposome fusion rates depend upon the conformation of polycation catalysts. *J Am Chem Soc* **2011,** *133* (9), 2881-3.

40. Banchereau, J.; Palucka, A. K. Dendritic cells as therapeutic vaccines against cancer. *Nat Rev Immunol* **2005,** *5* (4), 296-306.

41. Slutter, B., *et al.* Nasal vaccination with N-trimethyl chitosan and PLGA based nanoparticles: nanoparticle characteristics determine quality and strength of the antibody response in mice against the encapsulated antigen. *Vaccine* **2010,** *28* (38), 6282-91.

42. Uto, T., *et al.* Improvement of adaptive immunity by antigen-carrying biodegradable nanoparticles. *Biochem Biophys Res Commun* **2009,** *379* (2), 600-4.

43. Glynn, A., *et al.* Effect of homologous and heterologous prime-boost on the immune response to recombinant plague antigens. *Vaccine* **2005,** *23* (16), 1957-65.

44. Jones, T., *et al.* Intranasal Protollin/F1-V vaccine elicits respiratory and serum antibody responses and protects mice against lethal aerosolized plague infection. *Vaccine* **2006,** *24* (10), 1625-32.

45. Glynn, A., *et al.* Protection against aerosolized Yersinia pestis challenge following homologous and heterologous prime-boost with recombinant plague antigens. *Infect Immun* **2005,** *73* (8), 5256-61.

Chapter 3: Lipid-hyaluronic acid cross-linked nanoparticles for enhancement of antigen-specific T cell responses

3.1. Abstract

Recent outbreaks of emerging infectious diseases and their aftermath underscore the lack of effective countermeasures, especially prophylactic vaccines. Subunit proteins derived from whole-pathogens provide a safe antigen source but are often limited by their low immunogenicity. Nanoparticle vaccines have shown promise to enhance immune stimulation by stably delivering antigens and adjuvants. Inspired by the promising results shown in Chapter 2, here we have developed a lipid-hyaluronic acid (HA) crosslinked multilamellar vaccine particle (MVP) platform to co-deliver protein antigens and an adjuvant monophosphoryl lipid A (MPLA), a Toll-like receptor four agonist. Compared to multilamellar lipid vesicles without crosslinking and surface decoration by HA, ovalbumin (OVA) and MPLA co-loaded MVP accumulated more in CD44-expressing dendritic cells (DCs), enhanced antigen processing in DCs in vitro, therefore eliciting significantly stronger antigen-specific CD8+ and CD4+ T cell immune responses *in vivo*. Ebola glycoprotein (GP) and MPLA co-loaded MVP also significantly enhanced

GP-specific cellular immune responses, leading to prophylactic efficacy of 80% after single-dose immunization in mice against a lethal viral challenge. These results suggest the MVP could be a promising delivery platform for protein antigens and facilitate clinical translation of subunit vaccine candidates.

3.2. Introduction

Emerging infectious diseases, such as the Ebola and Zika outbreaks in recent years, have caused a severe burden of public health and economic loss.[1-2] Prophylactic vaccines have successfully controlled or even eradicated several deadly diseases in human history,[3-4] and would provide an effective countermeasure against those emerging infectious pathogens that are in lack of effective treatments. Although traditional vaccine approaches relying on inactivated or attenuated whole viruses or bacteria have shown ideal immune stimulation, their widespread use has been limited by undesired reactogenicity and safety concerns.[5-6] In contrast, molecularly defined subunit protein antigens, though providing safer alternatives, are often less immunogenic than whole-virus or -bacterium antigens, thus require co-administration of adjuvants to boost vaccine efficacy. In addition, soluble protein antigens are susceptible to deactivation or degradation. Nanoparticle systems have been widely investigated for subunit vaccine delivery,[7-10] with their advantages in protecting encapsulated antigens from degradation,

achieving co-localized delivery of adjuvants, and improving delivery efficiency to local draining lymph nodes (dLNs) following subcutaneous administration.[11-13]

In the current chapter, we developed a multilamellar lipid-polymer hybrid nanoparticle platform with cationic lipid interbilayers crosslinked by a biocompatible anionic polymer, thiolated hyaluronic acid (HA-SH) to form the multilamellar vaccine particle (MVP). We co-loaded protein antigens and MPLA as the adjuvant into the MVP and investigated its potential in the elicitation of antigen-specific immune responses *in vitro* and *in vivo*. The MVP achieved efficient and stable loading of protein antigens and activated dendritic cells (DCs) *in vitro* with the co-loaded MPLA. Compared with the previously developed platform of interbilayer-crosslinked multilamellar vesicle (ICMV) which was crosslinked by dithiothreitol (DTT), crosslinking and particle surface decoration with HA increased the accumulation of MVP in CD44-expressing DCs, and promoted antigen processing by DCs *in vitro*. Using ovalbumin (OVA) as the model antigen, immunization with OVA/MPLA co-loaded MVP elicited robust OVA-specific $CD8^+$ and $CD4^+$ T cells, and durable cellular and humoral immune responses *in vivo*. When tested with the Ebola glycoprotein (GP) antigen and compared to the nanoparticle platform without HA-mediated crosslinking and DC targeting, GP/MPLA co-loaded MVP elicited stronger GP-specific T cell immune responses *in vivo*, resulting in a prophylactic protection rate of 80% against a lethal viral challenge following a single vaccination dose. These results suggest MVP could be a promising delivery platform for

subunit protein antigens, leading to potent vaccine candidates against emerging infectious diseases.

3.3. Materials and Methods

3.3.1. Materials

Lipids including 1,2-dioleoyl-sn-glycero-3-phosphocholine (DOPC), 1,2-dioleoyl-sn-glycero-3-phosphoethanolamine-N-[4-(p-maleimidophenyl)butyramide] (MPB-PE), 1,2-dioleoyl-3-trimethylammonium-propane (DOTAP), N-(4-carboxybenzyl)-N,N-dimethyl-2,3-bis(oleoyloxy)propan-1-aminium (DOBAQ), monophosphoryl lipid A (MPLA), and 1-palmitoyl-2-(dipyrromethene boron difluoride)undecanoyl-sn-glycero-3-phosphocholine (TF-PC) were purchased from Avanti Polar Lipids. Hyaluronic acid (HA) sodium salt (average Mw = 29 kD) was from Lifecore Biomedical, and the thiolated hyaluronic acid (HA-SH) was synthesized as described previously.[9] Ovalbumin (OVA) was from Worthington Biochemical Corporation, and DQ-OVA was from ThermoFisher Scientific. The Ebola glycoprotein (GP) was kindly provided by Dr. Christopher L. Cooper (USAMRIID). All other materials were at least the reagent grade.

3.3.2. Synthesis of the maleimide-functional lipid DOBAQ-MAL

Maleimide-modified DOBAQ (DOBAQ-MAL) was synthesized by EDC/NHS chemistry. In brief, DOBAQ, N-(3-Dimethylaminopropyl)-N'-ethylcarbodiimide hydrochloride (EDC, ThermoFisher Scientific), and N-Hydroxysuccinimide (NHS, Sigma-Aldrich) were dissolved in dichloromethane at a molar ratio of 1 : 1.5 : 1.5 and reacted for 0.5 h at room temperature, followed by addition of N-(2-Aminoethyl)maleimide hydrochloride (MAL, 1.2 molar fold to DOBAQ, TCI America) and adjustment of pH to 8-9 with triethylamine (Sigma-Aldrich). The reaction was kept for another 24 h and monitored by thin layer chromatography (TLC) using developing media composed of chloroform : methanol : acetonitrile : water = 70 : 21 : 5 : 4 (v/v/v/v) and colorization by iodine gas. DOBAQ-MAL was purified by multiple washes through 0.1 M hydrochloride solution, saturated sodium chloride solution, and acetonitrile. Reaction rate was quantified by high performance liquid chromatography (HPLC, SHIMADZU) using a diphenyl column (4.6 mm ID × 250 mm, GRACE) with elution phase composed of water : methanol : acetonitrile : trifluoroacetic acid = 34.98 : 32.48 : 32.48 : 0.05 (v/v/v/v), and detection wavelength at 220 nm. The molecular structure of DOBAQ-MAL was determined by ^{1}H-NMR (Varian, USA) using d^{6}-DMSO (Sigma-Aldrich) as the solvent.

3.3.3. Synthesis and characterization of ICMVs and MVPs

The ICMV platform was synthesized according to the previous protocol with some modifications.[8] In brief, MBP-PE and DOPC (1:1, m/m) plus varying amounts of MPLA were dissolved in chloroform and dried under reduced pressure to form the lipid film in a glass vial, which was then hydrated in the Bis-Tris buffer (pH 7.4) containing proteins (400 μg OVA or 40 μg GP / 1.26 μmol of total lipids) at room temperature for 1 h under intermittent vortex, followed by brief sonication, addition of $CaCl_2$ solution (40 μl of 0.2 M solution / 1.26 μmol of total lipids) and DTT (4 μl of 0.15 M solution / 1.26 μmol of total lipids), and incubation at 37 ^{o}C for 1 h to promote complexation and cross-linking. The resulting particles were washed by centrifuge (20817 ×g, 5 min) for three times, dispersed by brief sonication, and stored at 4 ^{o}C before use. To synthesize the MVP, lipids composed of DOTAP, DOPC, DOBAQ-MAL (1:0.5:0.5, m/m) plus MPLA were dried to form the lipid film, which was then hydrated with proteins (50 μg OVA or 40 μg GP / 1.26 μmol of total lipids) dissolved in the PBS buffer (pH 7.4) at room temperature for 1 h under intermittent vortex, followed by brief sonication, addition of HA-SH (200 μg / 1.26 μmol of total lipids), and incubation at 37 ^{o}C for one hour under 700 rpm constant shaking to promote complexation and crosslinking. The resulting particles were then washed and stored similarly as ICMV. For fluorescent probe-labeled and MPLA alone-loaded particles, a small portion of DOPC in the lipid composition was replaced by TF-PC, and particles were hydrated in buffers without proteins.

Particle size and surface charge were measured by the dynamic laser scattering

(DLS) using Zetasizer Nano (Malvern, UK). The encapsulation efficiency of proteins was measured by SDS-PAGE followed by Coomassie Blue staining. Lamellarity of MVPs was measured as previously.[14] *In vitro* leakage of the encapsulated protein antigen was measured by a fluorescence-based assay. In brief, particles loaded with Alexa Fluor 647-labeled OVA (OVA-AF647) or soluble OVA-AF647 (control) were added into a 300 kD MWCO dialysis tube (Spectrum G235060) and incubated in PBS supplemented with 10% or 50% fetal bovine serum (FBS) at 37 ^{o}C under constant shaking at 120 rpm. Samples outside the dialysis tube were collected at pre-determined time points within one week and quantified for fluorescence intensity using a plate reader (Synergy Neo, BioTek, USA).

To determine the display of proteins on the surfaces of MVPs, OVA-loaded and DiD-labeled (0.1% mol of total lipids) particles were stained by an anti-OVA-FITC antibody (Abcam ab85584, 1:100 dilution) at room temperature for 1 h, followed by multiple washing using an airfuge (200000 ×g, 10 min). The pellet was resuspended in 1% Triton PBS, and measured for fluorescence intensity at Ex/Em = 488/520 (FITC) nm and 650/680 nm (DiD) using a plate reader. Ebola GP-loaded particles were first stained by a mouse 13C6 primary antibody (provided by Dr. Christopher L. Cooper, USAMRIID, 1:100 dilution), followed by washing and staining with a goat anti-mouse IgG-PE secondary antibody (eBioscience 12-4010-87, 1:50 dilution), and measured for fluorescence intensity as above.

3.3.4. Activation of DCs by MPLA-loaded ICMVs and MVPs in vitro

BMDCs were prepared according to a previous protocol,[15] and used within days 7-11 of culture. DCs were seeded into a 24-well plate at 2×10^5 cells / well, treated with soluble MPLA, ICMVs or MVPs with or without MPLA loading at 0.5 ug/ml MPLA for 24 h. Cells were then collected and measured for expression of CD86 (eBioscience 12-0862) by flow cytometry (CytoFLEX, Beckman Coulter, USA). Cell culture supernatant was also collected for measurements of DC secretion of TNF-α and IL-6 by ELISA.

3.3.5. Antigen uptake and processing by BMDCs in vitro

For antigen uptake studies, DCs were seeded into a 24-well plate at 2×10^5 cells / well, and incubated with TF-PC-labeled (0.2% mol of total lipids), MPLA-loaded ICMVs or MVPs at 0.5 ug/ml MPLA for 24 h, followed by measurement of fluorescence intensity among $CD11c^+CD44^{high}$ and $CD11c^+CD44^{low}$ DC populations by flow cytometry. For antigen processing studies, ICMVs and MVPs were loaded with MPLA and DQ-OVA (OVA labeled with a self-quenched fluorescent probe, which will fluoresce upon protein degradation), and added to DC culture at a dose of 2 μg DQ-OVA and 0.25 μg MPLA / 2×10^5 cells, followed by incubation for 24 h and measurement of fluorescence intensity in DCs by flow cytometry. A soluble mixture of DQ-OVA and MPLA was also included

as a control group. Antigen processing was also confirmed by confocal microscopy. In brief, DCs were seeded on glass coverslips put into a 24-well plate and incubated with the soluble mixture of DQ-OVA and MPLA, DQ-OVA/MPLA ICMVs, or DQ-OVA/MPLA MVPs at 1 μg DQ-OVA and 0.2 μg MPLA / 2×10^5 cells for 24 h, followed by washing and staining of cells with 0.1 μM Lysotracker (ThermoFisher L7528) and 1 μg/ml Hoechst 33342 (ThermoFisher H3570) at 37 ^{o}C for 1 h. Cells were then fixed using 4% paraformaldehyde solution, coated on a glass slide using the ProLong Diamond Antifade Mountant (ThermoFisher P36965), and visualized using a confocal microscope (Nikon A1, USA).

3.3.6. Draining and DC uptake of ICMVs and MVPs in lymph nodes

All animal experiments were performed under approval from the Institutional Animal Care and Use Committee (IACUC) at the University of Michigan. TF-PC-labeled (2% mol of total lipids) ICMVs or MVPs were subcutaneously injected into the tail base of C57BL/6 mice (six-week-old, female, n = 3, Envigo, USA) under the same fluorescence dose. On days one and three, inguinal lymph nodes (LNs) were collected and visualized using the IVIS (PerkinElmer, USA). LNs were then dissociated with 1 mg/ml collagenase IV (Sigma-Aldrich C5138) and 100 U/ml DNase I (Sigma-Aldrich D4263) at 37 ^{o}C for 30 min under constant shaking, followed by washing with FACS buffer (1% BSA in PBS,

1500 ×g, 5 min), blocking with an anti-CD16/32 antibody (eBioscience 14-0161) at room temperature for 10 min, and staining with CD44 (BD 560569) and CD11c (Biolegend 117309) at 4 ^{o}C for 30 min. Cells were then washed with FACS buffer and resuspended in 2 μg/ml DAPI (Sigma-Aldrich D9542) and measured for the percent of $CD11c^{+}CD44^{+}$ population among $DAPI^{-}$ or $DAPI^{-}particle^{+}$ populations by flow cytometry.

3.3.7. Proliferation of antigen-specific $CD4^{+}$ T cells in vivo

$CD45.1^{+}$ C57BL/6 mice (six-week-old, female, n = 3, The Jackson Laboratory, USA) were intravenously transferred with 3×10^{5} naïve $CD4^{+}$ T cells isolated from $CD45.2^{+}$ OT-II mice (kindly provided by Dr. Lonnie Shea, University of Michigan) using an EasySep™ kit (STEMCELL 19765). One day later, recipient mice were immunized with PBS, soluble OVA + MPLA, OVA/MPLA ICMVs, or OVA/MPLA MVPs at 10 μg OVA and 2 μg MPLA / mouse. One week later, splenocytes from recipients were collected and stained with CD4 (BD 560569) and CD45.2 (BD 561874) for quantification of the percent of transferred $CD45.2^{+}$ cells among total $CD4^{+}$ splenocytes using flow cytometry.

3.3.8. Immunization studies

For studies using the OVA antigen, C57BL/6 mice (n = 5-7) were immunized s.c. with PBS, soluble OVA and MPLA, OVA/MPLA ICMVs, or OVA/MPLA MVPs every three

weeks for three doses. Each dose was composed of 10 μg OVA and 2.5 μg MPLA. At one week after the 1st and 2nd doses and 17 weeks after the 3rd dose, splenocytes were collected and purified using the lymphocyte separation medium (Lonza 17-829), seeded into the IFN-γ ELISPOT plate (BD 551083) at 2×10^5 cells / well, and cultured with 20 μg/ml $OVA_{257-264}$ or $OVA_{323-339}$ peptide for 18 h. $IFN\gamma^+$ spots were measured according to the manufacture protocol (BD 551083). At 17 weeks after the 3rd dose, blood was also collected for quantification of the percent of peripheral OVA-specific $CD8^+$ T cells using a SIINFEKL-$H2K^b$-PE tetramer (MBL, USA).[16] Under the same immunization scheme, sera were collected at three weeks after each dose and nine weeks after the 3rd dose for analysis of serum titers of anti-OVA total IgG, IgG_1, and IgG_{2c} by ELISA. Titers were designated as the reciprocal of the highest dilution factors with OD_{450} values at least two times higher than the background values obtained from the PBS immunization group.

For studies using the Ebola GP antigen, C57BL/6 mice (n = 3-5) were immunized s.c. with PBS, soluble GP and MPLA, GP/MPLA ICMVs, or GP/MPLA MVPs every three weeks for two doses. Each dose was composed of 3 μg GP and 2.5 μg MPLA. Splenocytes were collected at one week after the second dose, re-stimulated *ex vivo* with 4 μg/ml of a GP-derived WE15 peptide (sequence: WIPYFGPAAEGIYTE), and quantified for GP-specific IFN-γ^+ T cells or B cells by ELISPOT. Re-stimulated splenocytes were also quantified for the percent of intracellular TNF-α^+ or IFN-γ^+ by flow cytometry. In another study, mice (n = 10) received a single vaccine dose, followed

by serum collection two weeks later for analysis of anti-GP IgG titers by ELISA. Immunized mice were challenged i.p. with 1000 pfu of a mouse-adapted Ebola virus strain (ma-EBOV) one month later, and monitored for animal survival.

3.3.9. Statistical analysis

Data were analyzed by unpaired *t*-test, or one- or two-way analysis of variance (ANOVA) followed by the *Bonferroni's* post-test for comparison of multiple groups using the Prism 5.0 (GraphPad Software). *P* values less than 0.05 were considered statistically significant. All values are presented as mean ± SEM with indicated sample size.

3.4. Results and discussion

3.4.1. Design and synthesis of the multilamellar vaccine particles (MVPs)

We previously developed the ICMV platform for successful encapsulation and delivery of subunit protein antigens.[17-18] Although loading of lipoid molecules, such as the adjuvant MPLA, into the multi-lipid layer nanostructure enhanced immune stimulation, there was an only moderate increase in antigen-specific T cell immune responses *in vivo* by OVA/MPLA ICMVs compared to unilamellar and multilamellar liposomal vaccines. In the current work, we purpose the optimized MVP platform by incorporating a functional

biopolymer, thiolated hyaluronic acid (HA-SH), as the cross-linker of inter-lipid layers as well as a surface ligand to achieve targeted delivery to antigen-presentation cells, thus improving antigen-specific T cell immune responses. As shown in the schematic illustration in **Figure 3.1**, compared to the ICMV platform, there are two major differences in the design of the MVP delivery system: (1) cationic lipids including DOTAP and DOBAQ-MAL were employed in the lipid composition to facilitate encapsulation of protein antigens which were negatively charged; and (2) lipid bilayers were cross-linked and further stabilized by the polymer thiolated hyaluronic acid (HA-SH). The adjuvant MPLA was similarly incorporated into the lipid portion of both platforms.

We first synthesized the functional lipid DOBAQ-MAL using the EDC/NHS chemistry (**Figure 3.2A**). DOBAQ was successfully modified with a maleimide group, as shown by the results of thin layer chromatography (**Figure 3.2B**) and ^{1}H-NMR (**Figure 3.3**), with the reaction rate of 95% as determined by high-performance liquid chromatography (**Figure 3.2C**). We then formulated OVA/MPLA co-loaded ICMVs and MVPs, which were ~ 150 nm and ~ 280 nm in diameter, respectively, and both showed negative surface charges (**Table 3.1**). The conversion of particle surface charge from the positive liposomes to the negative lipid/HA-SH hybrid particles also demonstrated surface coating of MVPs by the HA polymer. The Ebola GP-loaded MVPs showed an increased particle size of ~ 350 nm in diameter (**Table 3.1**), possibly due to a larger

molecular size of the GP antigen (monomer Mw 150 kD) than OVA (43 kD). We determined the multilamellar structure of MVPs by a lamellarity assay as reported previously,[14] showing decreased values from 0.57 for unilamellar liposomes to 0.39 for MVPs, suggesting a decrease of the fraction of lipids exposed on the outer layer (**Table 3.2**).

3.4.2. MVPs stably encapsulate and display protein antigens

We next measured encapsulation efficacy (EE%) of protein antigens by MVPs using SDS-PAGE followed by Coomassie blue staining. Mean EE% of OVA and GP were ~ 18% and ~ 36%, respectively (**Table 3.3**), corresponding to ~ 9 μg OVA or ~ 15 μg GP / mg lipids. Further, protein antigen was stably loaded in both ICMVs and MVPs, demonstrated by ~ 10% or ~ 20% leakage of the loaded protein from particles following one-week incubation in 10% or 50% serum-containing media, respectively (**Figure 3.4**).

Since recognition and internalization of antigens by B cell receptors is the prerequisite for B cell activation and production of antigen-specific antibodies,[19] we confirmed the display of protein antigens on the surfaces of MVPs by an immunofluorescence assay (**Figure 3.5A**). The same amount of MVPs (indicated by the same recovery rate of the particle fluorescence) loaded with or without OVA was stained by a fluorophore-labeled, anti-OVA antibody. The OVA-loaded particle showed 6.6-fold

higher antibody fluorescence intensity than the particle without protein loading (**Figure 3.5B**), suggesting successful antigen display. GP was also displayed on the surfaces of GP-loaded MVPs, indicated by a 2.6-fold higher antibody fluorescence intensity than the empty particle (**Figure 3.5C**).

3.4.3. Adjuvant MPLA activates DCs

To enhance DC activation and promote antigen-specific immune responses, we employed MPLA, a Toll-like receptor four agonist which has been intensively investigated in clinical trials and approved for use in vaccine products.[20-21] Compared to soluble MPLA, both MPLA-loaded ICMVs and MVPs significantly ($p < 0.001$) up-regulated expression of the maturation marker CD86 in DCs (**Figure 3.6A**). We also measured the release of inflammatory cytokines from the DC culture. Both empty ICMVs and MVPs were not immunostimulatory, while the incorporation of MPLA induced significant DC release of TNF-α (**Figure 3.6B**) and IL-6 (**Figure 3.6C**), demonstrating the potent DC activation driven by the MPLA adjuvant.

3.4.4. MVPs preferentially accumulate in $CD44^{high}$ DCs

We next compared engulfment of ICMVs and MVPs by DCs using the fluorescent probe-labeled particles. Compared to ICMVs, MVPs significantly ($p < 0.001$) enhanced

DC uptake of particles, showing an average 4.6-fold and 1.4-fold increase in fluorescence intensity among $CD44^{high}$ (**Figure 3.7B**) and $CD44^{low}$ (**Figure 3.7C**) DC populations, respectively. The preferential accumulation of MVP in the $CD44^{high}$ population might be due to the HA coated on the particle surface, as HA is a natural ligand of CD44, and has been employed to modify nanoparticle platforms to improve delivery of antigens and/or adjuvants to DCs.[22-23] We also investigated accumulation of ICMVs and MVPs in DCs in draining lymph nodes (dLNs) following subcutaneous administration. Although the overall accumulation of particles in dLNs was similar between ICMVs and MVPs within three days after administration (**Figure 3.8**), there was significantly ($p < 0.05$, an average three-fold) more $CD44^{+}$ DCs engulfing MVPs than ICMVs on day one (**Figure 3.7D, F**), while ICMVs achieved a similar accumulation level in $CD44^{+}$ DCs as MVPs on day three (**Figure 3.7E, F**). Overall, surface decoration of HA increased the accumulation of MVPs in CD44-expressing DCs both *in vitro* and *in vivo*.

3.4.5. MVPs promote processing of protein antigens by DCs

We then investigated impacts of a higher level of DC uptake of MVPs than ICMVs on intracellular processing of the particle-loaded protein antigen. Particles were co-loaded with MPLA and DQ-OVA, OVA labeled with a self-quenched fluorescent dye which will fluoresce upon protein degradation. Compared to the soluble mixture and ICMVs, MVPs

significantly ($p < 0.001$) enhanced intracellular processing of DQ-OVA, demonstrated by an average four-fold increase of fluorescence intensity in DCs (**Figure 3.9A**). These results were further confirmed by confocal microscopy. The strong fluorescence signal from MVP-treated DCs was observed both inside and outside lysosomes (**Figure 3.9B**), suggesting promotion of antigen presentation by both MHC-II and MHC-I, and following activation of $CD4^+$ and $CD8^+$ T cell immune responses, respectively.[24]

3.4.6. MVPs elicit stronger antigen-specific T cell immune responses than ICMVs

To compare immune activation elicited by ICMVs and MVPs, we performed immunization studies using the model antigen OVA. Naïve mice were subcutaneously immunized with three doses of vaccine particles every three weeks (**Figure 3.10A**), and tested for antigen-specific $CD8^+$ and $CD4^+$ T cell immune responses by re-stimulating splenocytes *ex vivo* with the OT-I and OT-II peptides, respectively, and quantifying IFN-γ^+ cells by an ELISPOT assay. After the first dose, both OVA/MPLA co-loaded ICMV and MVP elicited significantly ($p < 0.05$ and 0.001, respectively) more OVA-specific $CD8^+$ T cells than the soluble mixture of OVA and MPLA, with the MVP group showing a further ~ two-fold increase than the ICMV group (**Figure 3.10B**). Only OVA/MPLA MVPs elicited significantly ($p < 0.05$) more OVA-specific $CD4^+$ T cells than the soluble vaccine, while showing an insignificant increasing trend compared to the

ICMV group (**Figure 3.10E**). The levels of antigen-specific T cells were maintained after the second dose, while only MVPs eliciting significantly more OVA-specific $CD8^+$ ($p < 0.001$) and $CD4^+$ ($p < 0.01$) T cells than the soluble vaccine (**Figure 3.10C, F**), and still eliciting ~ two-fold more OVA-specific $CD8^+$ T cells than ICMVs (**Figure 3.10C**). We then performed the third vaccination and analyzed the durability of antigen-specific T cell immune responses elicited by vaccine particles four months later. Immunization with MVPs maintained significantly ($p < 0.05$) and slightly more OVA-specific $CD8^+$ T cells compared to the soluble vaccine and ICMVs, respectively (**Figure 3.10D**). These results were also confirmed in the peripheral blood by staining PBMCs with a SIINFEKL-$H2K^b$-tetramer (**Figure 3.11**). Immunization with MVPs also maintained significantly ($p < 0.05$) more OVA-specific $CD4^+$ T cells than both the soluble vaccine and ICMVs (**Figure 3.10G**).

We further confirmed the activation of antigen-specific $CD4^+$ T cells by an adoptive transfer experiment. Mice bearing the syngeneic marker CD45.1 were transferred with OT-II T cells, then vaccinated with OVA and MPLA in soluble or particle forms, and analyzed for the proliferation of transferred T cells in spleen one week later (**Figure 3.12A**). Compared to the soluble vaccine, both ICMV and MVP vaccines induced significantly ($p < 0.001$) more proliferation of antigen-specific $CD4^+$ T cells, and MVPs showed further significant ($p < 0.01$) increase than ICMVs (**Figure 3.12B,C**). Overall, OVA/MPLA formulated by MVPs elicited stronger antigen-specific $CD8^+$ and $CD4^+$ T

cell immune responses than both soluble and ICMV vaccines.

3.4.7. Both ICMVs and MVPs enhance antigen-specific humoral immune responses

Under the immunization scheme shown in **Figure 3.10A**, we also collected serum at three weeks after each dose and analyzed antigen-specific humoral immune responses by measuring anti-OVA total IgG, IgG_1, and IgG_{2c} titers. Titers of all three IgG subtypes reached the highest plateau after the second immunization with OVA/MPLA ICMVs or MVPs, or after the third immunization of the soluble mixture of OVA and MPLA, with the MVP group eliciting significantly higher titers than the soluble vaccine after the second or third dose (**Figure 3.13**). OVA/MPLA ICMVs and MVPs elicited similar serum anti-OVA IgG titers, which robustly maintained untill at least three months after the final dose.

3.4.8. GP/MPLA MVPs as an effective subunit vaccine against the Ebola disease

Inspired by the promising immune stimulation results by OVA/MPLA ICMVs and MVPs, we tested both platforms for vaccine delivery of a subunit Ebola glycoprotein (GP) antigen,[25] aiming to develop a potent vaccine against this disastrous disease. Although the viral vector-based Ebola vaccine has achieved promising prophylactic efficacy in recent clinical trials,[26] subunit Ebola vaccines may further relieve concerns about reactogenicity

and adverse effects related to the delivery carrier, and facilitate vaccine production and distribution. We formulated GP/MPLA into ICMVs and MVPs, immunized mice every three weeks for two doses, and analyzed antigen-specific T cell immune responses following re-stimulating splenocytes with a GP-derived WE15 peptide (sequence: WIPYFGPAAEGIYTE) *ex vivo* (**Figure 3.14A**). GP/MPLA MVPs elicited significantly ($p < 0.05$) more GP-specific T cells than both the soluble and GP/MPLA ICMV vaccines (**Figure 3.14B**), and enhanced both $CD8^+$ (**Figure 3.14D, E**) and $CD4^+$ (**Figure 3.14F, G**) T cell responses, demonstrated by the staining of intracellular TNF-α (**Figure 3.14D, F**) and IFN-γ (**Figure 3.14E, G**) in splenocytes. All vaccines induced robust levels of GP-specific B cells in the spleen (**Figure 3.14C**).

Further, we performed a viral challenge study in mice vaccinated with a single dose of different GP/MPLA vaccines (**Figure 3.15A**). Similar to results from the OVA immunization study (**Figure 3.13**), both ICMV and MVP vaccines significantly ($p < 0.001$) enhanced serum titers of GP-specific IgG (**Figure 3.15B**). Notably, GP/MPLA MVPs protected 80% of vaccinated mice from the lethal challenge of a mouse-adapted Ebola virus strain, while the survival rate was only 40% and 10% for GP/MPLA ICMVs and the soluble vaccine, respectively (**Figure 3.15C**). These results indicate MVPs elicit robust antigen-specific T cell and B cell immune responses with strong efficacy against viral challenge.

3.5. Conclusion

We developed a new cationic lipid-hyaluronic acid crosslinked nanocarrier MVP for co-delivery of subunit protein antigens and a molecular adjuvant MPLA, which potentiated immune responses by activating DCs. Compared to the previously developed ICMV platform, the hyaluronic acid-coated MVPs increased accumulation and processing of antigens in CD44-expressing DCs, leading to stronger antigen-specific $CD8^+$ and $CD4^+$ T cell immune response *in vivo*. A single dose of the Ebola GP/MPLA co-loaded MVPs protected 80% of mice against the viral infection, suggesting the MVP could be a promising nanocarrier for delivery of subunit protein antigens and facilitate the development of subunit vaccines against emerging infectious diseases.

3.6. Figures and tables

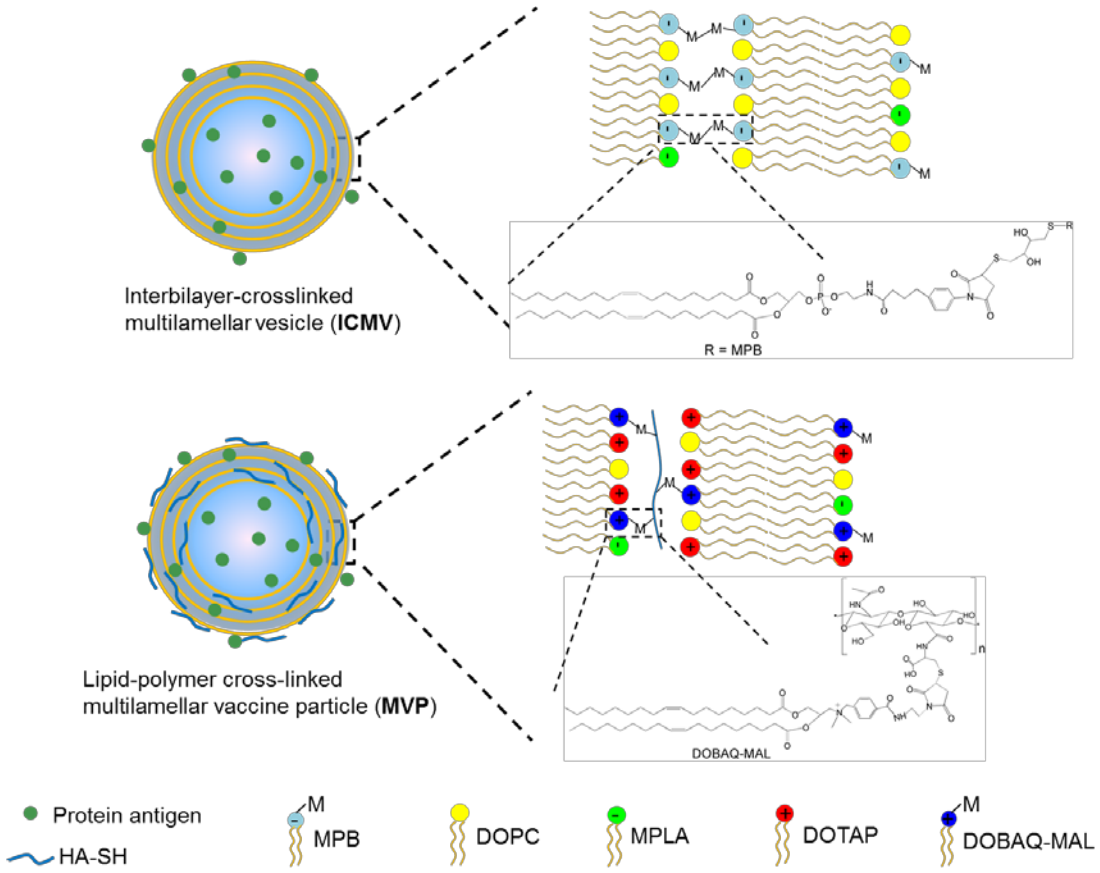

Figure 3.1. Schemes of protein and MPLA co-loaded ICMV and MVP platforms. Lipid bilayers are cross-linked by the small molecule DTT and the thiolated hyaluronic acid (HA-SH) through thiol-maleimide conjugation in the ICMV and MVP, respectively.

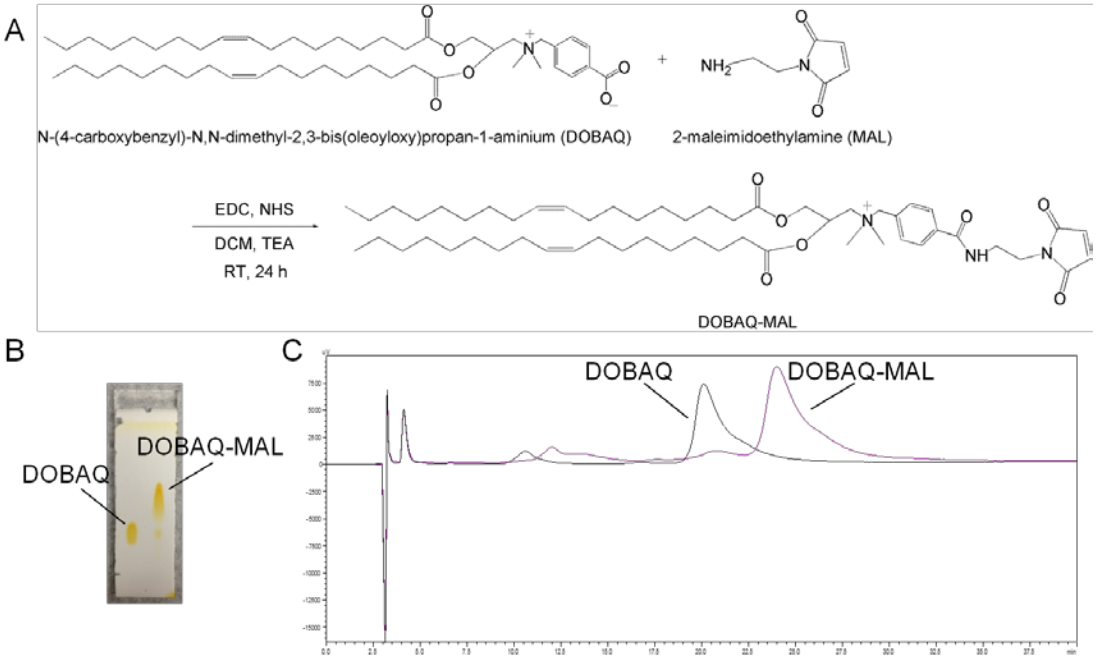

Figure 3.2. Synthesis of DOBAQ-MAL. **(A)** Synthesis scheme. DOBAQ was modified with maleimide via EDC/NHS chemistry. **(B)** Thin layer chromatography (TLC) and **(C)** high performance liquid chromatography (HPLC) show successful modification of maleimide to DOBAQ, with reaction efficiency = 95.0 ± 1 % (mean ± SEM, n = 3) calculated by peak areas from HPLC results.

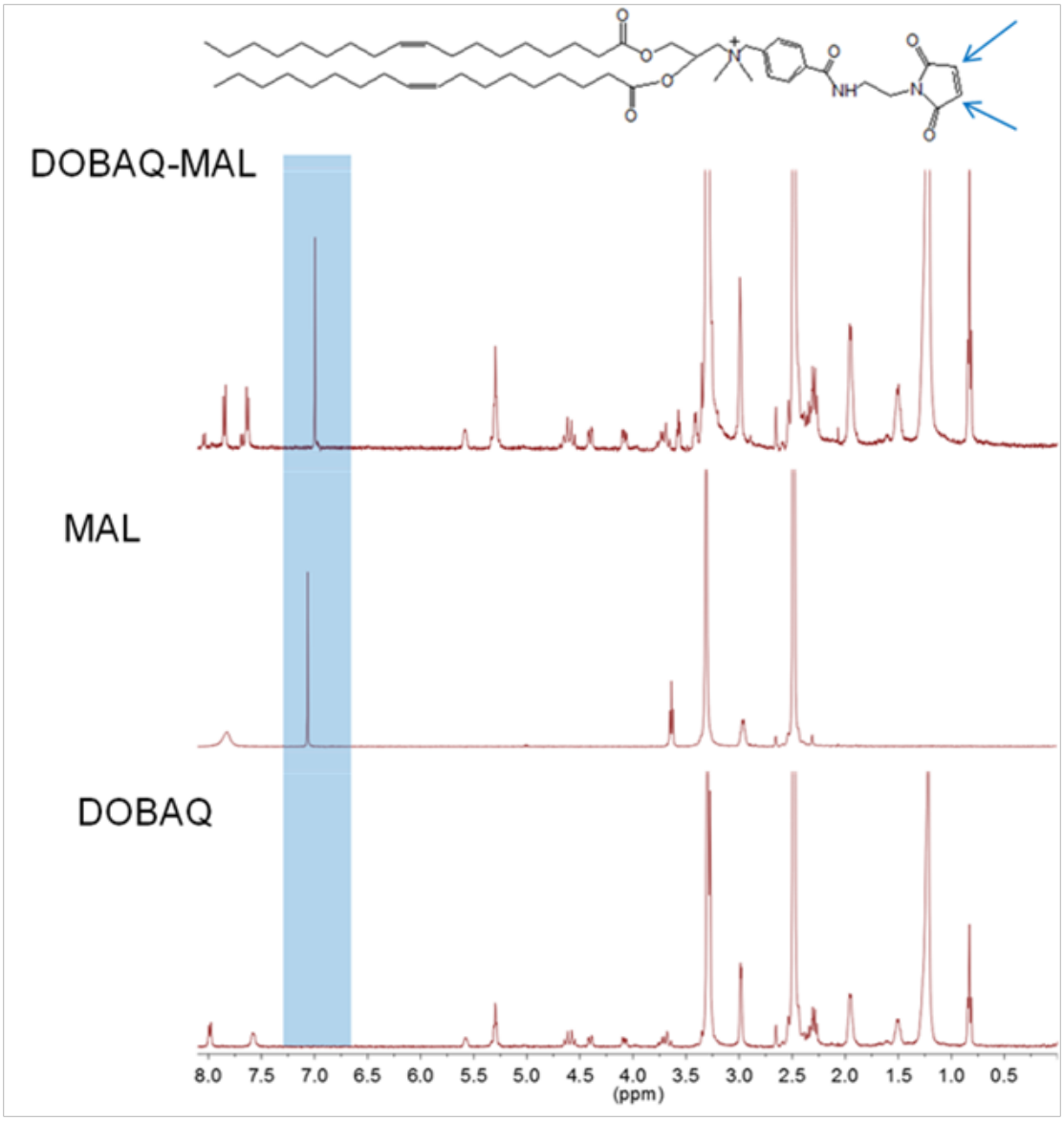

Figure 3.3. ^{1}H-NMR identification of DOBAQ-MAL, MAL, and DOBAQ. The shaded area indicates the characteristic peak of hydrogen atoms in the maleimide group.

Table 3.1. Particle size and surface charge of protein/MPLA co-loaded ICMVs and MVPs. Results are reported as mean ± SEM, *n* = 3.

Particle types	Z-average (nm)	PDI	Zeta (mV)
OVA/MPLA ICMV	153 ± 2	0.173 ± 0.004	-31.8 ± 0.8
Unilamellar liposome*	128 ± 20	0.266± 0.05	19.5 ± 0.2
MPLA MVP	225 ± 10	0.149± 0.01	-17.8 ± 0.4
OVA/MPLA MVP	284 ± 40	0.179 ± 0.03	-18.0 ± 0.4
Ebola GP/MPLA MVP	351 ± 5	0.256 ± 0.03	-14.0 ± 0.3

* Contains the same lipid composition as MVP but w/o thiolated hyaluronic acid and protein.

Table 3.2. Lamellarity of protein-loaded unilamellar liposomes and MVPs. Results are reported as mean ± SEM, *n* = 3.

Particle type	OVA liposome	OVA MVP
Lamellarity (fraction of exposed lipid)	0.57 ± 0.01	0.39 ± 0.02

Table 3.3. Encapsulation efficiency (EE%) of proteins in MVPs measured by SDS-PAGE followed by Coomassie blue staining. Results are reported as mean ± SEM, *n* = 3.

Particles	OVA/MPLA MVP	GP/MPLA MVP
EE% of protein	17.8 ± 0.6	36.3 ± 1

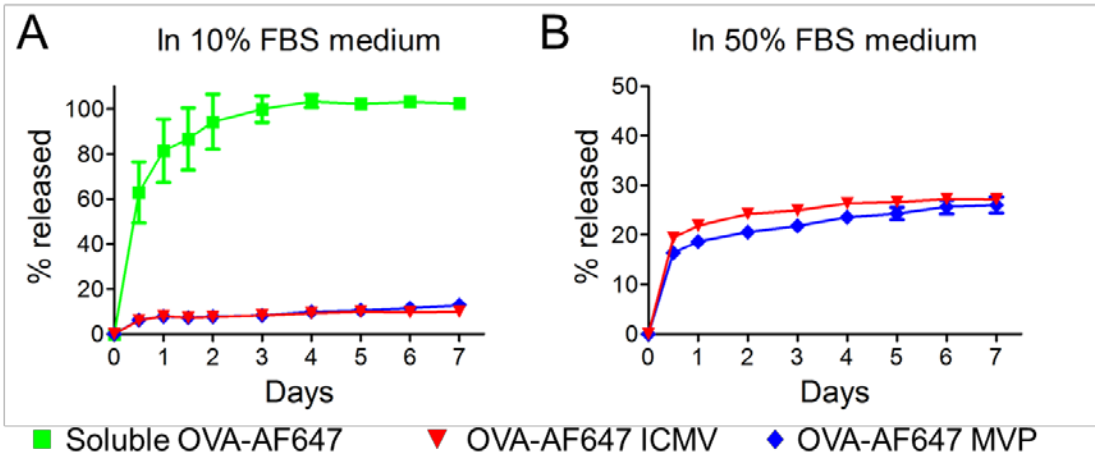

Figure 3.4. Protein antigen is stably encapsulated in ICMVs and MVPs. Leakage of OVA-AF647 from ICMVs and MVPs within one week after incubation in PBS supplemented with 10% **(A)** or 50% **(B)** FBS under constant shaking. Soluble OVA-AF647 was used as the control in **(A)**. Results are presented as mean ± SEM, $n = 3$, except $n = 4$ for the MVP in panel **(B)**.

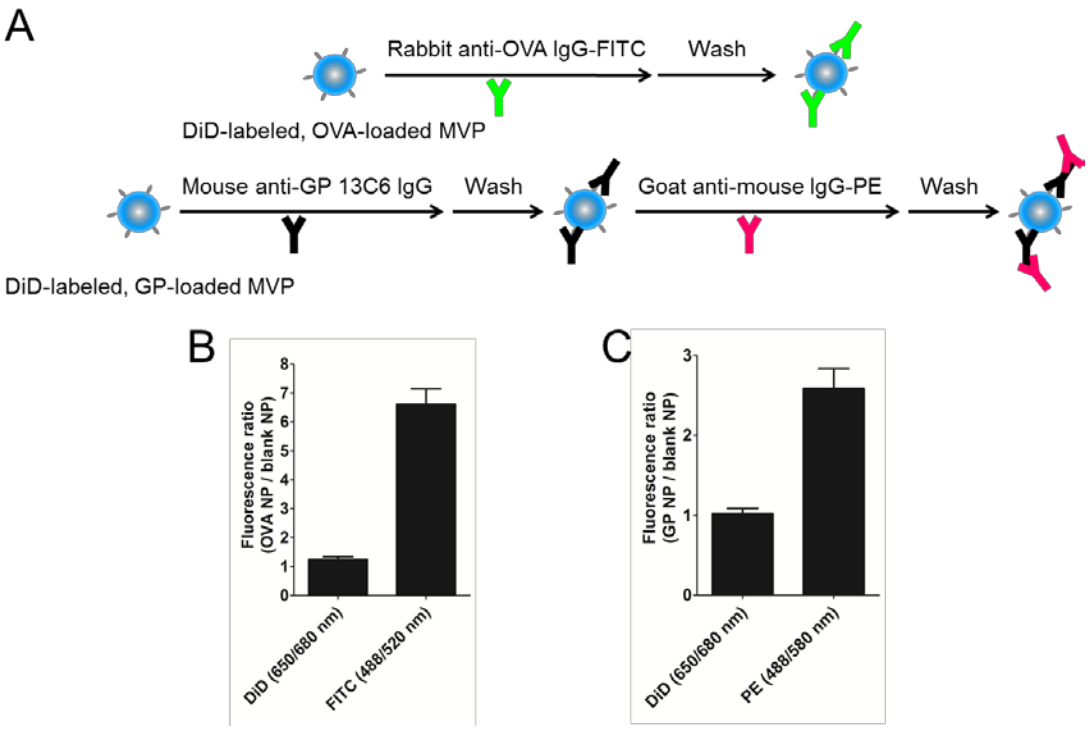

Figure 3.5. Portions of encapsulated proteins are displayed on the MVP surface. **(A)** Experiment scheme. Protein-loaded and DiD-labeled MVPs were stained by a fluorophore-labeled, anti-OVA primary antibody, or an anti-Ebola GP primary antibody and a fluorophore-labeled secondary antibody, and quantified for the ratio of fluorescence intensity between MVP w/ and w/o protein loading (negative control). A DiD fluorescence ratio about one indicated that similar amounts of protein-loaded and empty MVPs were stained, under which circumstance fluorescence ratios of antibodies higher than one indicated the display of OVA **(B)** or GP **(C)** on the MVP surface. Results are presented as mean ± SEM, $n = 3$.

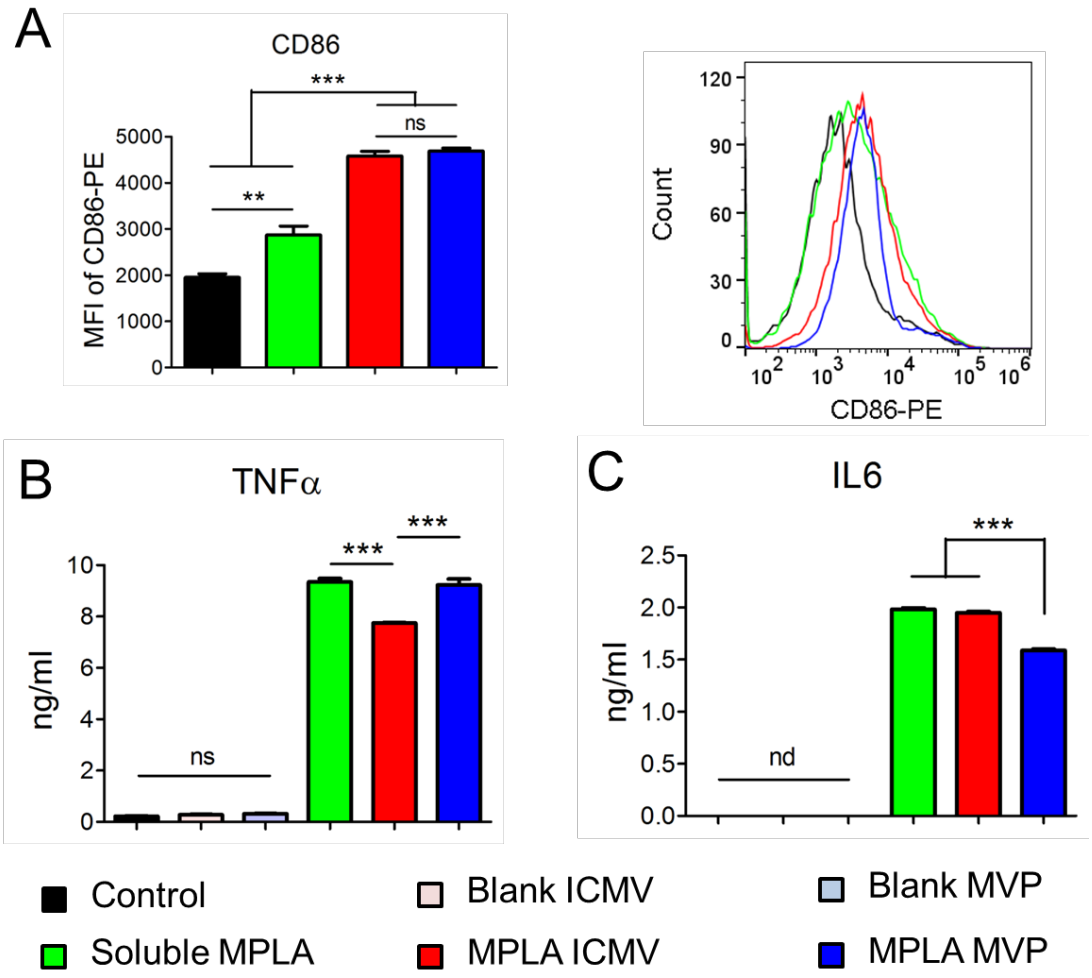

Figure 3.6. MPLA-loaded ICMVs and MVPs activate DCs *in vitro*. BMDCs were treated with soluble MPLA, or ICMVs or MVPs loaded with or without MPLA for 24 h, followed by measurement of DC expression of CD86 **(A)**. Cell culture supernatant was also collected for measurements of DC secretion of TNF-α **(B)** and IL-6 **(C)** by ELISA. Results are presented as mean ± SEM, $n = 3$. ** $p < 0.01$, *** $p < 0.001$, analyzed by one-way ANOVA with Bonferroni multiple comparison post-test; ns, not significant; nd, not detected.

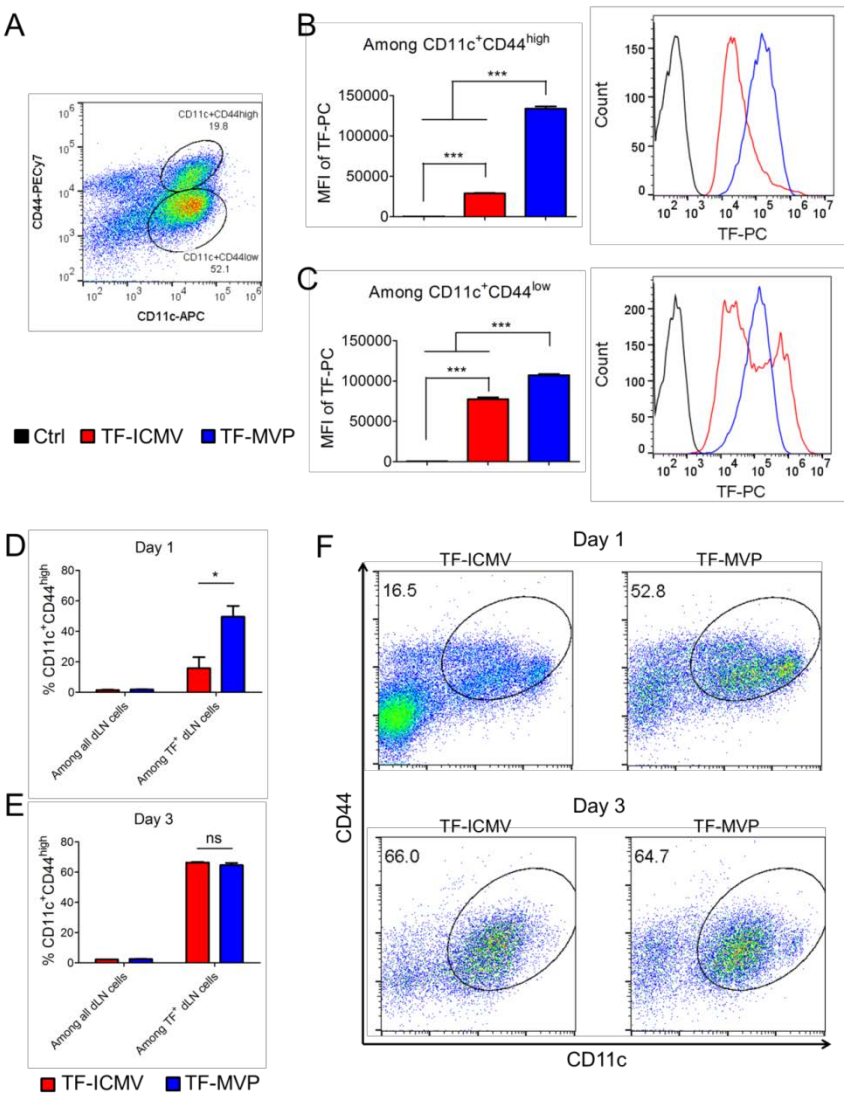

Figure 3.7. MVPs are preferentially engulfed by CD44-expressing DCs. **(A)-(C)** BMDCs were incubated with TopFluor PC (TF-PC)-labeled ICMVs or MVPs for 24 h, followed by quantification of particle uptake by $CD11c^{+}CD44^{high}$ **(B)** and $CD11c^{+}CD44^{low}$ **(C)** DCs using flow cytometry. A representative gating chart of DC populations is shown in **(A)**. **(D)-(F)** C57BL/6 mice were injected with TF-PC-labeled ICMVs or MVPs s.c. at the tail base. Single cell suspension was obtained from dLNs, and quantified for the percent of $CD11c^{+}CD44^{+}$ population among all dLN cells or dLN cells that engulfed particles on days one **(D)** and three **(E)** post injection by flow cytometry. **(F)** Representative flow charts showing the gating and percent of the $CD11c^{+}CD44^{+}$ population among dLN cells that engulfed particles. Results are presented as mean ± SEM, $n = 3$. **(B,C)** *** $p < 0.001$, analyzed by one-way ANOVA with Bonferroni multiple comparison post-test; **(D,E)** * $p < 0.05$, analyzed by unpaired *t*-test.

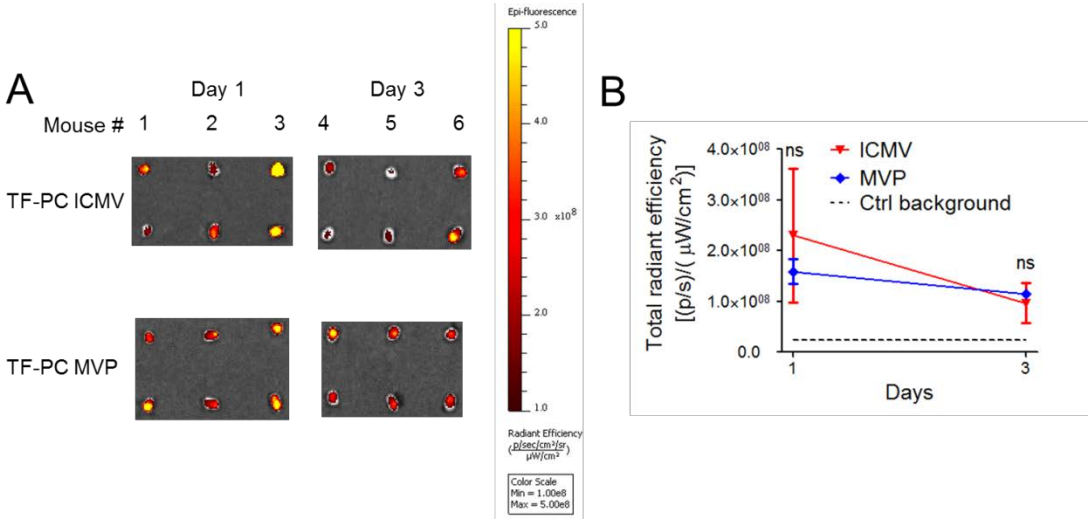

Figure 3.8. ICMVs and MVPs are similarly drained to lymph nodes (LNs). C57BL/6 mice were injected with fluorescent lipid-labeled ICMVs or MVPs s.c. at the tail base. On days one and three post injection, fluorescence intensity in draining LNs (inguinal LNs) was visualized **(A)** and quantified **(B)** by IVIS. Representative results from two independent experiments are presented as mean ± SEM, $n = 3$; ns, not significant.

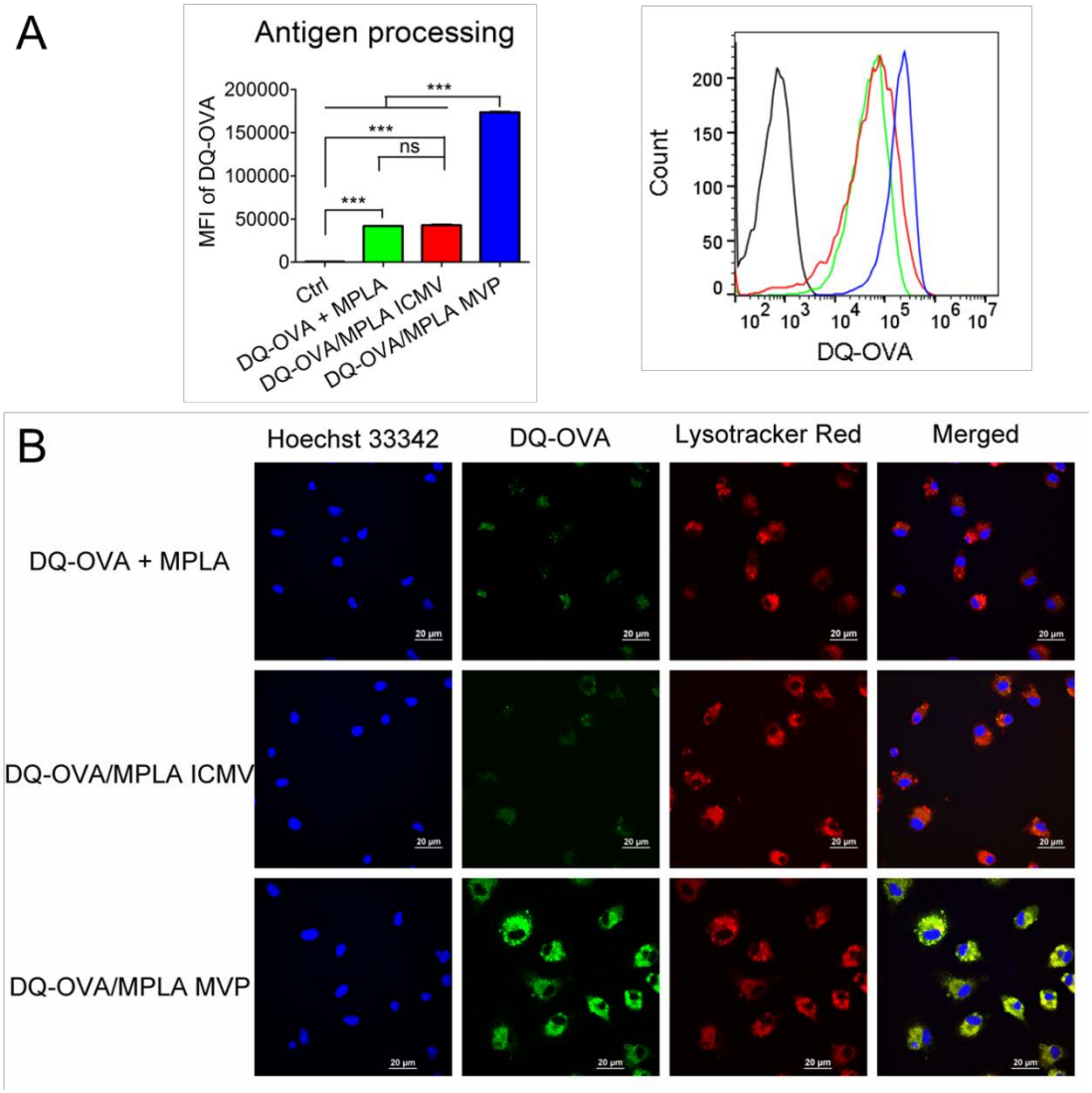

Figure 3.9. MVPs promote antigen processing by DCs *in vitro*. DCs were treated by ICMVs or MVPs co-loaded with MPLA and DQ-OVA (OVA labeled with a self-quenched fluorescent dye, which will fluoresce upon protein degradation) for 24 h, and measured for fluorescence intensity by flow cytometry **(A)** and confocal microscopy **(B)**. Nuclei and lysosomes were stained with Hoechst 33342 and the Lysotracker Red, respectively. Results in **(A)** are shown as mean ± SEM, $n = 3$. *** $p < 0.001$, analyzed by one-way ANOVA with Bonferroni multiple comparison post-test.

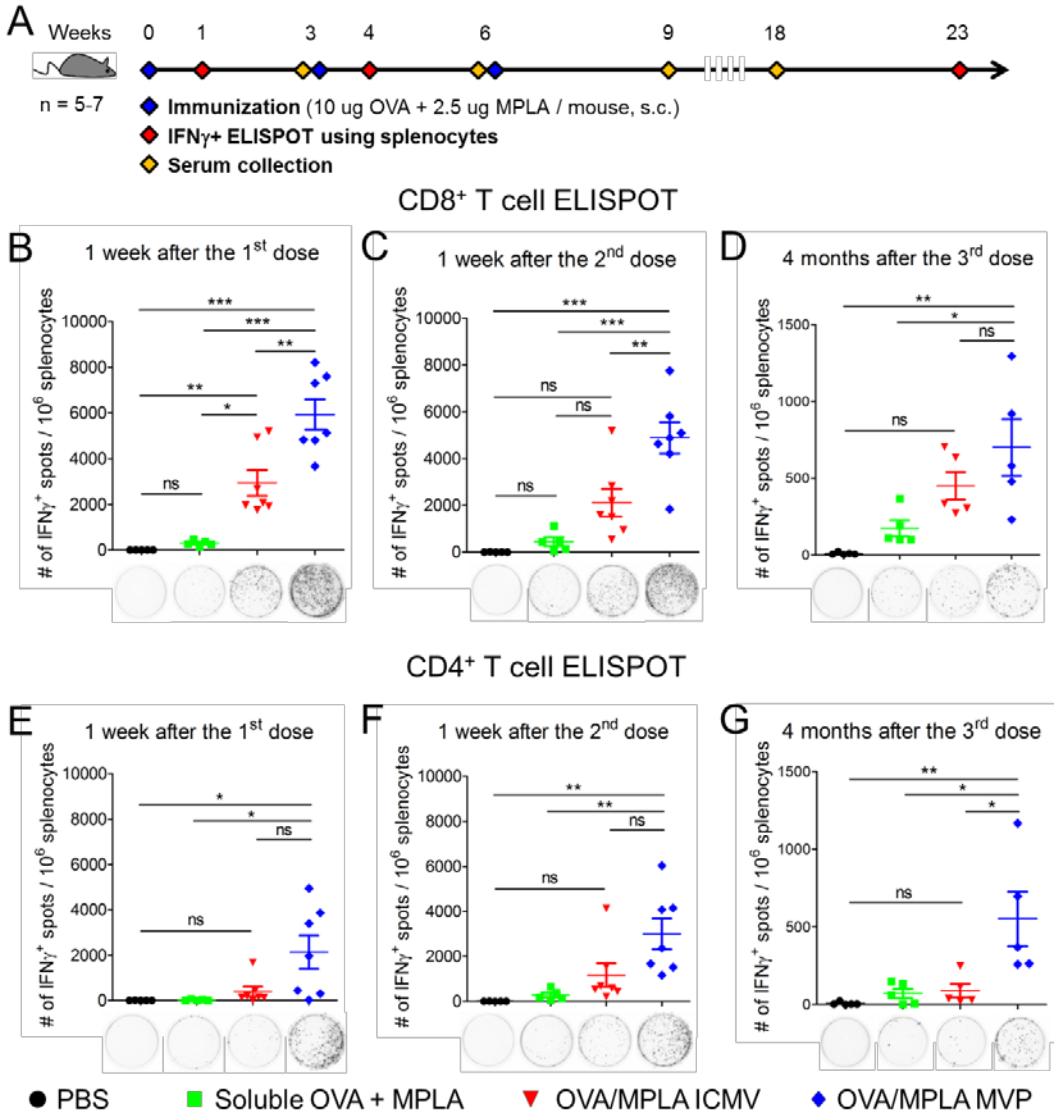

Figure 3.10. OVA/MPLA MVPs elicit stronger antigen-specific T cell immune responses than OVA/MPLA ICMVs *in vivo*. **(A)** Immunization scheme. C57BL/6 mice were immunized s.c. with three doses of PBS, soluble OVA and MPLA, OVA/MPLA ICMVs, or OVA/MPLA MVPs at a three-week interval. Each dose was composed of 10 μg OVA and 2.5 μg MPLA / mouse. At one week after the 1st **(B,E)** and 2nd **(C,F)** doses, and four months after the 3rd dose **(D,G)**, splenocytes were collected and re-stimulated *ex vivo* with the $OVA_{257-264}$ **(B-D)** or $OVA_{323-339}$ **(E-G)** peptide for quantification of IFN-γ^+CD8^+ or IFN-γ^+CD4^+ T cells by the ELISPOT assay, respectively. Results are presented as mean ± SEM, n = 5-7 **(B,C,E,F)**, or n = 5 **(D,G)**. Representative images of individual wells are shown at the bottom of each graph. * $p < 0.05$, ** $p < 0.01$, *** $p < 0.001$, analyzed by one-way ANOVA with Bonferroni multiple comparison post-test.

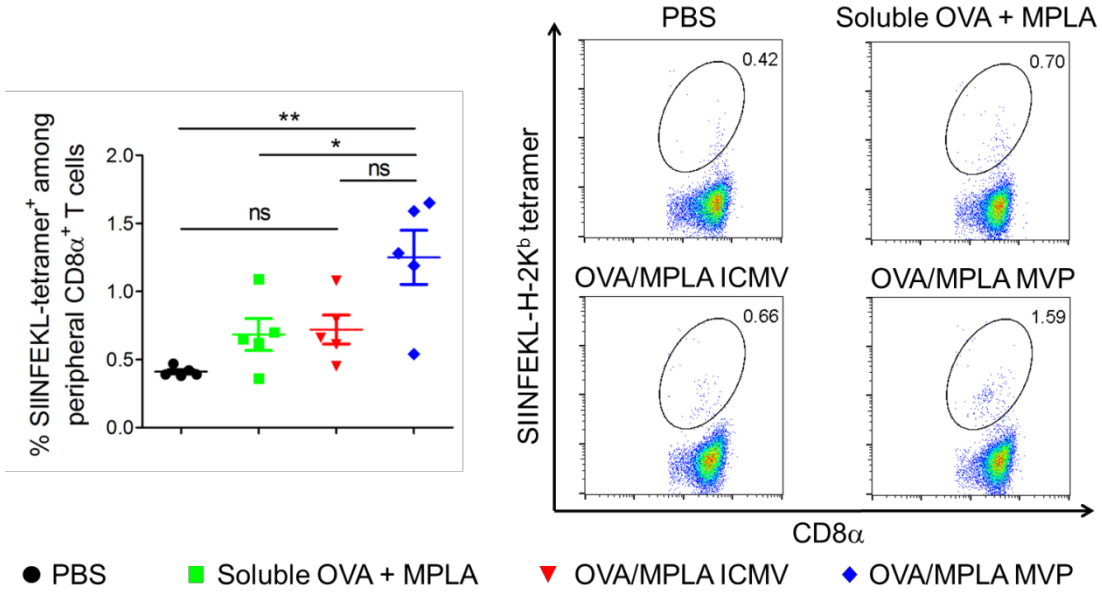

Figure 3.11. Long-term antigen-specific $CD8^+$ T cell response measured by tetramer staining. At four months after the 3rd dose (**Figure 3.10A**), percent of SIINFEKL-specific $CD8^+$ T cells in the peripheral blood was quantified by a tetramer staining assay using flow cytometry. Results are presented as mean ± SEM, $n = 5$. * $p < 0.05$, ** $p < 0.01$, analyzed by one-way ANOVA with Bonferroni multiple comparison post-test.

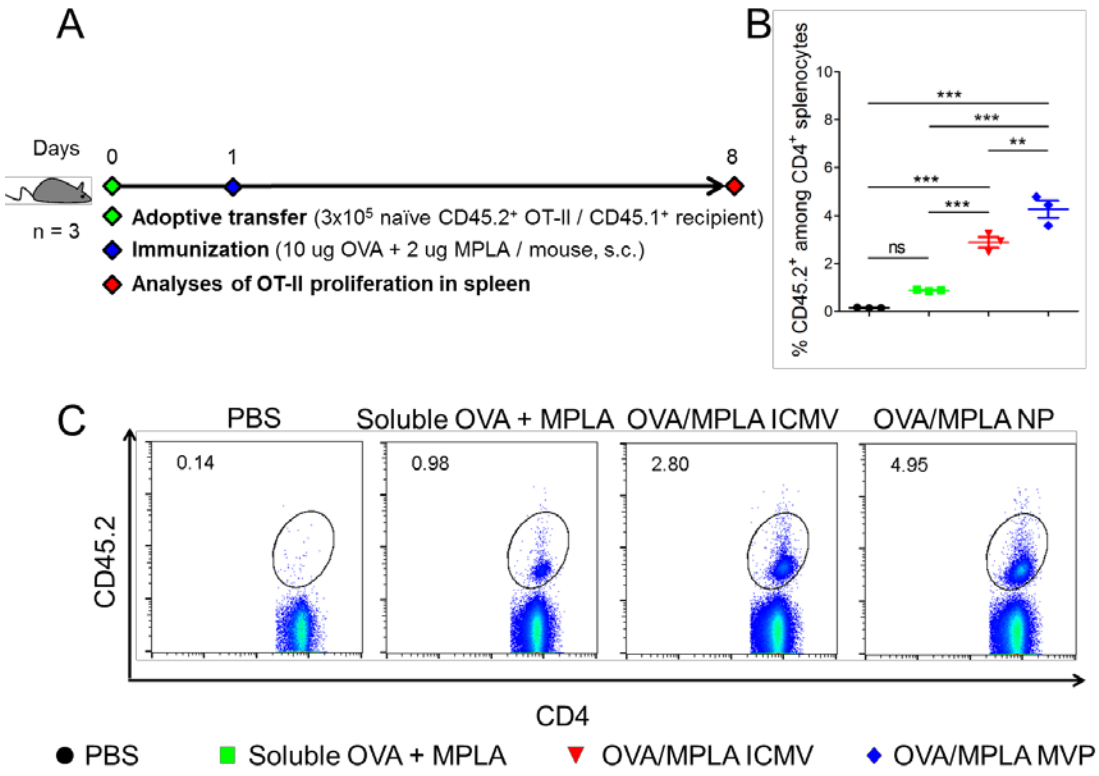

Figure 3.12. OVA/MPLA MVPs elicit stronger proliferation of antigen-specific $CD4^+$ T cells than OVA/MPLA ICMV *in vivo*. **(A)** $CD45.1^+$ C57BL/6 mice were adoptively transferred with naïve $CD45.2^+CD4^+$ T cells ($3x10^5$ / recipient, i.v.) isolated from OT-II mice on day zero, followed by immunization s.c. with different formulations (10 μg OVA and 2 μg MPLA) on day one. One week later, splenocytes from the recipient mice were collected for quantification of proliferation of the transferred OT-II T cells by flow cytometry **(B,C)**. Results are presented as mean ± SEM, $n = 3$. ** $p < 0.01$, *** $p < 0.001$, analyzed by one-way ANOVA with Bonferroni multiple comparison post-test.

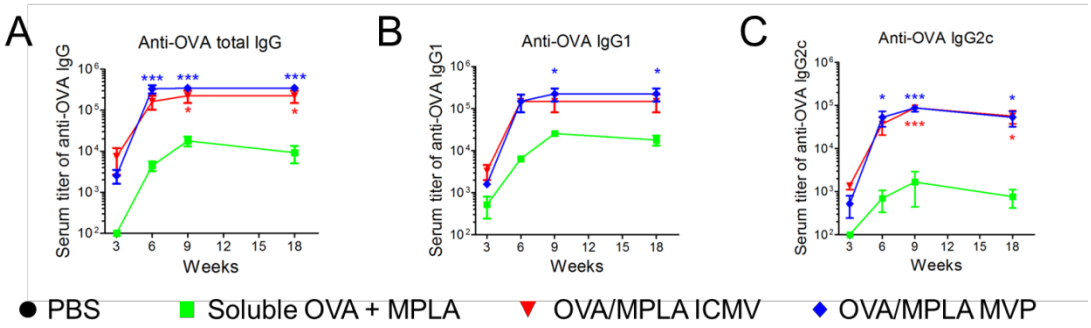

Figure 3.13. OVA/MPLA MVPs and OVA/MPLA ICMVs elicit potent antigen-specific humoral immune responses *in vivo*. C57BL/6 mice were immunized as shown in the **Figure 3.10A**. Sera were collected at three weeks after each dose and three months after the 3rd dose for quantification of serum titers of anti-OVA total IgG **(A)**, IgG_1 **(B)**, and IgG_{2c} **(C)** by ELISA. Results are presented as mean ± SEM, $n = 5$. * $p < 0.05$, *** $p < 0.001$ *vs*. soluble OVA + MPLA, analyzed by two-way ANOVA with Bonferroni multiple comparison post-test.

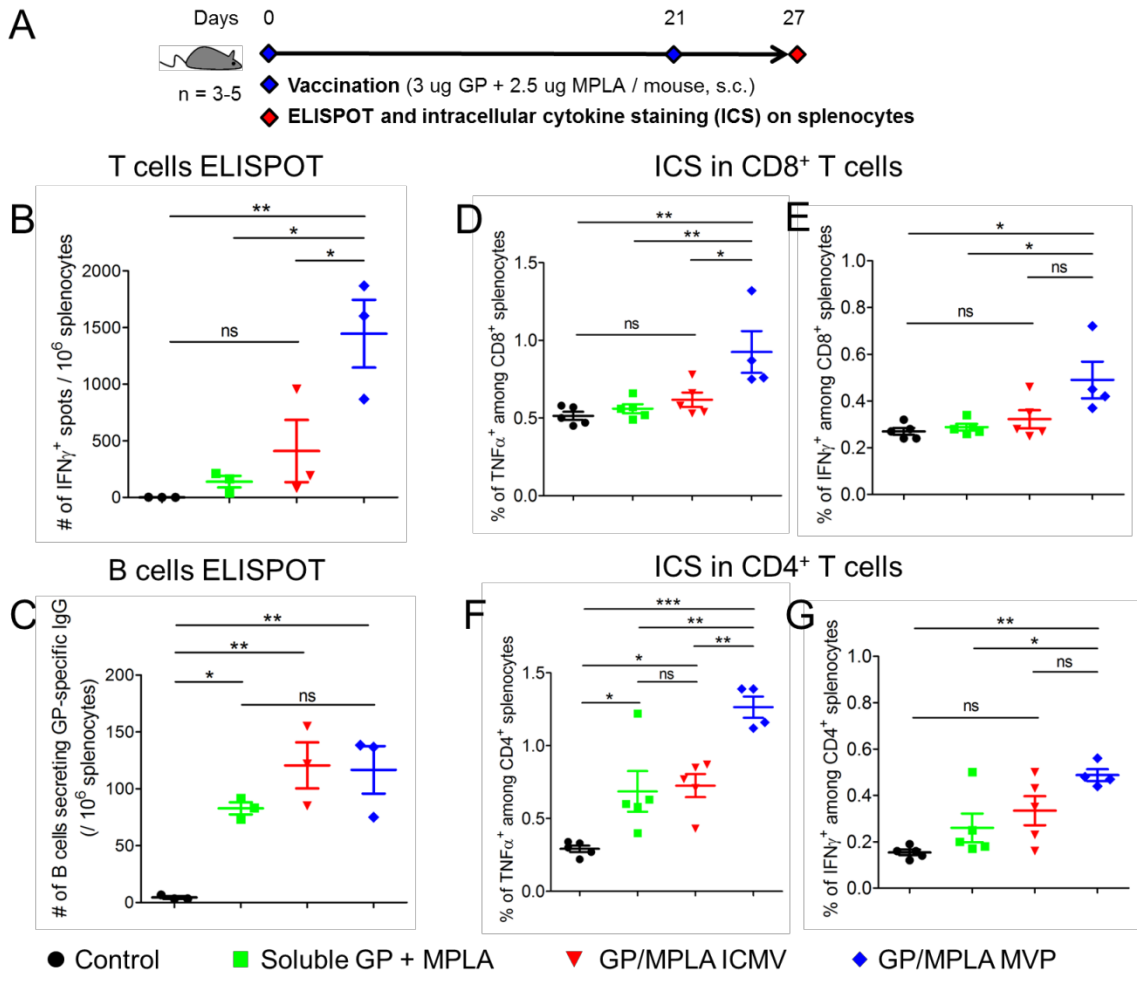

Figure 3.14. Ebola GP/MPLA MVPs elicit stronger GP-specific T cell responses than GP/MPLA ICMVs. **(A)-(G)** C57BL/6 mice were immunized s.c. with soluble GP + MPLA, GP/MPLA ICMVs, or GP/MPLA MVPs on days 0 and 21. Each dose was composed of 3 μg GP and 2.5 μg MPLA / mouse. At one week after the final dose, splenocytes were collected and re-stimulated *ex vivo* for quantification of antigen-specific IFN-γ^+ T cells **(B)** and B cells **(C)** by ELISPOT, and the percent of TNF-α^+ **(D,F)** and INF-γ^+ **(E,G)** among CD8$^+$ **(D,E)** and CD4$^+$ **(F,G)** T cells by intracellular cytokine staining. Results are presented as mean ± SEM, n = 3 **(B,C)**, n = 4-5 **(D,E,F,G)**. * $p < 0.05$, ** $p < 0.01$, *** $p < 0.001$, analyzed by one-way ANOVA with Bonferroni multiple comparison post-test.

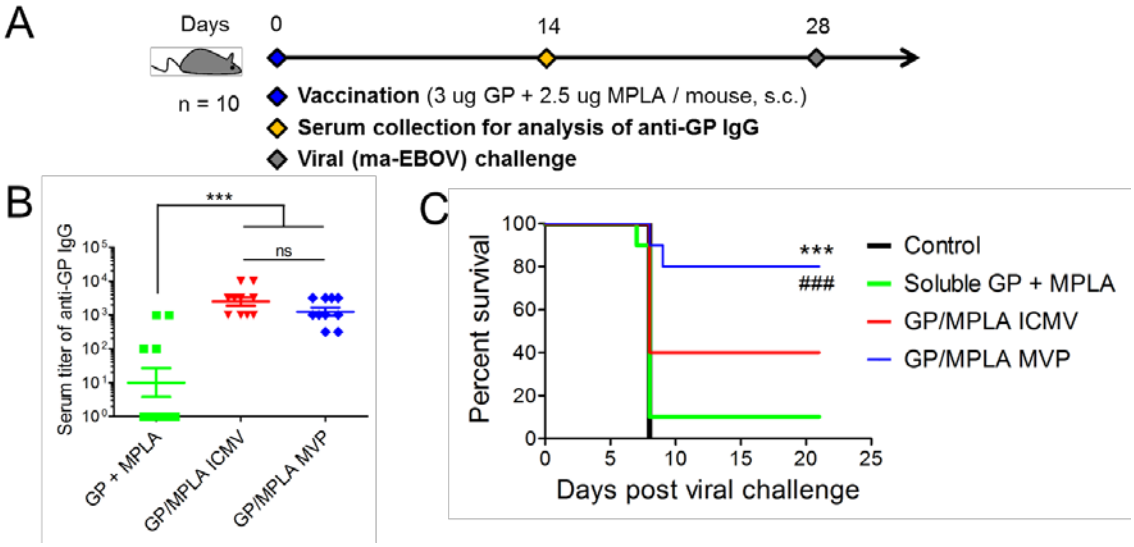

Figure 3.15. Ebola GP/MPLA MVP as a strong prophylactic subunit vaccine. **(A)-(C)** Mice (n = 10) were immunized with a single vaccine dose, followed by collection of serum for analysis of GP-specific IgG titers by ELISA **(B)**, and a viral challenge and monitored for animal survival **(C)**. **(B)** *** $P < 0.001$, analyzed by one-way ANOVA with Bonferroni multiple comparison post-test; **(C)** *** $p < 0.001$ *vs.* the control, $^{###}$ $p < 0.001$ *vs.* the soluble group, analyzed by log-rank (Mantel-Cox) test.

3.7. References

1. Mullan, Z. The cost of Ebola. *Lancet Glob Health* **2015,** *3* (8), e423.

2. Gostin, L. O.; Hodge, J. G., Jr. Zika virus and global health security. *Lancet Infect Dis* **2016,** *16* (10), 1099-1100.

3. Riedel, S. Edward Jenner and the history of smallpox and vaccination. *Proc (Bayl Univ Med Cent)* **2005,** *18* (1), 21-5.

4. Schiller, J. T.; Lowy, D. R. Understanding and learning from the success of prophylactic human papillomavirus vaccines. *Nat Rev Microbiol* **2012,** *10* (10), 681-92.

5. Freed, G. L., *et al.* Parental vaccine safety concerns in 2009. *Pediatrics* **2010,** *125* (4), 654-9.

6. Minor, P. D. Live attenuated vaccines: Historical successes and current challenges. *Virology* **2015,** *479-480*, 379-92.

7. Fan, Y.; Moon, J. J. Particulate delivery systems for vaccination against bioterrorism agents and emerging infectious pathogens. *Wiley Interdiscip Rev Nanomed Nanobiotechnol* **2017,** *9* (1).

8. Moon, J. J., *et al.* Interbilayer-crosslinked multilamellar vesicles as synthetic vaccines for potent humoral and cellular immune responses. *Nat Mater* **2011,** *10* (3), 243-51.

9. Fan, Y., *et al.* Cationic liposome-hyaluronic acid hybrid nanoparticles for intranasal vaccination with subunit antigens. *J Control Release* **2015,** *208*, 121-129.

10. Kuai, R., *et al.* Designer vaccine nanodiscs for personalized cancer immunotherapy. *Nat Mater* **2017,** *16* (4), 489-496.

11. Irvine, D. J., *et al.* Engineering synthetic vaccines using cues from natural immunity. *Nat Mater* **2013,** *12* (11), 978-90.

12. Irvine, D. J., *et al.* Synthetic Nanoparticles for Vaccines and Immunotherapy. *Chem Rev* **2015,** *115* (19), 11109-46.

13. Fan, Y.; Moon, J. J. Nanoparticle Drug Delivery Systems Designed to Improve Cancer Vaccines and Immunotherapy. *Vaccines (Basel)* **2015,** *3* (3), 662-85.

14. Girard, P., *et al.* A new method for the reconstitution of membrane proteins into giant unilamellar vesicles. *Biophys J* **2004,** *87* (1), 419-29.

15. Lutz, M. B., *et al.* An advanced culture method for generating large quantities of highly pure dendritic cells from mouse bone marrow. *J Immunol Methods* **1999,** *223* (1), 77-92.

16. Ochyl, L. J.; Moon, J. J. Whole-animal imaging and flow cytometric techniques for analysis of antigen-specific CD8+ T cell responses after nanoparticle vaccination. *J Vis Exp* **2015,** (98), e52771.

17. Moon, J. J., *et al.* Enhancing humoral responses to a malaria antigen with nanoparticle vaccines that expand Tfh cells and promote germinal center induction. *Proc Natl Acad Sci U S A* **2012,** *109* (4), 1080-5.

18. Li, A. V., *et al.* Generation of effector memory T cell-based mucosal and systemic immunity with pulmonary nanoparticle vaccination. *Sci Transl Med* **2013,** *5* (204), 204ra130.

19. Heesters, B. A., *et al.* Antigen Presentation to B Cells. *Trends Immunol* **2016,** *37* (12), 844-854.

20. Kaczanowska, S., *et al.* TLR agonists: our best frenemy in cancer immunotherapy. *J Leukoc Biol* **2013,** *93* (6), 847-63.

21. Vacchelli, E., *et al.* Trial watch: FDA-approved Toll-like receptor agonists for cancer therapy. *Oncoimmunology* **2012,** *1* (6), 894-907.

22. Sahdev, P., *et al.* Biomaterials for nanoparticle vaccine delivery systems. *Pharm Res* **2014,** *31* (10), 2563-82.

23. Kim, K. S., *et al.* Noninvasive Transdermal Vaccination Using Hyaluronan Nanocarriers and Laser Adjuvant. *Adv Funct Mater* **2016,** *26* (15), 2512-2522.

24. Blum, J. S., *et al.* Pathways of antigen processing. *Annu Rev Immunol* **2013,** *31*,

443-73.

25. Martins, K., *et al.* Cross-protection conferred by filovirus virus-like particles containing trimeric hybrid glycoprotein. *Viral Immunol* **2015,** *28* (1), 62-70.

26. Henao-Restrepo, A. M., *et al.* Efficacy and effectiveness of an rVSV-vectored vaccine in preventing Ebola virus disease: final results from the Guinea ring vaccination, open-label, cluster-randomised trial (Ebola Ca Suffit!). *Lancet* **2017,** *389* (10068), 505-518.

Chapter 4: Lipid-polymer crosslinked nanoparticles for co-localized delivery of immunogenically dying tumor cells and adjuvant for cancer immunotherapy

4.1. Abstract

Despite their potential, conventional whole-cell cancer vaccines prepared by freeze-thawing or irradiation have shown limited therapeutic efficacy in clinical trials. Recent studies have shown that cancer cells treated with certain chemotherapeutics, such as mitoxantrone, can undergo immunogenic cell death (ICD) and initiate anti-tumor immune responses. However, it remains unclear how to exploit ICD for cancer immunotherapy. In this section, we explore the delivery of molecular adjuvants by the MVP platform. In specific, we present a new material-based strategy for converting immunogenically dying tumor cells into a powerful platform for cancer vaccination and demonstrate their therapeutic potential in murine models of melanoma and colon carcinoma. We have generated immunogenically dying tumor cells surface-modified with adjuvant-loaded nano-depots. Dying tumor cells laden with nano-depots efficiently promote activation and antigen cross-presentation by dendritic cells *in vitro* and elicit robust antigen-specific $CD8\alpha^+$ T cells *in vivo*. Furthermore, whole tumor-cell vaccination

combined with immune checkpoint blockade leads to complete tumor regression in ~ 78% of CT26 tumor-bearing mice and establishes long-term immunity against tumor recurrence. Our strategy presented here may open new doors to “personalized” cancer immunotherapy tailored to individual patient’s tumor cells.

4.2. Introduction

While various technologies, including micelles, lipid vesicles, polymers, and inorganic nanomaterials, have been developed as the delivery platforms for cancer vaccination,[1-8] it remains challenging to achieve robust anti-tumor efficacy with therapeutic potential against established tumors. Cancer vaccines employing defined tumor antigens require extensive antigen discovery and optimization processes, but tumor cells can escape the immune pressure by antigen down-regulation and immunosuppression.[9] Notably, recent reports suggest that cancer cells treated with certain anthracyclines undergo immunogenic cell death (ICD),[10-11] during which dying tumor cells release immunostimulatory ‘danger’ signals (e.g. high mobility group box 1 (HMGB1),[12] calreticulin,[13] and ATP[14]) to break immune tolerance and initiate anti-tumor immune responses.[11, 15] While this discovery suggests an entirely new therapeutic approach, it remains unclear how to exploit ICD as a new basis for cancer vaccination. This unmet need is underscored by the limited patient response rates to immune checkpoint blockers (ICBs) that remove immunosuppressive

"brakes" on T cells.[16-17] If we can harness the potency of ICD to initiate anti-tumor immunity against a wide repertoire of antigens released from patients' dying tumor cells and "liberate" anti-tumor T-cells with ICBs, this could lead to a powerful and generalizable strategy for "personalized" cancer immunotherapy.

Here, we present a novel synthetic approach for converting immunogenically dying tumor cells into a versatile platform for cancer vaccination and demonstrate their therapeutic potential in multiple murine tumor models. Specifically, we have utilized immunogenically dying tumor cells as the source of both tumor antigens and 'danger' signals and amplified their potency by surface-modification of dying tumor cells with adjuvant-loaded nano-depots (**Figure 4.1**). We demonstrate that our whole tumor-cell vaccine approach efficiently promotes activation and antigen presentation by antigen-presenting cells (APCs) and elicits strong anti-tumor immune responses in murine models of melanoma and colon carcinoma. Importantly, dying tumor cells laden with adjuvants in combination with ICBs exhibited remarkable therapeutic potential, leading to complete tumor regression and long-term protection against tumor recurrence in ~ 78% of tumor-bearing animals.

4.3. Materials and methods

4.3.1. Synthesis and characterization of lipid-polymer cross-linked nano-depots

Lipid-polymer cross-linked nanoparticles were synthesized using cationic lipids and thiolated hyaluronic acid (HA-SH). Briefly, 0.63 μmol of lipids including DOBAQ-MAL, 1,2-dioleoyl-sn-glycero-3-phosphocholine (DOPC), 1,2-dioleoyl-3-trimethylammonium-propane (DOTAP) at a ratio of 50:25:25 (m/m/m) were dissolved in chloroform and dried under vacuum to form a lipid film, which was then hydrated with PBS and sonicated to produce unilamellar liposomes. One hundred μg of HA-SH and 25 μg of CpG were added to liposomes, followed by incubation for 1 h at 37 ^{o}C with constant shaking to promote complexation and cross-linking between lipids and HA-SH. NPs were centrifuged (20817 ×g, 5 min) and washed three times with PBS, resuspended in PBS, dispersed by brief sonication, and stored at 4 ^{o}C until use. In some cases, portions of DOPC were replaced by fluorephore-labeled lipids, including TopFluor PC or Liss Rhod PE (both from Avanti Polar Lipids) to label NPs. Size distribution and zeta potential of NPs were measured by dynamic laser scattering (Zetasizer Nano ZSP, Malvern, UK). NPs were visualized by a transmission electron microscope (JEOL 1400 Plus, USA) with negative staining. The amount of CpG encapsulated in NPs was measured by absorbance at 260 nm using a plate reader (Synergy Neo, BioTek, USA). Reactive maleimide groups on the surfaces of NPs were measured by labeling maleimide with a fluorescent probe. In brief, Bodipy FL L-cystine (ThermoFisher Scientific) was reduced by 20 molar fold of tris(2-carboxyethyl)phosphine (TCEP, ThermoFisher Scientific) for 2 h at 37 ^{o}C, then incubated with NPs for another 0.5 h at 37 ^{o}C, followed

by removal of excess dye using a desalting column (MWCO 7 kD, ThermoFisher Scientific). The same amount of NPs was pre-incubated with an excess amount of L-cysteine (Sigma-Aldrich) for 0.5 h at 37 ^{o}C to block reactive maleimide and served as the control. Fluorescence intensity at 488/520 nm was measured by a plate reader and converted to the number of reactive maleimide groups, while the number of NPs was calculated from particle concentration measured by nanoparticle tracking analysis (NTA, NanoSight, Malvern, USA).[18] The multilamellar structure of NPs was determined by a lamellarity assay,[19] using unilamellar liposomes as the control.

4.3.2. Tumor cell culture and elicitation of immunogenic cell death by chemo-treatment

Murine melanoma B16F10, B16F10 expressing ovalbumin (B16F10OVA, both were provided by Dr. Darrell Irvine, MIT), and murine colon carcinoma CT26 (ATCC) were cultured in RPMI 1640 media supplemented with 10% fetal bovine serum and 1% penicillin-streptomycin at 37 ^{o}C under 5% CO_2. Cells were tested free from mycoplasma. Tumor cells were treated by 10 μM mitoxantrone (Mit) for 12 h to induce immunogenic cell death. For determination of cell death and ICD, 10^5 tumor cells were seeded into a 12-well plate, followed by chemo-treatment described above, and measurements of cell death and cellular release of high mobility group box 1 (HMGB1) protein by Annexin V / PI staining using a flow cytometer (Cyan 5, Beckman Coulter, USA), and an ELISA kit

(IBL International), respectively. Sulfhydryl groups expressed in cell-surface proteins were stained by Oregon Green-labeled maleimide (ThermoFisher Scientific). In brief, live or Mit-treated B16F10 cells were incubated with PBS or 1 mM TCEP for 0.5 h at room temperature with constant shaking, followed by washing and labeling with 1 μg/ml of Oregon Green-labeled maleimide for 15 min at room temperature. For maleimide blocking of the dye, 1 μg/ml of Oregon Green-maleimide was incubated with 100 molar fold excess of L-cysteine for 1 h at room temperature, then used for staining. Cells were washed, resuspended in 2 μg/ml DAPI solution, and analyzed for fluorescence intensity of Oregon Green among the DAPI-negative population by flow cytometry. For confocal experiments, live or Mit-treated cells were labeled with eFluor 450 (eBioscience 65-0842), followed by TCEP treatment and staining with Oregon Green-maleimide as described above.

4.3.3. Conjugation of CpG-loaded NPs (CpG-NPs) on the surfaces of dying tumor cells

Various amounts of CpG-NPs were incubated with 10^6 Mit- and TCEP-treated tumor cells suspended in 1 ml PBS for 12 h at 4 ^oC with constant shaking, followed by two washes with PBS using centrifuge (1500 ×g, 5 min), then resuspended in PBS and used freshly. The number of NPs associated per cell was measured using TopFluor PC-labeled NPs and calculated with particle concentration measured by NTA. Oregon Green-labeled

dying tumor cells conjugated with Liss Rhod PE-labeled NPs on their surfaces were visualized by a confocal microscope (Nikon A1, Japan). The fraction of NPs on cell surfaces was quantified by a fluorescence quenching experiment using 0.25 mg/ml trypan blue, a membrane impermeable dye that can specifically quench cell surface-bound fluorescence, and calculated as $[1 - (F_3 - F_1) / (F_2 - F_1)] \times 100\%$, where F_1, F_2, and F_3 were geometric mean fluorescence intensity (MFI) of cells without particle conjugation, cells with particle conjugation but without quenching, and cells with particle conjugation and quenching, respectively.

4.3.4. Migration of dendritic cells to immunogenically dying tumor cells in vitro

Murine bone marrow-derived dendritic cells (BMDCs) were prepared as reported previously.[20] Migration of BMDCs was measured with the Transwell system (5 μm pore size, Costar 3421, Corning). Briefly, 2×10^5 live, Mit-treated B16F10 cells (Mit-B16F10), or Mit-B16F10 conjugated with CpG-NPs (Mit-B16F10-CpG-NPs) were seeded into the lower chamber and cultured for 2 h for cell adherence, followed by seeding of 5×10^5 CFSE-labeled BMDCs into the upper chamber, and cell culture for another 12 h. Culture media without tumor cells in the lower chamber served as the negative control. DCs that migrated to the lower chamber were collected, and $CFSE^+DAPI^-$ DCs were counted by flow cytometry.

4.3.5. Uptake and cross-presentation of antigens by BMDCs in vitro

BMDCs were seeded into a 24-well plate at a density of 2×10^5 cells / well, followed by seeding of 6×10^5 Oregon Green-labeled, live or Mit-treated B16F10OVA cells with or without CpG, and co-culture for 24 h. DCs alone served as the negative control. Cells were collected, stained with a PE-labeled 25-D1.16 monoclonal antibody directed against SIINFEKL-H-$2K^b$ complexes (eBioscience 12-5743) and a PECy7-labeled anti-CD11c (BD 558079) antibody, and analyzed for the percent of dye positive within the DC population, and MFI of PE within DCs engulfing tumor antigens by flow cytometry.

4.3.6. Activation of BMDCs in vitro

BMDCs were seeded into a 12-well plate at a density of 5×10^5 cells / well, followed by seeding of 10^5 live or Mit-treated B16F10OVA cells with or without CpG, and co-culture for 24 h. DCs alone cultured in media was the negative control. Co-culture supernatant was collected and analyzed for DC secretion of inflammatory cytokines, including IL-12p70, TNF-α, and IFN-β by ELISA kits (R&D Systems DY419, DY410, and Biolegend 79838, respectively). Cells were collected and measured for expression of maturation markers, including CD86 (eBioscience 12-0862) and CD40 (eBioscience 12-0401) in DCs by flow cytometry.

4.3.7. In vivo immunization and cancer immunotherapeutic studies

All animal experiments were performed under approval from the Institutional Animal Care and Use Committee (IACUC) at the University of Michigan. Female, 6 week-old C57BL/6 mice (Envigo) were subcutaneously (in two sides of the tail base) immunized with PBS, Mit-treated B16F10OVA cells with or without CpG on day 0, followed by the assessment of SIINFEKL-specific $CD8\alpha^+$ T cells on day 7 by the tetramer staining assay. The single vaccine dose per mouse was composed of 4×10^6 Mit-treated tumor cells with or without 382 ng CpG. Mice were subcutaneously (in one side of flank) inoculated with 10^5 live B16F10OVA cells on day 8, and monitored for tumor initiation. In a separate experiment, ~ $5x10^5$ splenocytes from immunized mice were collected on day 8 and co-cultured with 10^5 live B16F10OVA cells for 20 h in the presence of Brefeldin A, followed by staining with CD8α (BD 553035) and CD4 (BD 552775), fixation and permeabilization with 4% paraformaldehyde, and staining with IFN-γ (BD 562020). Percentages of IFN-γ^+ among $CD8\alpha^+$ and $CD4^+$ splenocytes were quantified by flow cytometry.

For therapeutic studies using the CT26 model, female, 6 week-old BALB/c mice (Envigo) were subcutaneously inoculated with 2×10^5 CT26 cells on day 0, followed by a single subcutaneous vaccine dose on day 4 with Mit-treated CT26 cells (Mit-CT26),

Mit-CT26 conjugated with CpG-loaded NPs (Mit-CT26-CpG-NPs), Mit-CT26 admixed with CpG-loaded NPs, or soluble CpG. The single vaccine dose per mouse was composed of 10^6 Mit-CT26 with or without 117 ng CpG. For combination therapy against CT26 tumors, mice were vaccinated with Mit-CT26-CpG-NPs as above, followed by intraperitoneal administration of an anti-PD1 IgG antibody (BioXcell BP0146, clone: RMP1-14; 100 μg / mouse) on days 5, 8, 11, 14, 17, 20, 23, and 26. Length and width of tumors were measured every two days starting day 6, and tumor volumes were calculated as [0.5 × length × width^2]. Mice were euthanized if the length of tumor > 1.5 cm, or tumors became ulcerated, according to requirements by IACUC. Mice cured by the combination therapy were re-challenged with 2×10^5 CT26 cells in the contralateral flank on day 70, and monitored for tumor initiation.

4.3.8. Statistical analysis

Data are presented as representative or compiled results obtained from two to three independent experiments. Animal experiments were performed after randomization. Data were analyzed by one- or two-way analysis of variance (ANOVA), followed by Bonferroni *post hoc* tests for comparison of multiple groups or log-rank (Mantel-Cox) test using the GraphPad Prism 5.0 software. *P* values < 0.05 are considered statistically significant. All values are reported as mean ± SEM with indicated sample size.

4.4. Results and discussion

4.4.1. Synthesis and characterization of the adjuvant-loaded nano-depot

First, we used the MVP platform developed in the previous chapter to achieve co-localized delivery of immunostimulatory ligands with immunogenically dying tumor cells. We chose to work with CpG oligonucleotide, a potent Toll-like receptor nine (TLR-9) agonist known to promote antigen cross-presentation and cross-priming of $CD8^+$ T cell responses.[21] We constructed cross-linked lipid-polymer nano-depots by utilizing the charge-mediated complexation between cationic lipid vesicles containing a maleimide-modified lipid and a thiolated anionic biopolymer, hyaluronic acid (HA-SH).[22] Subsequent chemical cross-linking led to the formation of multilamellar lipid-polymer hybrid nano-depots (**Figure 4.2**). Briefly, we used the DOBAQ-MAL synthesized in the previous chapter and prepared unilamellar liposomes (composed of DOBAQ-MAL, DOTAP, and DOPC) and incubated them with HA-SH and CpG, resulting in stable NPs. Maleimide-sulfhydryl-mediated cross-linking was crucial for the formation of homogeneous NPs, as aggregates were formed when we replaced DOBAQ-MAL (+1 charge) with DOTAP (+1 charge), or when we replaced HA-SH with HA-bearing the same amount of negative charges.

We also optimized nano-depots by varying the amounts of HA-SH. Homogenous

NPs with a diameter < 300 nm were formed when the charge ratio of cations to anions (from cationic lipids and HA subunits, respectively) was set at ≤ 2 (**Figure 4.3**). Therefore, we performed the subsequent studies using NPs formulated with 0.63 μmol of total lipids (DOBAQ-MAL : DOTAP : DOPC = 25 : 50 : 25, m/m/m) and 100 μg of HA-SH (~ 0.25 μmol of subunits) with the cation to anion ratio of 1.89. Compared with unilamellar liposomes, these lipid-polymer hybrid NPs exhibited a slightly increased particle size of 250 ± 13 nm with their surface charge converted to -16 ± 0.4 mV (**Table 4.1**). The resulting NPs had an average of ~2300 reactive maleimide molecules displayed on each particle, with 28% of lipids exposed on the external surfaces of NPs (as opposed to 45% for unilamellar liposomes) with 81 ± 2 % of CpG loading efficiency (**Table 4.1 and 4.2**). These results indicate the successful synthesis of maleimide-displaying, multilamellar NPs loaded with CpG (CpG-NPs).

4.4.2. Conjugation of CpG-NPs on the surfaces of immunogenically dying tumor cells

We then tethered CpG-NPs on the surfaces of dying tumor cells. We first characterized tumor cells undergoing ICD after treatment with mitoxantrone (Mit), a potent ICD-inducing anthracenedione agent.[13] B16F10OVA melanoma cells expressing an exogenous antigen, ovalbumin (OVA), were exposed to 10 μM Mit for 12 h and washed. After two days of culture, the majority of tumor cells exhibited signs of apoptosis, as

indicated by ~ 80% of the Annexin V^+ cell population (**Figure 4.4A**) and released HMGB1 (**Figure 4.4B**), a marker of ICD.[12] Live as well as immunogenically dying tumor cells have free sulfhydryls on endogenous cell-membrane proteins (as shown by cells stained with Oregon Green-Maleimide, **Figure 4.5A**). Thus, we have sought to utilize free sulfhydryls on the surfaces of immunogenically dying tumor cells to attach maleimide-displaying CpG-NPs. A brief treatment of dying tumor cells with 1 mM TCEP, a reducing agent, increased free sulfhydryls on the cell membrane by a 2.5-fold, compared with dying tumor cells without the TCEP treatment (**Figure 4.5B**). Pre-blocking Oregon Green-Maleimide with 100 molar excess of L-cysteine led to ~ 27-fold reduction in the MFI of cells, showing its specificity toward free thiols on the cells (**Figure 4.5B**). Overnight incubation of Mit- and TCEP-treated cells with NPs at 4 ^{o}C led to the successful surface-conjugation of NPs in a dose-dependent manner (**Figure 4.6A, B**). When cell-NP conjugates were treated with trypan blue, a cell membrane-impermeable fluorescence-quencher,[23-24] ~ 96% of the cell-associated fluorescence signal was quenched (**Figure 4.6C**), indicating cell-surface conjugation, rather than internalization, of NPs. In contrast, elevating the incubation temperature from 4 ^{o}C to 37 ^{o}C resulted in ~ 50% of the NPs internalized by tumor cells within 1 h (**Figure 4.7**). Mit-treated B16F10OVA cells decorated with NPs displayed the prototypical markers of ICD (**Figure 4.8**).

4.4.3. Activation of DCs in vitro by the dying tumor cell-CpG-NP conjugates

We next asked whether dying tumor cells modified with CpG-NPs can recruit and activate dendritic cells (DCs). In particular, successful cross-priming of $CD8\alpha^+$ T cells by DCs requires three signals: (1) antigen processing and presentation in the context of major histocompatibility complex (MHC) class I molecule; (2) up-regulation of co-stimulatory markers, such as CD40, CD80, and 86; and (3) secretion of TNF-α and IFN-β that mediate inflammatory and innate immune responses,[25-26] as well as Th_1 cytokines, such as IL-12.[27-28] Indeed, we observed that Mit-treated tumor cells significantly increased DC recruitment (a 2.4-fold increase than live tumor cells, $p < 0.001$, **Figure 4.9**). DCs engulfed Mit-treated tumor cells 4.2-fold more efficiently than live tumor cells ($p < 0.001$, **Figure 4.10A**). We next examined the cross-presentation of tumor antigens engulfed by DCs. As shown by staining with a 25-D1.16 monoclonal antibody directed against SIINFEKL-H-$2K^b$ complexes,[7] cross-presentation of OVA protein from B16F10OVA cells was significantly enhanced when DCs were co-cultured with dying tumor cell-CpG-NP conjugates, compared with tumor cells admixed with the equivalent dose of free CpG or CpG-NPs ($p < 0.001$, **Figure 4.10B**). Moreover, surface-decoration of dying tumor cells with CpG-NPs was important for maturation and up-regulation of CD40 and CD86 in DCs ($p < 0.001$, **Figure 4.11A, B**). Similarly, dying tumor cell-CpG-NP conjugates promoted the robust secretion of inflammatory cytokines from DCs, including IL-12p70 (only detected for dying tumor cell-CpG-NP conjugates,

Figure 4.12A), TNF-α, and IFN-β (p < 0.001, **Figure 4.12B, C**). Overall, surface-conjugation of CpG-NPs on dying tumor cells, rather than their physical mixture, was crucial for strong DC maturation, antigen cross-presentation, and cytokine secretion.

4.4.4. Elicitation of antigen-specific $CD8^+$ T cells in vivo

Having shown DC activation *in vitro*, we examined whether the whole tumor-cell vaccine can elicit anti-tumor $CD8\alpha^+$ T cell responses *in vivo*. We immunized naive C57BL/6 mice subcutaneously (s.c.) at the tail base with a single dose of vaccine ($4x10^6$ Mit-treated B16F10OVA cells with 380 ng CpG per dose). On day 7, the frequency of $CD8\alpha^+$ T cells against the immunodominant epitope of OVA, SIINFEKL, was measured by the tetramer staining assay on the peripheral blood mononuclear cells (PBMCs) (**Figure 4.13A**).[29-30] Whereas vaccination with dying tumor cells alone resulted in minimal induction of SIINFEKL-specific $CD8\alpha^+$ T cells, dying tumor cell-CpG-NP conjugates generated strong antigen-specific $CD8\alpha^+$ T cell responses (3.2-fold greater than PBS, p < 0.01; and 2.4-fold greater than dying tumor cells, p < 0.05, **Figure 4.13B**). Similar results were also found among splenocytes (**Figure 4.13C**). We also re-stimulated splenocytes from immunized mice with whole B16F10OVA cells and found that dying tumor cell-CpG-NP conjugates elicited significantly higher levels of IFN-γ^+ $CD8\alpha^+$ and $CD4^+$ T cells, compared with dying tumor cells without CpG (p < 0.05, **Figure 4.14A, B**). To assess the

functionality of these CD8α^+ T cells, we inoculated the animals with 10^5 B16F10OVA tumor cells s.c. on day 8. A single immunization with dying tumor cell-CpG-NP conjugates protected all animals against tumor initiation (**Figure 4.15**). In contrast, vaccination with dying tumor cells alone failed to stop B16F10OVA tumor growth ($p < 0.01$, **Figure 4.15A**) with only 20% survival rate ($p < 0.05$, **Figure 4.15B**). Taken together, these results demonstrate the potency of the dying tumor cell-CpG-NP conjugates to generate anti-tumor T-cell immune responses *in vivo*, and we therefore kept the single vaccine dose in therapeutic studies.

4.4.5. Therapeutic efficacy of the whole-cell cancer vaccine in vivo

Next, we evaluated our vaccination strategy in a therapeutic setting against established CT26 colon carcinoma (without any exogenous antigen) to provide a more rigorous condition than the prophylactic setting shown above. We confirmed that Mit treatment induced ICD in CT26 cells (**Figure 4.16A**) and that CpG-NPs were successfully conjugated on CT26 cells (**Figure 4.16B**). BALB/c mice were inoculated at s.c. flank with $2x10^5$ CT26 cells, and on day 4 when tumors were palpable, a single dose of vaccine was administered. The dying tumor cell-CpG-NP conjugates significantly inhibited CT26 tumor growth ($p < 0.001$, compared with PBS or dying tumor cells alone, **Figure 4.17**), whereas dying tumor cells physically admixed with the equivalent dose of soluble CpG

or CpG-NPs failed to reduce the tumor size. Taken together with the DC activation data, these results show that surface-conjugation of CpG-NPs on dying tumor cells, rather than their physical mixture, was crucial for potent immune responses and anti-tumor efficacy.

4.4.6. Combination therapy using the whole-cell cancer vaccine and immune checkpoint blocker

Lastly, we sought to amplify the therapeutic potential of our whole-cell vaccine by combining with ICBs. This was motivated by the low patient response rates to ICBs,[31-32] highlighting the need to improve the outcomes of cancer immunotherapy. We treated CT26 tumor-bearing mice with dying tumor cell-CpG-NP conjugates combined with anti-PD1 IgG therapy (**Figure 4.18A**). The combination immunotherapy exerted robust anti-tumor efficacy, leading to potent inhibition of average tumor growth ($p < 0.001$, **Figure 4.18B**) and complete elimination of tumors in ~ 78% of animals (**Figure 4.18C**). In contrast, mice that received anti-PD1 monotherapy or dying tumor-cell vaccine alone failed to stop the average tumor growth in this model. Importantly, 100% of the survivors in the whole tumor-cell vaccine plus anti-PD1 treatment group rejected engraftment of $2x10^5$ CT26 tumor cells re-challenged on day 70 ($p < 0.001$, **Figure 4.18D**), demonstrating long-term immunity against tumor recurrence. Moreover, throughout our studies, we did not observe any signs of weight loss, toxicity, reactogenicity at the sites of

vaccination, nor autoimmunity in animals treated with the combination immunotherapy. Collectively, these studies show that surface-modification of immunogenically dying tumor cells with adjuvant-carrying nano-depots rendered them into a potent vaccine platform with therapeutic potential.

4.5. Conclusion

In summary, we induced ICD of tumor cells by treating them with mitoxantrone and exploited immunogenically dying tumor cells as the platform for co-delivery of tumor antigens and immunostimulatory agents. To promote immune activation, we tethered CpG-NPs onto the surfaces of dying tumor cells via sulfhydryl-maleimide chemistry, a facile cell-engineering approach that has been utilized on therapeutic T cells.[33-34] Notably, our strategy based on nano-depots achieve co-delivery of adjuvants without their pre-modification with cell-anchoring structures,[35-36] or pre-labeling of cells with metabolic ligands or antibodies,[37-38] and could deliver a single or potentially multiple synergistic TLR agonists.[39] We have demonstrated that immunogenically dying tumor cells decorated with CpG-NPs recruited DCs, promoted DC maturation, uptake of tumor antigens, and subsequent antigen cross-presentation, thereby triggering robust antigen-specific T cell responses with anti-tumor efficacy *in vivo*. Importantly, by employing a combination approach with anti-PD1 therapy, we achieved regression of

established CT26 tumors in ~78% of mice and protected them against future tumor relapse. Furthermore, a single vaccine dose employed in this study would simplify the immunization scheme and increase the translational potential of our strategy. To the best of our knowledge, we demonstrate for the first time that immunogenically dying tumor cells engineered to release exogenous adjuvants can exert potent prophylactic as well as therapeutic anti-tumor efficacy in multiple murine tumor models. We are currently exploring ways to co-deliver ICD inducers and immunostimulatory molecules to tumors *in vivo* and optimizing therapeutic schemes so that we can generate whole tumor-cell vaccines *in situ* without *ex vivo* manipulations. Looking forward, we provide a general framework for exploiting ICD of tumor cells for elicitation of immunity against a wide repertoire of antigens found in whole tumor cells, without *a priori* knowledge of antigens. Our strategy may open new avenues to “personalized” cancer immunotherapy tailored to individual patient’s tumor cells.[40]

4.6. Figures and tables

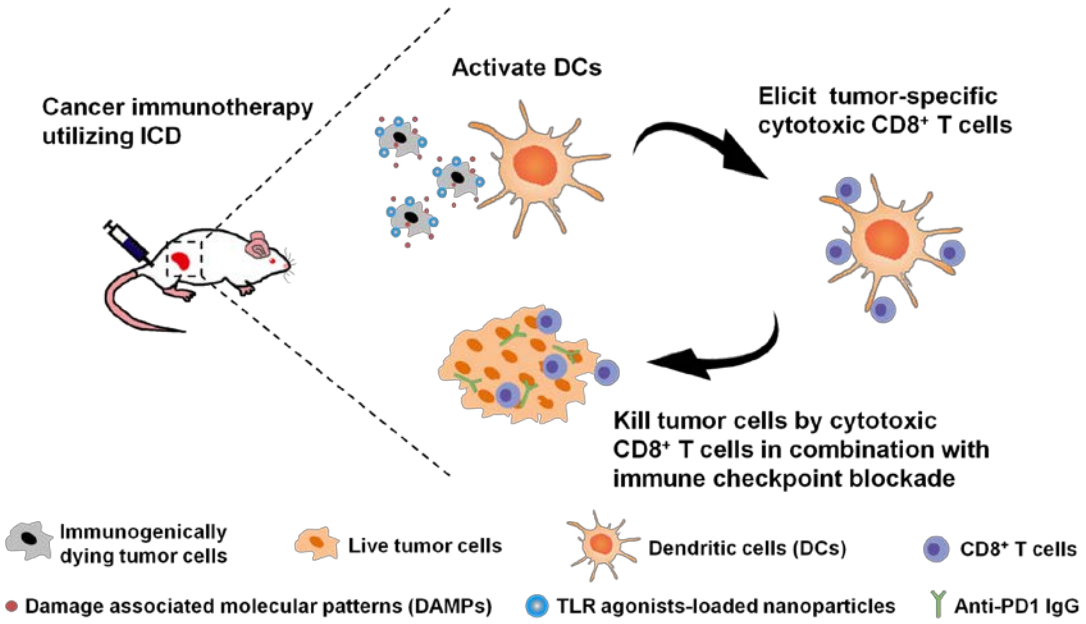

Figure 4.1. Immunogenically dying tumor cells surface-decorated with TLR agonist-loaded nanoparticles release tumor antigens and damage associated molecular patterns (DAMPs), triggering activation of dendritic cells and induction of tumor-specific $CD8^+$ T cells that can kill tumor cells. Combination of the whole-cell vaccine with PD1 blockade further improves therapeutic efficacy.

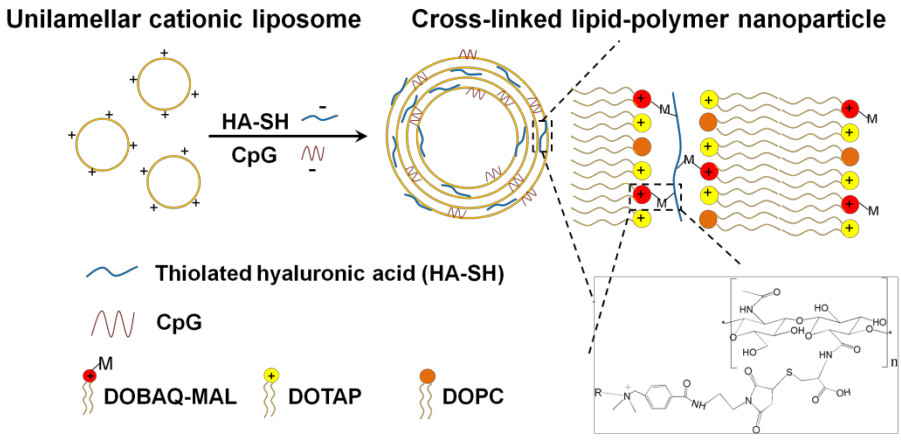

Figure 4.2. The nano-depot encapsulating the TLR-9 agonist CpG was constructed by complexation between cationic liposomes and thiolated hyaluronic acid (HA-SH), an anionic biopolymer, followed by crosslink-mediated stabilization.

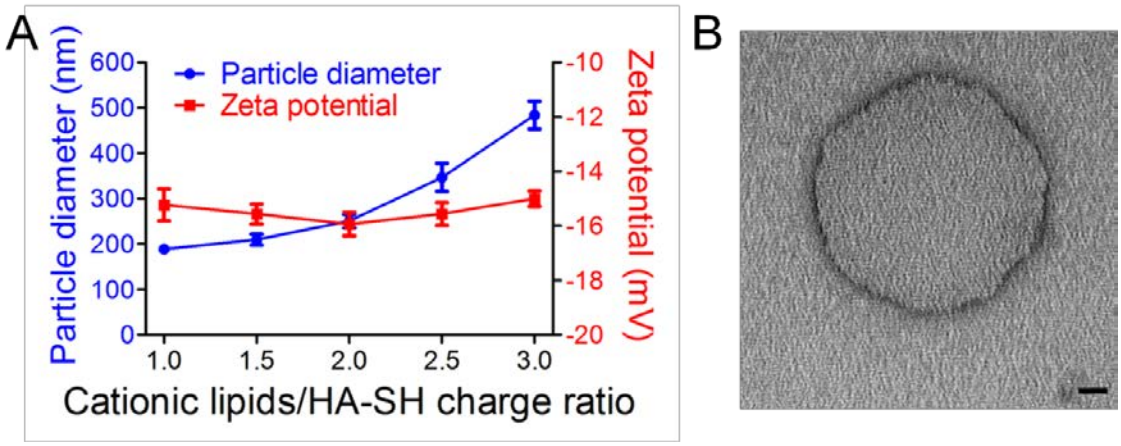

Figure 4.3. Optimization of the NP formulation. **(A)** NP synthesis was optimized by varying the charge ratio between cationic lipids and HA-SH. Particle size and zeta potential were measured by dynamic laser scattering (DLS). Results are shown as mean ± SEM, *n* = 3. **(B)** A representative CpG-loaded NP visualized by transmission electron microscopy with negative staining. Scale bar, 20 nm.

Table 4.1. Characterization of CpG-loaded NPs. The data show mean ± SEM, *n* = 3.

Particles	Z-average (nm)	PDI	Zeta potential (mV)	% Encapsulation efficiency of CpG	Reactive maleimide on NP surfaces (ave. # x10^3 molecules / particle)
Unilamellar liposomes	108 ± 4	0.234 ± 0.02	20.3 ± 0.6	N.A.	N.A.
Blank NPs without CpG	254 ± 10	0.222 ± 0.03	-16.4 ± 0.4	N.A.	2.19 ± 0.3
CpG-loaded NPs	290 ± 10	0.177 ± 0.02	-17.7 ± 0.5	81.2 ± 2	2.34 ± 0.4

Table 4.2. Lamellarity of liposomes and CpG-loaded NPs. The data show mean ± SEM, *n* = 3.

Particles	Unilamellar liposomes	CpG-loaded NPs
Lamellarity	0.45 ± 0.04	0.28 ± 0.02

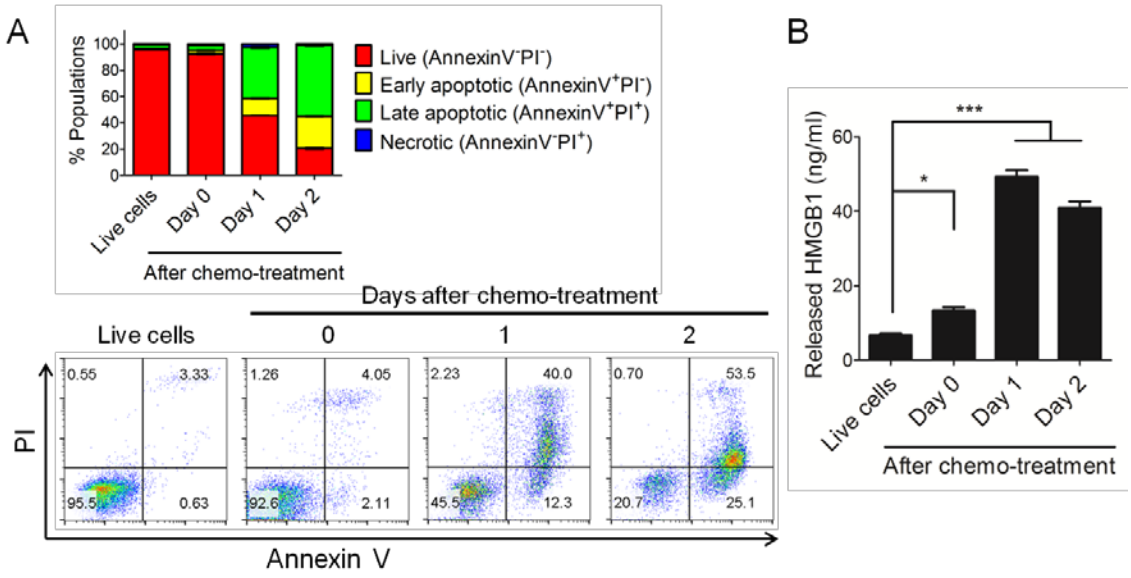

Figure 4.4. Mitoxantrone (Mit) induced immunogenic cell death of tumor cells. B16F10OVA cells were treated by 10 μM mitoxantrone for 12 h, followed by media change and cell culture for two days. **(A)** Cell death and **(B)** cellular release of HMGB1 were measured by Annexin V / PI staining and ELISA, respectively. Numbers in the representative flow cytometry plots indicate the percentage of live, apoptotic, and necrotic cell populations. Data show mean ± SEM (n = 3), representative from 2-3 independent experiments. * $p < 0.05$, *** $p < 0.001$, analyzed by one-way ANOVA with Bonferroni multiple comparison post-test.

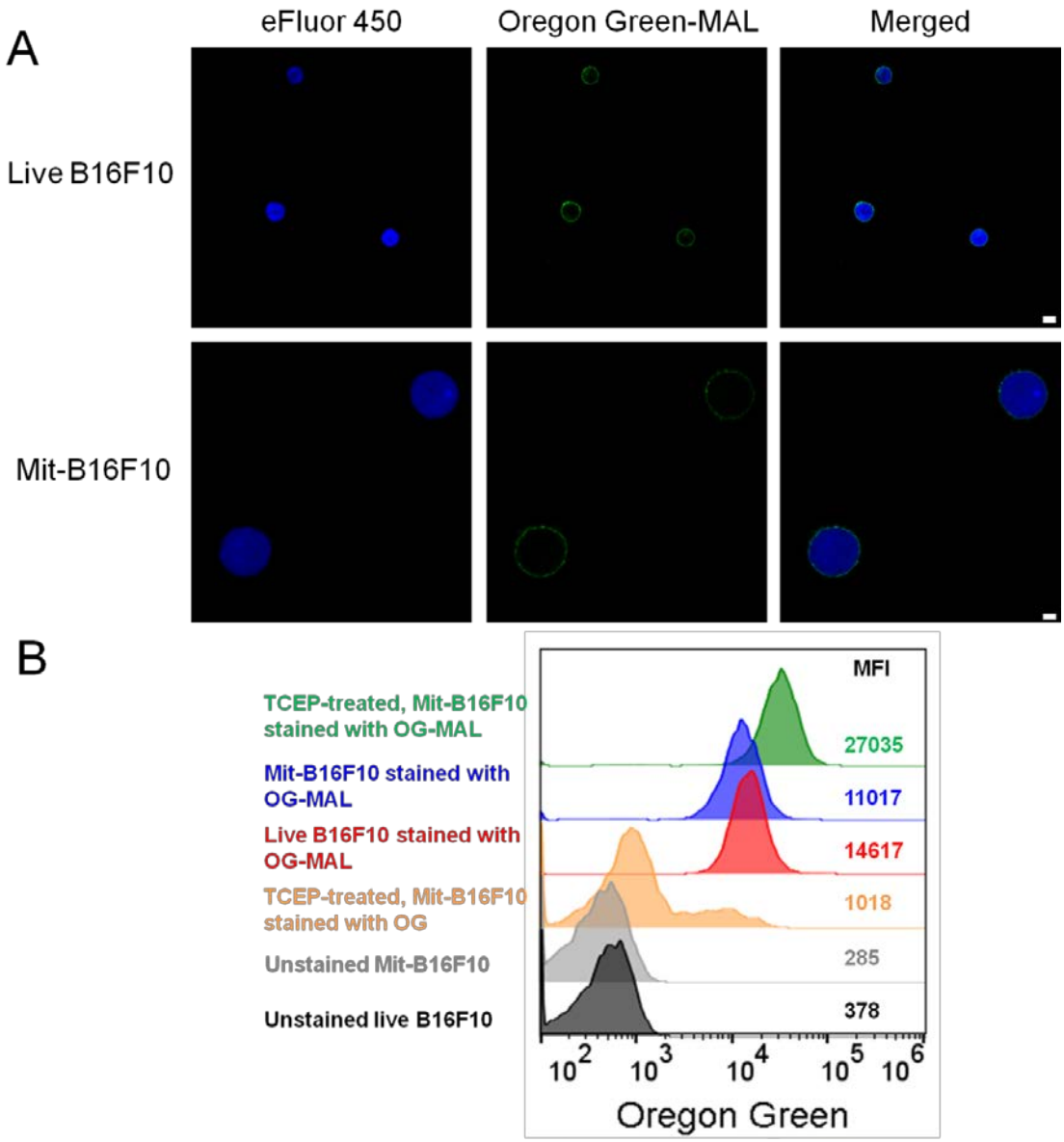

Figure 4.5. Expression of sulfhydryls on the surface of tumor cells. **(A)** Live or Mit-treated B16F10 cells were stained by eFluor 450 (blue), treated by 1 mM TCEP at room temperature for 30 min, followed by staining with Oregon Green-maleimide (green). The data show representative confocal images. Scale bar, 10 μm for live cells; 5 μm for Mit-treated cells. **(B)** Mit-treated tumor cells exhibited free thiol groups on their surfaces, and treatment with 1 mM TCEP further increased the level of free thiols, as shown by the representative flow cytometry analysis from two independent experiments. MFI, geometric mean fluorescence intensity. Pre-blocking of Oregon Green-Maleimide (OG-MAL) with 100 molar-excess L-cysteine (OG) decreased the MFI.

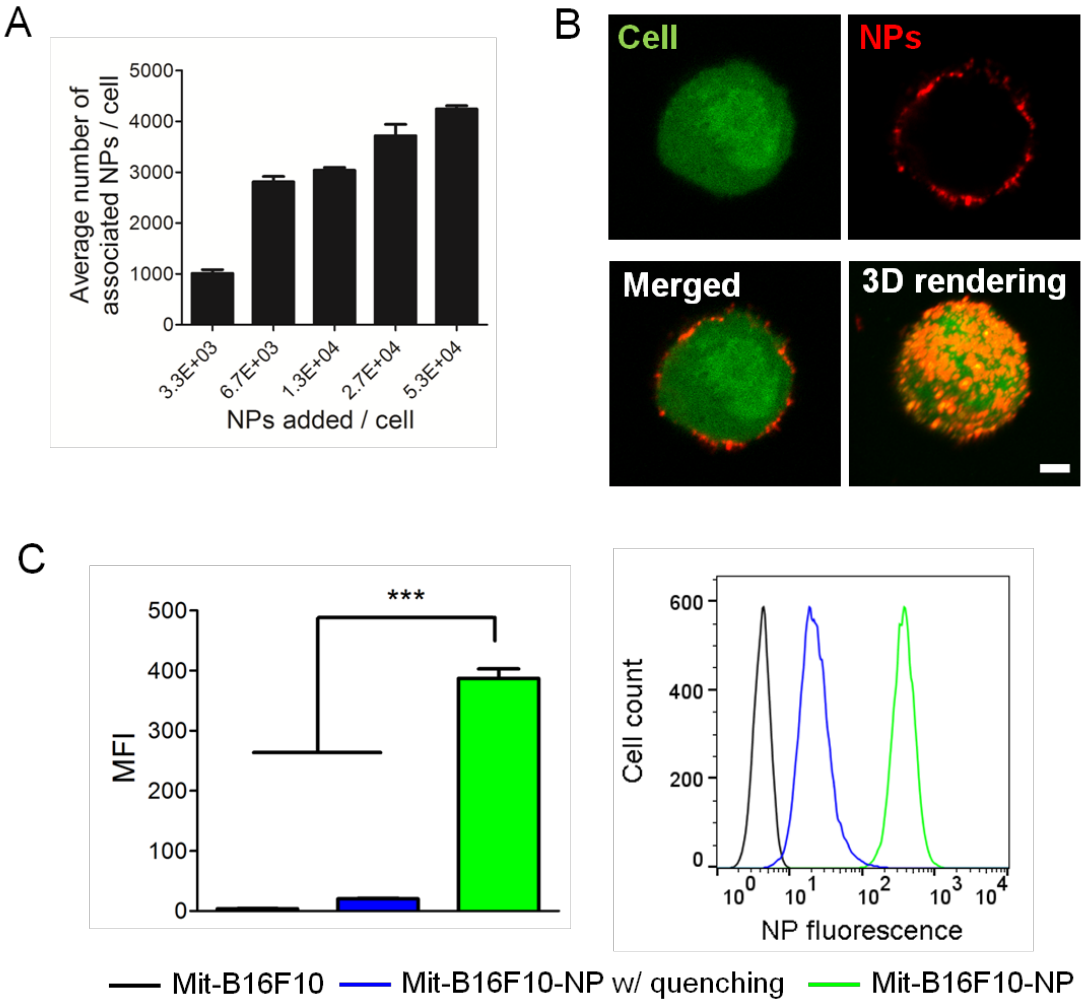

Figure 4.6. Conjugation of CpG-NPs on the surfaces of dying tumor cells **(A)** The number of NPs bound on dying tumor cells was quantified after incubation of 10^6 Mit-treated B16F10 cells at 4 ^{o}C for 12 h with varying doses of fluorophore-labeled, CpG-NPs. **(B)** The representative confocal images of a dying tumor cell (green) conjugated with NPs (red) and their 3D re-construction. Scale bar, 5 μm. **(C)** In the presence of trypan blue (a membrane-impermeable quencher), fluorescence signal from cell-associated NPs was lost, indicating that NPs were attached externally to the cell membrane. Data show mean ± SEM (n = 3), representative from 2-3 independent experiments. *** $p < 0.001$, analyzed by one-way ANOVA with Bonferroni multiple comparison post-test.

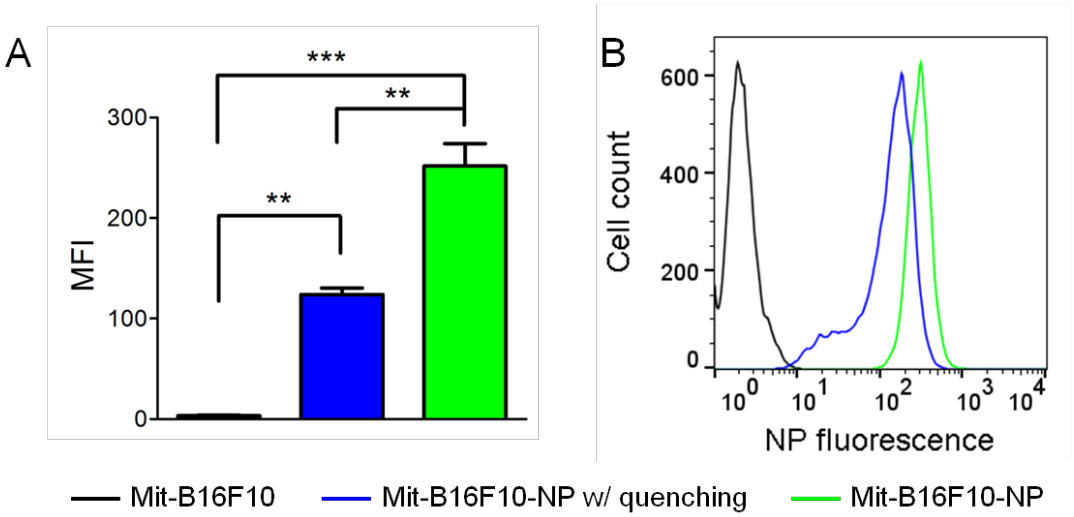

Figure 4.7. Incubation of chemo-treated tumor cells with NPs at 37 ^{o}C results in significant cellular uptake of NPs. Fluorophore-labeled, CpG-loaded NPs were incubated with Mit-treated B16F10 cells at 37 ^{o}C for 1 h with constant shaking, followed by washing and quantification of cell-surface bound NPs. Cell-surface fraction of NPs = 50.3 ± 5 %, determined by MFI. The data show mean ± SEM, $n = 3$. ** $p < 0.01$, *** $p < 0.001$, analyzed by one-way ANOVA with Bonferroni multiple comparison post-test.

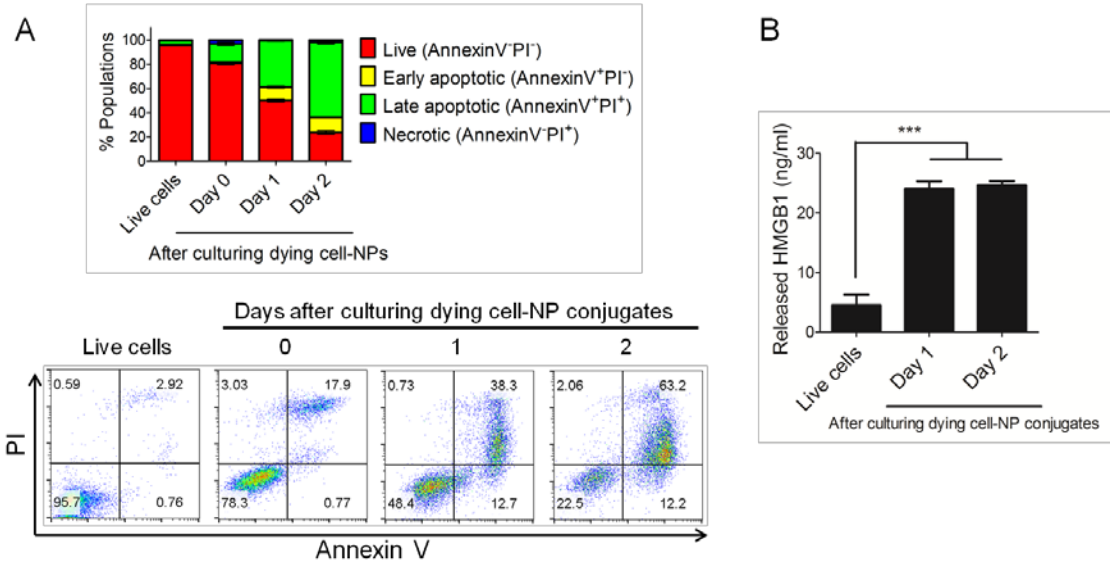

Figure 4.8. Dying tumor cell-NP conjugates undergo immunogenic cell death. B16F10OVA cells were treated with 10 μM mitoxantrone for 12 h, followed by conjugation with NPs on their surfaces and cell culture for two days. **(A)** Cell death and **(B)** cellular release of HMGB1 were measured by Annexin V / PI staining and ELISA, respectively. The data show mean ± SEM, $n = 3$. *** $p < 0.001$, analyzed by one-way ANOVA with Bonferroni multiple comparison post-test.

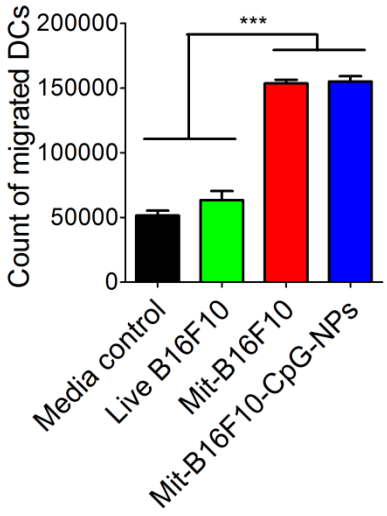

Figure 4.9. Mit-treated B16F10OVA tumor cells promoted recruitment of BMDCs as measured by the Transwell migration assay. The data show mean ± SEM, from a representative experiment (n = 3) from 2-3 independent experiments. *** $p < 0.001$, analyzed by one-way ANOVA with Bonferroni multiple comparison post-test.

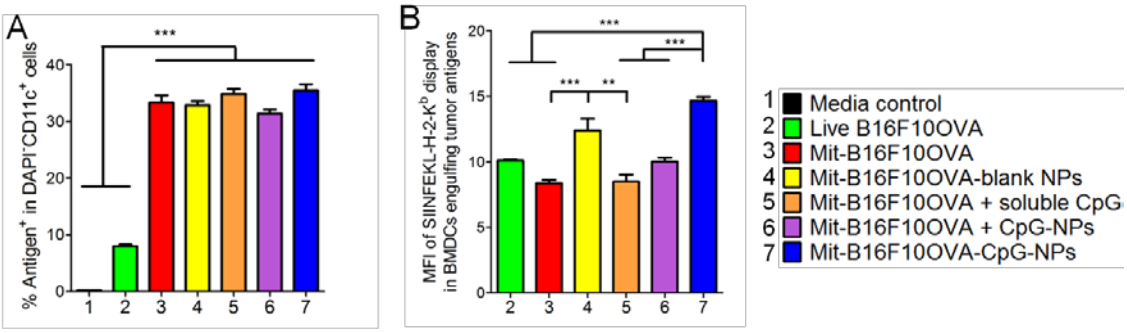

Figure 4.10. Mit-treated tumor cells were efficiently engulfed and cross-presented by BMDCs. BMDCs were co-cultured with Oregon Green-labeled, Mit-treated B16F10OVA cells for 24 h, followed by **(A)** quantification of tumor antigen-positive BMDCs and **(B)** SIINFEKL display among antigen-positive BMDCs by flow cytometry. The data show mean ± SEM, from a representative experiment (n = 3) from 2-3 independent experiments. ** $p < 0.01$, *** $p < 0.001$, analyzed by one-way ANOVA with Bonferroni multiple comparison post-test.

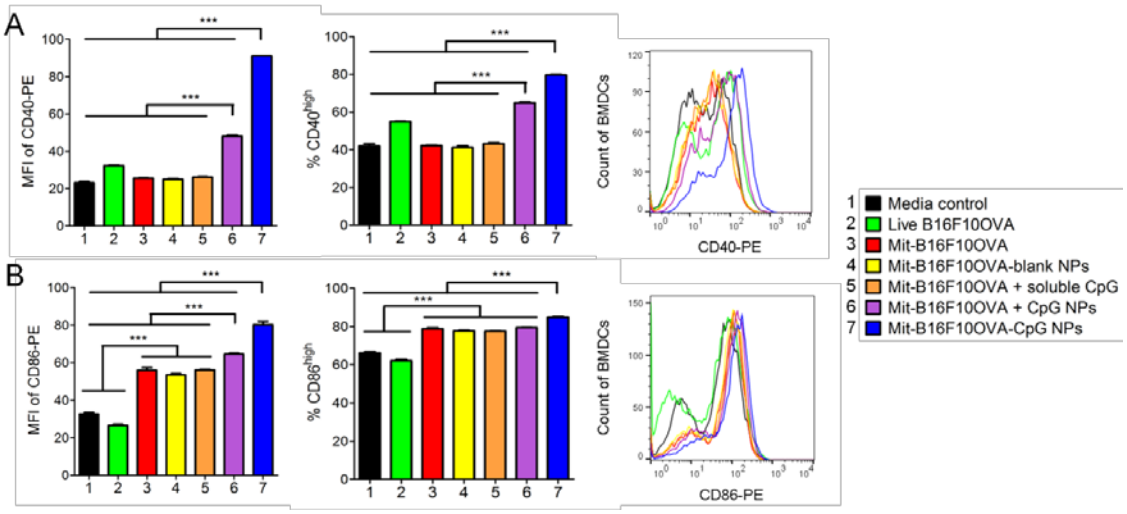

Figure 4.11. Dying tumor cells conjugated with CpG-NPs induced up-regulation of **(A)** CD40 and **(B)** CD86 in BMDCs *in vitro*. The data show mean ± SEM, from a representative experiment (n = 3) from 2-3 independent experiments. *** $p < 0.001$, analyzed by one-way ANOVA with Bonferroni multiple comparison post-test.

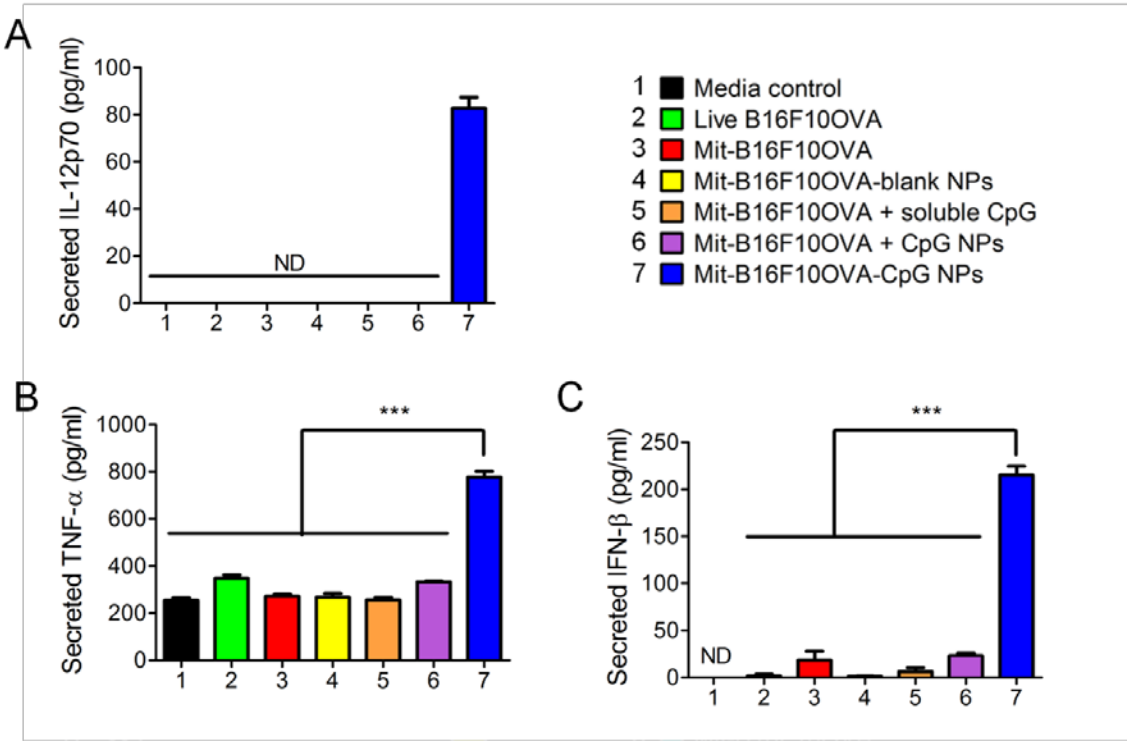

Figure 4.12. Dying tumor cells conjugated with CpG-NPs promoted BMDCs to secrete inflammatory cytokines, including **(A)** IL-12p70, **(B)** TNF-α, and **(C)** IFN-β, as measured by ELISA. ND, not detected. The data show mean ± SEM, from a representative experiment (n = 3) from 2-3 independent experiments. *** $p < 0.001$, analyzed by one-way ANOVA with Bonferroni multiple comparison post-test.

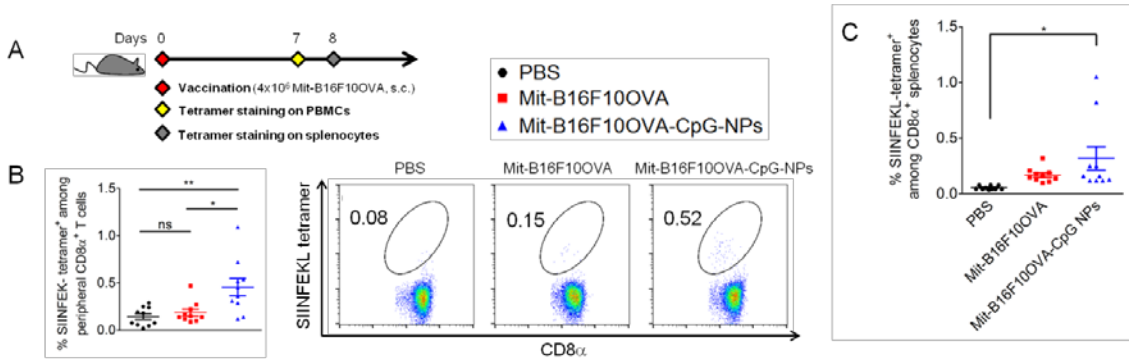

Figure 4.13. Immunogenically dying tumor cells membrane-decorated with CpG-NPs elicit anti-tumor T-cell responses *in vivo*. **(A)** C57BL/6 mice were vaccinated with $4x10^6$ Mit-treated B16F10OVA cells, followed by tetramer staining for antigen-specific $CD8\alpha^+$ T cells among PBMCs and splenocytes on days 7 and 8, respectively. **(B)** The frequency of SIINFEKL-specific $CD8\alpha^+$ T cells among peripheral blood mononuclear cells (PBMCs) and their representative flow cytometry scatter plots are shown. **(C)** Frequency of SIINFEKL-specific $CD8\alpha^+$ T cells among splenocytes. The data show mean ± SEM, $n = 10$. * $p < 0.05$, ** $p < 0.01$, analyzed by one-way ANOVA with Bonferroni multiple comparison post-test.

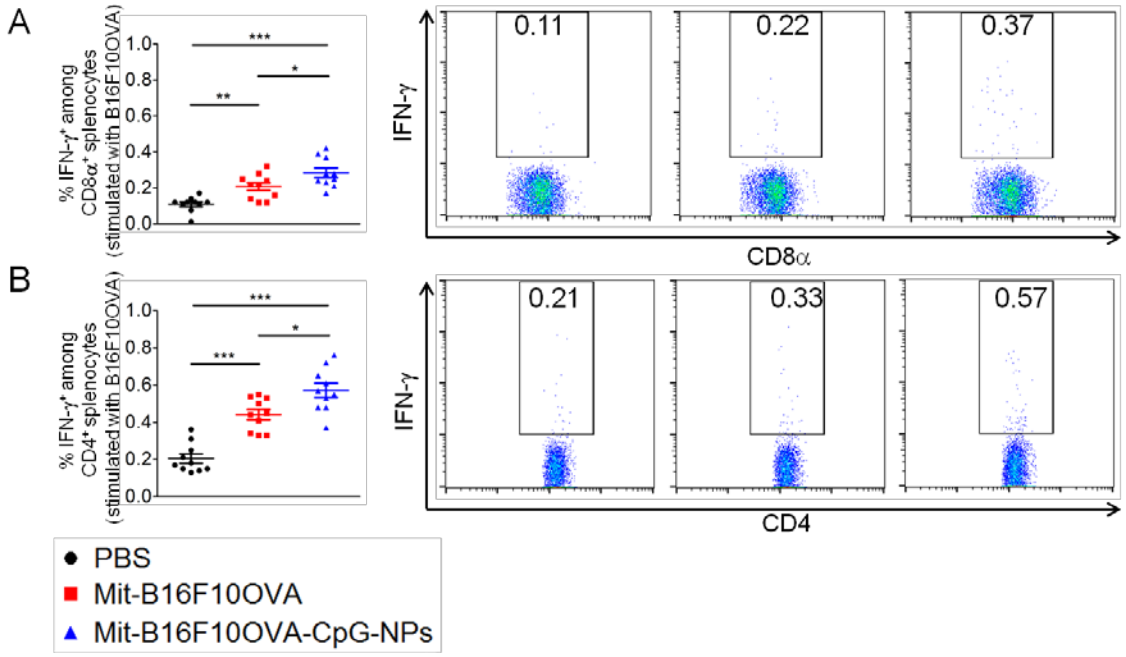

Figure 4.14. Splenocytes from immunized mice were re-stimulated with live B16F10OVA cells *ex vivo* on day 8, and the percentage of IFN-γ^+ among **(A)** CD8α^+ and **(B)** CD4$^+$ splenocytes are shown. The data show mean ± SEM, $n = 10$. * $p < 0.05$, ** $p < 0.01$, *** $p < 0.001$, analyzed by one-way ANOVA with Bonferroni multiple comparison post-test.

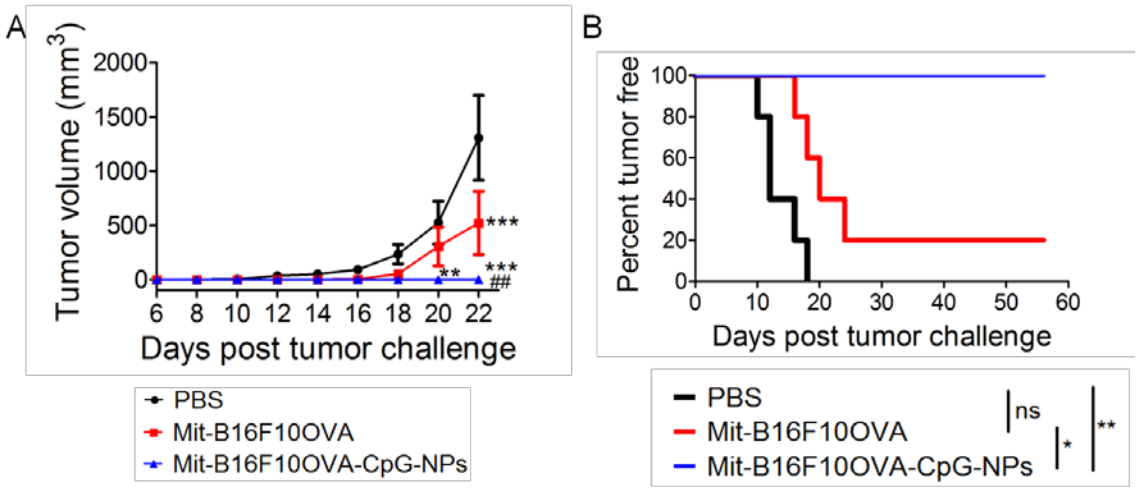

Figure 4.15. Vaccinated mice were challenged with live B16F10OVA cells, and **(A)** average tumor volumes and **(B)** tumor-free percentage are shown. The data show mean ± SEM (n = 4-5), analyzed by **(A)** two-way ANOVA with the Bonferroni multiple comparison post-test, or **(B)** the log-rank (Mantel-Cox) test. **(A)** ** $p < 0.01$, *** $p < 0.001$ *vs.* the PBS control; $^{\#\#}P < 0.01$ *vs.* the Mit-B16F10OVA group. **(B)** ** $p < 0.01$, *** $p < 0.001$.

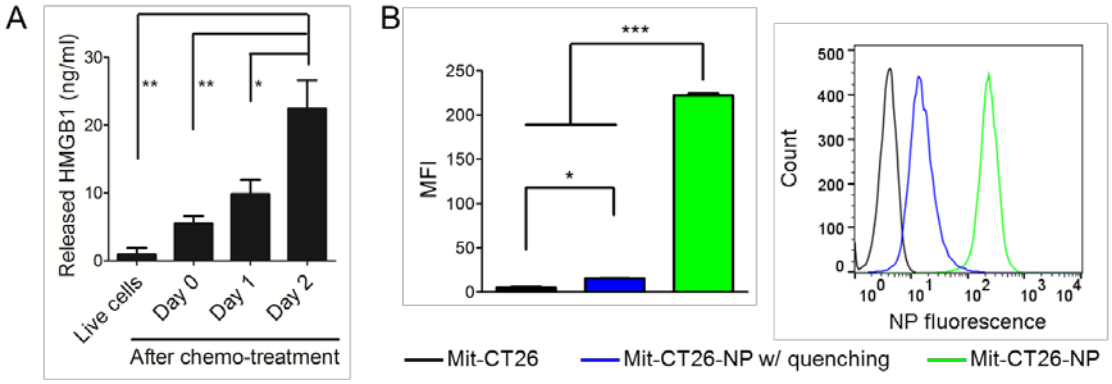

Figure 4.16. ICD and cell-surface conjugation of NPs on CT26 cells. **(A)** HMGB1 release from mitoxantrone-treated CT26 cells. CT26 cells were treated by 10 μM mitoxantrone for 12 h, followed by media change and cell culture for two days. Cellular release of HMGB1 was measured by ELISA. **(B)** NPs were mainly located on the surfaces of dying CT26 cells. Cell-surface fraction of NPs = 94.6 ± 0.2 % determined by MFI. The data show mean ± SEM, $n = 3$. * $p < 0.05$, ** $p < 0.01$, *** $P < 0.001$, analyzed by one-way ANOVA with Bonferroni multiple comparison post-test.

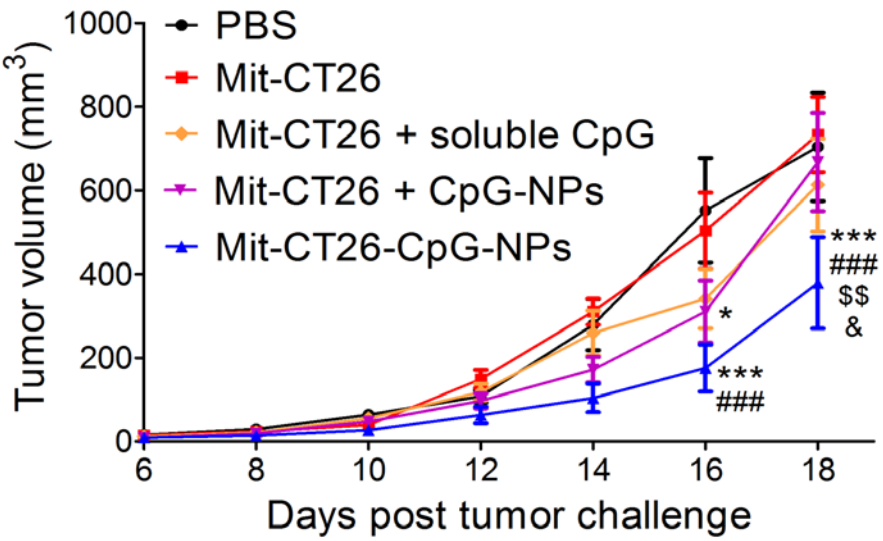

Figure 4.17. Anti-tumor efficacy of dying tumor cells decorated with CpG-loaded NPs. BALB/c mice were inoculated with $2x10^5$ CT26 cells subcutaneously on day 0, and on day 4 when tumors were palpable, animals were treated with a single dose of whole-cell vaccines along with various CpG formulations (10^6 Mit-CT26 cells plus 117 ng CpG / mouse). The average tumor growth volumes are shown until day 18 when mice bearing large or ulcerated tumors had to be euthanized. The data show mean ± SEM, from a representative experiment (n = 8) from two independent experiments, analyzed by two-way ANOVA with Bonferroni multiple comparison post-test. * $p < 0.05$, *** $p < 0.001$ *vs.* the PBS control; $^{###}$ $p < 0.001$ *vs.* Mit-CT26; $^{\$\$}$ $p < 0.01$ *vs.* Mit-CT26 + CpG NPs; $^{\&}$ $p < 0.05$ *vs.* Mit-CT26 + soluble CpG.

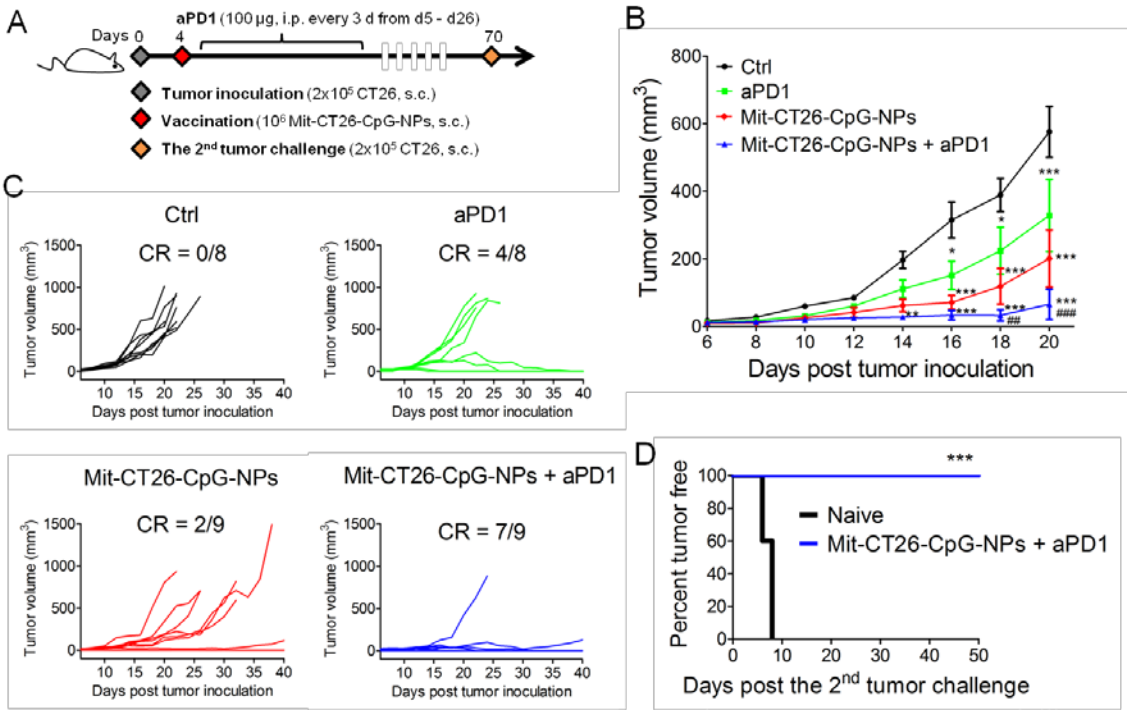

Figure 4.18. Immunogenically dying tumor cells conjugated with CpG-NPs exert potent anti-tumor efficacy in combination with immune checkpoint blockade. **(A-D)** BALB/c mice were inoculated with $2x10^5$ CT26 cells subcutaneously on day 0, then treated with a single dose of the whole-cell vaccine (10^6 Mit-CT26-CpG-NPs) on day 4 when tumors were palpable, followed by anti-PD1 IgG therapy (clone: RMP1-14, 100 µg) every three days from days 5 to 26. **(B)** The average tumor growth volumes are shown until day 20 when mice bearing large or ulcerated tumors had to be euthanized. **(C)** Individual tumor growth curves are shown. CR, complete regression. **(D)** Tumor growth was monitored after re-challenge of mice cured by the combination therapy (n = 7) with $2x10^5$ CT26 tumor cells on day 70. Naive mice (n = 5) were used as control. The data show mean ± SEM, from a representative experiment with n = 8-9 for panel **(B,C)** from two independent experiments, analyzed by **(B)** two-way ANOVA with Bonferroni multiple comparison post-test, or **(D)** log-rank (Mantel-Cox) test. **(B)** $^{*}p < 0.05$, $^{**}p < 0.01$, $^{***}p < 0.001$ *vs.* the control group; $^{\#\#}p < 0.01$, $^{\#\#\#}p < 0.001$ *vs.* the anti-PD1 group. **(D)** $^{***}p < 0.001$.

4.7. References

1. Moon, J. J., *et al.* Engineering nano- and microparticles to tune immunity. *Adv Mater* **2012,** *24* (28), 3724-46.

2. Irvine, D. J., *et al.* Engineering synthetic vaccines using cues from natural immunity. *Nat Mater* **2013,** *12* (11), 978-90.

3. Sahdev, P., *et al.* Biomaterials for nanoparticle vaccine delivery systems. *Pharm Res* **2014,** *31* (10), 2563-82.

4. Liu, H., *et al.* Structure-based programming of lymph-node targeting in molecular vaccines. *Nature* **2014,** *507* (7493), 519-22.

5. Fan, Y.; Moon, J. J. Nanoparticle Drug Delivery Systems Designed to Improve Cancer Vaccines and Immunotherapy. *Vaccines (Basel)* **2015,** *3* (3), 662-85.

6. van der Burg, S. H., *et al.* Vaccines for established cancer: overcoming the challenges posed by immune evasion. *Nat Rev Cancer* **2016,** *16* (4), 219-33.

7. Kuai, R., *et al.* Designer vaccine nanodiscs for personalized cancer immunotherapy. *Nat Mater* **2017,** *16* (4), 489-496.

8. Wang, C., *et al.* Tailoring Biomaterials for Cancer Immunotherapy: Emerging Trends and Future Outlook. *Adv Mater* **2017,** *29* (29).

9. Melero, I., *et al.* Therapeutic vaccines for cancer: an overview of clinical trials. *Nat Rev Clin Oncol* **2014,** *11* (9), 509-24.

10. Kroemer, G., *et al.* Immunogenic cell death in cancer therapy. *Annu Rev Immunol* **2013,** *31*, 51-72.

11. Galluzzi, L., *et al.* Immunogenic cell death in cancer and infectious disease. *Nat Rev Immunol* **2017,** *17* (2), 97-111.

12. Apetoh, L., *et al.* Toll-like receptor 4-dependent contribution of the immune system to anticancer chemotherapy and radiotherapy. *Nat Med* **2007,** *13* (9), 1050-9.

13. Obeid, M., *et al.* Calreticulin exposure dictates the immunogenicity of cancer cell death. *Nat Med* **2007,** *13* (1), 54-61.

14. Ghiringhelli, F., *et al.* Activation of the NLRP3 inflammasome in dendritic cells induces IL-1beta-dependent adaptive immunity against tumors. *Nat Med* **2009,** *15* (10), 1170-8.

15. Casares, N., *et al.* Caspase-dependent immunogenicity of doxorubicin-induced tumor cell death. *J Exp Med* **2005,** *202* (12), 1691-701.

16. Teng, M. W., *et al.* Classifying Cancers Based on T-cell Infiltration and PD-L1. *Cancer Res* **2015,** *75* (11), 2139-45.

17. Zou, W., *et al.* PD-L1 (B7-H1) and PD-1 pathway blockade for cancer therapy: Mechanisms, response biomarkers, and combinations. *Sci Transl Med* **2016,** *8* (328), 328rv4.

18. Filipe, V., *et al.* Critical evaluation of Nanoparticle Tracking Analysis (NTA) by NanoSight for the measurement of nanoparticles and protein aggregates. *Pharm Res* **2010,** *27* (5), 796-810.

19. Girard, P., *et al.* A new method for the reconstitution of membrane proteins into giant unilamellar vesicles. *Biophys J* **2004,** *87* (1), 419-29.

20. Lutz, M. B., *et al.* An advanced culture method for generating large quantities of highly pure dendritic cells from mouse bone marrow. *J Immunol Methods* **1999,** *223* (1), 77-92.

21. Krieg, A. M. CpG motifs in bacterial DNA and their immune effects. *Annu Rev Immunol* **2002,** *20*, 709-60.

22. Fan, Y., *et al.* Cationic liposome-hyaluronic acid hybrid nanoparticles for intranasal vaccination with subunit antigens. *J Control Release* **2015,** *208*, 121-129.

23. Van Amersfoort, E. S.; Van Strijp, J. A. Evaluation of a flow cytometric fluorescence quenching assay of phagocytosis of sensitized sheep erythrocytes by polymorphonuclear leukocytes. *Cytometry* **1994,** *17* (4), 294-301.

24. Patino, T., *et al.* Surface modification of microparticles causes differential uptake

responses in normal and tumoral human breast epithelial cells. *Sci Rep* **2015,** *5*, 11371.

25. Balkwill, F. Tumour necrosis factor and cancer. *Nat Rev Cancer* **2009,** *9* (5), 361-71.

26. Yang, X., *et al.* Targeting the tumor microenvironment with interferon-beta bridges innate and adaptive immune responses. *Cancer Cell* **2014,** *25* (1), 37-48.

27. Trinchieri, G. Interleukin-12 and the regulation of innate resistance and adaptive immunity. *Nat Rev Immunol* **2003,** *3* (2), 133-46.

28. Zhu, J., *et al.* Differentiation of effector CD4 T cell populations (*). *Annu Rev Immunol* **2010,** *28*, 445-89.

29. Klenerman, P., *et al.* Tracking T cells with tetramers: new tales from new tools. *Nat Rev Immunol* **2002,** *2* (4), 263-72.

30. Ochyl, L. J.; Moon, J. J. Whole-animal imaging and flow cytometric techniques for analysis of antigen-specific CD8+ T cell responses after nanoparticle vaccination. *J Vis Exp* **2015,** (98), e52771.

31. Robert, C., *et al.* Pembrolizumab versus Ipilimumab in Advanced Melanoma. *N Engl J Med* **2015,** *372* (26), 2521-32.

32. Brahmer, J., *et al.* Nivolumab versus Docetaxel in Advanced Squamous-Cell Non-Small-Cell Lung Cancer. *N Engl J Med* **2015,** *373* (2), 123-35.

33. Stephan, M. T., *et al.* Therapeutic cell engineering with surface-conjugated synthetic nanoparticles. *Nat Med* **2010,** *16* (9), 1035-41.

34. Huang, B., *et al.* Active targeting of chemotherapy to disseminated tumors using nanoparticle-carrying T cells. *Sci Transl Med* **2015,** *7* (291), 291ra94.

35. Liu, H., *et al.* Membrane anchored immunostimulatory oligonucleotides for in vivo cell modification and localized immunotherapy. *Angew Chem Int Ed Engl* **2011,** *50* (31), 7052-5.

36. Tom, J. K., *et al.* Covalent modification of cell surfaces with TLR agonists improves & directs immune stimulation. *Chem Commun (Camb)* **2013,** *49* (83), 9618-20.

37. Mongis, A., *et al.* Coupling of Immunostimulants to Live Cells through Metabolic Glycoengineering and Bioorthogonal Click Chemistry. *Bioconjug Chem* **2017,** *28* (4), 1151-1165.

38. Ahmed, K. K., *et al.* Surface engineering tumor cells with adjuvant-loaded particles for use as cancer vaccines. *J Control Release* **2017,** *248*, 1-9.

39. Napolitani, G., *et al.* Selected Toll-like receptor agonist combinations synergistically trigger a T helper type 1-polarizing program in dendritic cells. *Nat Immunol* **2005,** *6* (8), 769-76.

40. Fan, Y., *et al.* Immunogenic Cell Death Amplified by Co-localized Adjuvant Delivery for Cancer Immunotherapy. *Nano Lett* **2017,** *17* (12), 7387-7393.

Chapter 5 Conclusion

5.1. Significance

Recent outbreaks of emerging infectious diseases have raised global concerns about the lack of effective countermeasures, especially prophylactic vaccines. Subunit proteins that contain the epitope responsible for the protective immunity may offer a safer antigen source than traditional whole pathogen-based antigens, which are often accompanied by undesirable reactogenicity.[1] However, protein antigens are susceptible to degradation and limited by their low immunogenicity, necessitating co-administration of adjuvants. Although alum- and emulsion-based adjuvants have been widely used in vaccine products,[2-3] they often elicit strong humoral instead of cellular immune responses, while recent studies have shown antigen-specific T cells are important for combating against infectious pathogens and cancer cells.[4-6] Toll-like receptor (TLR) agonists have been investigated as a new generation of molecular adjuvants potentiating both humoral and cellular immune responses,[7-8] therefore could be co-delivered with subunit antigens and formulated into potent vaccines. Nanoparticle (NP) platforms have been investigated for vaccine delivery and showed advantages in stable encapsulation of antigens, co-localized

delivery of antigens and adjuvants, and enhanced accumulation of antigens and adjuvants in draining lymph nodes.[9-10]

In this thesis, we first designed a cationic lipid-biopolymer hybrid nanoparticle platform for vaccine delivery of subunit protein antigens and TLR agonists as adjuvants. Liposomal formulations have been successfully translated in clinics,[11-12] and incorporation of cationic lipids in the lipid composition could increase protein loading by ionic complexation, while TLR agonists could be co-loaded by the ionic or hydrophobic interaction with lipids. The protein and adjuvant co-loaded liposomes were further stabilized by complexation with self-crosslinked thiolated hyaluronic acid (HA-SH). First, we used these NPs as an intranasal vaccine platform,[13] which exhibited improved colloidal stability and prolonged antigen release. Notably, cytotoxicity associated with cationic liposomes (LC_{50} ~ 0.2 mg/ml) was significantly reduced by at least 20 fold with these NPs (LC_{50} > 4 mg/ml), as measured with bone marrow dendritic cells (BMDCs). NPs co-loaded with the model antigen ovalbumin (OVA) and the TLR-4 agonist monophosphoryl lipid A (MPLA) promoted BMDC maturation *in vitro*, and elicited robust OVA-specific $CD8\alpha^+$ T cell and antibody responses *in vivo*. Importantly, intranasal vaccination with NPs co-loaded with F1-V, a candidate recombinant antigen for *Yersinia pestis* which is the causative agent of plague, and MPLA induced potent humoral immune responses with 11-, 23-, and 15-fold increases in F1-V-specific total IgG, IgG_1, and IgG_{2c} titers in immune sera by day 77, respectively, and induced balanced Th1/Th2 humoral

immune responses, compared with the lack of sero-conversion in mice immunized with the equivalent doses of soluble F1-V vaccine. We next optimized the nanostructure design by introducing a maleimide-modified lipid to promote inter-lipid layer crosslinking and particle surface modification by HA-SH, and formulated the multilamellar vaccine particle (MVP). Compared with the previously developed interbilayer-crosslinked multilamellar vesicle (ICMV) platform [14] without HA, the MVP accumulated more in CD44-expressing DCs, increased antigen processing in DCs, and therefore elicited significantly stronger antigen-specific $CD8^+$ and $CD4^+$ T cell immune responses *in vivo*. A single dose of Ebola glycoprotein (GP)/MPLA co-loaded MVPs protected 80% of mice against a lethal viral challenge. Overall, these results suggest the MVP could be a potent platform for vaccine delivery of subunit antigens. In addition, we further explored our lipid-HA crosslinked NPs for co-localized delivery of adjuvants with immunogenically dying tumor cells to formulate a novel whole-cell cancer vaccine.[15] Recent studies have shown that cancer cells treated with certain chemotherapeutics can undergo immunogenic cell death (ICD) and initiate anti-tumor immune responses.[16] However, it remains unclear how to exploit ICD for cancer immunotherapy. To this end, we generated immunogenically dying tumor cells surface-modified with adjuvant-loaded NPs, as there were sulfhydryl and maleimide groups displayed by cell-surface proteins and NPs, respectively. Dying tumor cells laden with NPs encapsulating the TLR-9 agonist CpG efficiently promoted activation and antigen cross-presentation by DCs *in*

vitro and elicited robust antigen-specific CD8α^+ T cells *in vivo*. Furthermore, whole tumor-cell vaccination combined with immune checkpoint blockade led to complete tumor regression in ~ 78% of CT26 tumor-bearing mice and established long-term immunity against tumor recurrence. This whole-cell vaccine strategy may open new doors to “personalized” cancer immunotherapy.

5.2. Future directions

Our future studies should be directed to provide mechanistic insights into how the multilamellar, lipid-biopolymer hybrid nanostructure design could impact immune responses, such as the kinetics of co-localized delivery of antigens and adjuvants to antigen-presenting cells within lymphoid tissues following mucosal and subcutaneous vaccinations, and the immunological effects of HA. Further, we will try to delineate the impacts of Th1/Th2-balanced humoral immune responses and antigen-specific T cell responses on the prophylactic vaccine efficacy against viral or bacterial infections. Inspired by the promising results on murine models, we seek to test the MVP platform in more rigorous animal models and demonstrate its vaccine efficacy against other infectious diseases. In addition, we will explore alternative ways to co-deliver ICD inducers and immunostimulatory molecules, e.g. single or combination of TLR agonists, STING agonist, and/or immune checkpoint modulators, to tumors *in vivo* for generating

whole tumor-cell vaccines *in situ* without *ex vivo* manipulations, therefore promoting the clinical translation of our whole-cell cancer vaccination strategy and benefiting cancer patients. Overall, we have developed a cationic lipid-HA crosslinked NP platform to improve delivery efficiency of antigens and adjuvants and enhance antigen-specific immune stimulation in different murine disease models. We will further explore the translational potential of this platform for the development of promising vaccine candidates against infectious diseases and cancer.

5.3. References

1. Fan, Y.; Moon, J. J. Particulate delivery systems for vaccination against bioterrorism agents and emerging infectious pathogens. *Wiley Interdiscip Rev Nanomed Nanobiotechnol* **2017,** *9* (1).

2. Reed, S. G., *et al.* Key roles of adjuvants in modern vaccines. *Nat Med* **2013,** *19* (12), 1597-608.

3. Fox, C. B.; Haensler, J. An update on safety and immunogenicity of vaccines containing emulsion-based adjuvants. *Expert Rev Vaccines* **2013,** *12* (7), 747-58.

4. Chen, D. S.; Mellman, I. Oncology meets immunology: the cancer-immunity cycle. *Immunity* **2013,** *39* (1), 1-10.

5. Chahal, J. S., *et al.* Dendrimer-RNA nanoparticles generate protective immunity against lethal Ebola, H1N1 influenza, and Toxoplasma gondii challenges with a single dose. *Proc Natl Acad Sci U S A* **2016,** *113* (29), E4133-42.

6. Sakabe, S., *et al.* Analysis of CD8(+) T cell response during the 2013-2016 Ebola epidemic in West Africa. *Proc Natl Acad Sci U S A* **2018,** *115* (32), E7578-E7586.

7. Steinhagen, F., *et al.* TLR-based immune adjuvants. *Vaccine* **2011,** *29* (17), 3341-55.

8. Kaczanowska, S., *et al.* TLR agonists: our best frenemy in cancer immunotherapy. *J Leukoc Biol* **2013,** *93* (6), 847-63.

9. Sahdev, P., *et al.* Biomaterials for nanoparticle vaccine delivery systems. *Pharm Res* **2014,** *31* (10), 2563-82.

10. Fan, Y.; Moon, J. J. Nanoparticle Drug Delivery Systems Designed to Improve Cancer Vaccines and Immunotherapy. *Vaccines (Basel)* **2015,** *3* (3), 662-85.

11. Watson, D. S., *et al.* Design considerations for liposomal vaccines: influence of formulation parameters on antibody and cell-mediated immune responses to liposome associated antigens. *Vaccine* **2012,** *30* (13), 2256-72.

12. Chang, H. I.; Yeh, M. K. Clinical development of liposome-based drugs: formulation,

characterization, and therapeutic efficacy. *Int J Nanomedicine* **2012,** *7*, 49-60.

13. Fan, Y., *et al.* Cationic liposome-hyaluronic acid hybrid nanoparticles for intranasal vaccination with subunit antigens. *J Control Release* **2015,** *208*, 121-129.

14. Moon, J. J., *et al.* Interbilayer-crosslinked multilamellar vesicles as synthetic vaccines for potent humoral and cellular immune responses. *Nat Mater* **2011,** *10* (3), 243-51.

15. Fan, Y., *et al.* Immunogenic Cell Death Amplified by Co-localized Adjuvant Delivery for Cancer Immunotherapy. *Nano Lett* **2017,** *17* (12), 7387-7393.

16. Kroemer, G., *et al.* Immunogenic cell death in cancer therapy. *Annu Rev Immunol* **2013,** *31*, 51-72.